Arab American University

Faculty of Graduate Studies

Department of Natural, Engineering and Technology Sciences

Ph.D. Program in Physics

Magnetic and Thermal Properties of a Monolayer of WS_2 Transition Metal Dichalcogenides (TMD) in a Magnetic Field

Eman Omer Hasan Nazzal

201920268

Dissertation Committee:

Assoc. Prof. Dr. Muayad Abu Saa

Assoc. Prof. Dr. Adli Saleh

Prof. Dr. Mohammad Elsaid

Prof. Hazem Khanfar

Prof. Sami Jaber

Prof. Jihad Asad

This Dissertation Was Submitted in Partial Fulfillment of the Requirements for the Doctor of Philosophy (Ph.D.) Degree in Physics.

Palestine, 9/2024

© Arab American University. All rights reserved.

Arab American University

Faculty of Graduate Studies

Department of Natural, Engineering and Technology Sciences

Ph.D. Program in Physics

Dissertation Approval

Magnetic and Thermal Properties of a Monolayer of WS_2 Transition Metal Dichalcogenides (TMD) in a Magnetic Field

Eman Omer Hasan Nazzal

201920268

This dissertation was defended successfully on 26/09/2024 and approved by:

Dissertation Committee Members:

	Name	Title	Signature
1.	Assoc. Prof. Dr. Muayad Abu Saa	Main Supervisor	
2.	Assoc. Prof. Dr. Adli Saleh	Members of Dissertation Committee	
3.	Prof. Dr. Mohammad Elsaid	Members of Dissertation Committee	M. Khalil
4.	Prof. Hazem Khanfar	Members of Dissertation Committee	
5.	Prof. Sami Jaber	Members of Dissertation Committee	Sami AL-Jaber
6.	Prof. Jihad Asad	Members of Dissertation Committee	

Palestine, 9/2024

Declaration

I declare that, except where explicit reference is made to the contribution of others, this dissertation, is substantially my own work and has not been submitted for any other degree at the Arab American University or any other institution.

Student Name: Eman Omer Hasan Nazzal

Student ID: 201920268

Signature:

Date of Submitting the Final Version of the Dissertation: 17/10/2024

Dedication

To My Parents, husband and children.

Eman Omer Hasan Nazzal

Acknowledgments

Began with a help of more than a hand, and suffered a lot of difficulties. Today, I am here, grateful to ALLAH and after whom to many people who have the right to thank, even though with a few words, suffice it is from my heart. I would like to express my sincere gratitude to my supervisors Assoc. Prof. Dr. Adli Saleh, Assoc. Prof. Dr. Moayad Abu Saa and Prof. Dr. Mohammad Elsaid for continuous support of my study and research. They lighted my way and answered demand questions using the right approach. For their helps, all thanks.

I would like to extend my gratitude to Prof. Dr. Atef Qasrawi, who nurtured our passion for scientific research. Growing up in his laboratories and being immersed in his research, we gleaned invaluable knowledge and experience from him. Additionally, I would want to express my sincere gratitude to Dr. Hanan Nazzal for her unwavering support during this stage.

Beside my supervisors, I would like to acknowledge the members of Department of Physics at Arab American University. I have greatly profited from the courses I took, the high-quality knowledge I reserved and all opportunities that I had when I worked as a teaching and research assistant and when I participated in conferences that held inside and outside the university. Also, I would like to express my gratitude to my thesis committee, for their efforts.

I want to express my special thanks to my best friends Olfat Omareya and Arwa Ghannam for their invaluable assistance with the programming tasks. They dedicated many late nights to numerous attempts, each culminating in success. My deep affection and love extend to them and their children.

Now, let me steal a line to whom the characters will not be able to reward them, made my ambition a coordinated way seeing it in their eyes. Dad and Mum be confident that this line will not be sufficient for you. Again, I say thanks for my heart and life, for my brothers and sisters, Hiba, A'amar, Ihsan, Maram, Abduallh, Mohammed, Ahmed, Raed and Mohammed, for your support and patience all love. For you and for; the angels that filled our house with happiness and pureness, your children, all love.

I am immensely grateful to my husband's family for their support throughout my Ph.D. journey. From their words of encouragement to their practical assistance and understanding, they have been a constant source of strength. Their unwavering belief in me and their willingness to lend a helping hand whenever needed have made a significant difference. I feel incredibly fortunate to be a part of such a caring and supportive family.

Finally, and always, I am deeply grateful to my husband, Tamer Hamad, for his invaluable assistance in my Ph.D quest. His consistent support, whether offering a listening ear during times of academic stress or providing practical aid with domestic tasks, has proven effective. His conviction in my talents, as well as his sacrifices, have allowed me to devote my whole attention to my research and academic aspirations. I am blessed to have such a caring and supporting partner by my side during this difficult but rewarding journey. I'd like to express my heartfelt love and gratitude to my children, Eva and Omar, who are the center of my universe. Despite my absence owing to long hours of study and late lectures, they continue to show me love. I am eternally grateful to my beloved children for their everlasting support and adoration.

Magnetic and Thermal Properties of a Monolayer of WS_2 Transition Metal Dichalcogenides (TMD) in a Magnetic Field

Eman Omer Hasan Nazzal

Assoc. Prof. Dr. Muayad Abu Saa

Assoc. Prof. Dr. Adli Saleh

Prof. Dr. Mohammad Elsaid

Prof. Hazem Khanfar

Prof. Sami Jaber

Prof. Jihad Asad

Abstract

In this thesis, the effective Hamiltonian of a monolayer WS_2 in an electric field will be analyzed in order to get information about enhancing the energy band gap of the monolayer WS_2. After applying an external perpendicular magnetic field, the effective Hamiltonian of the WS_2 monolayer will be studied in the case of absence and presence of Zeeman term. The electronic properties such as the energy gap and the band structure of the monolayer in the presence of electric and magnetic fields will be considered. Using the utilized information other properties such as the density of states, and Fermi energy will be discussed at different strengths of magnetic fields and temperatures. The added magnetic field will alter the electronic spectra and the Landau levels of the monolayer WS_2 will appear. Using the partition function the average energy, specific heat capacity, the magnetization and magnetic susceptibility will be considered in the presence and absence of Zeeman term. The effect of increasing the band gap by increasing the applied electric field will be considered on electronic, thermal and magnetic properties for the K valley and K′ valley of the WS_2 monolayer.

Key Words: Tungsten Sulfide, thermal, magnetic, Fermi, magnetic field.

Table of Contents

List of Tables

List of Figures

List of Definitions of Abbreviations

Abbreviations	Title
$\propto_c$	The magnetic length
$\mathcal{H}^{s\eta}$	The effective low-energy Hamiltonian
$\sigma_{x,y,z}$	Pauli matrices
C_v	Specific heat capacity
$\overline{E}$	Average energy
E_f	Fermi energy
E_z	perpendicular electric field
M_z	Zeeman Term
g'	Landee factor
g_s	spin degeneracy
k_B	Boltzmann constant
v_F	Fermi Velocity
λ_c	spin-orbit coupling strength in conduction band
λ_v	spin-orbit coupling strength in valance band
μ_B	Bohr magneton
ω_c	Cyclotron frequency
ω_c	The cyclotron frequency
ΔS	Entropy change
B	Magnetic field strength
COF	Covalent Organic Framework
DFT	Density Functional Theory

$\mathcal{H}$	Hamiltonian in the absence of an electric field
LDH	Layered Double Hydroxide
LL	Landau level
MCE	Magnetocaloric Effect
MOF	Metal-Organic Framework
PL	Photoluminescence
TMD	Transition Metal Dichalcogenide
TMO	Transition Metal Oxide
WS2	Tungsten Sulfide
A	Vector potential
DOS	Density of states
M	Magnetization
S	Entropy
T	Temperature
Z	partition function
c	Speed of light
d	distance between the W and S atoms in the sub-lattice
e	Charge of electron
m	Rest mass of the particle
n	Principle quantum number
$\mathbf{I}$	Unit matrix
Γ	The broadening parameter
μ	Chemical potential

χ	Magnetic susceptibility
2Δ	Energy band gap
2D	Two-Dimensional

Chapter One: Introduction

Because of their distinct characteristics that set them apart from bulk materials, monolayers are essential to the study of materials science and nanotechnology. Monolayers, which are made up of just one layer of atoms or molecules, have unique mechanical, optical, and electrical properties. For example, materials such as transition metal dichalcogenides (TMDs) and graphene exhibit quantum phenomena, higher conductivity, and greater reactivity that are absent from their bulk counterparts. Monolayers are crucial for the advancement of technology because of these qualities, which can be used in a variety of applications such as energy storage devices, sensors, and transistors.

The dimensionality of monolayers and the resulting surface-to-volume ratio are the primary distinctions between them and bulk materials. Averaged qualities result from interactions that mostly take place inside the volume of bulk materials. On the other hand, surface interactions completely define monolayers and can control their behavior. For some applications, monolayers are more effective because of the enhanced phenomena such as charge transfer and catalytic activity brought about by the increased surface area in relation to volume. Additionally, new quantum effects like exciton binding energies that are drastically different from bulk materials can result from the reduced dimensionality, opening up fascinating possibilities for study and development in cutting-edge technology.

Techniques like mechanical exfoliation, chemical exfoliation, or liquid-phase exfoliation are commonly used to convert bulk materials into monolayers. In order to create thin sheets, mechanical exfoliation—made popular by the creation of graphene—involves removing layers from the bulk material using adhesive tape or other techniques. By intercalating between the layers using chemical agents, chemical exfoliation makes it easier for the layers to separate into monolayers. The bulk material is dispersed in a solvent by liquid-phase exfoliation, which uses shear or sonication forces to separate it into separate layers. Depending on the particular material and desired characteristics of the final monolayers, each technique can be customized and offers a variety of benefits.

An emerging class of materials with exceptional promise for many applications are two-dimensional (2D) nanomaterials. Such materials were characterized by unique physical, chemical, electrical, and optical characteristics that have been conferred by their planar topography. Furthermore, these characteristics make them ideal candidates for medicinal delivery, biosensing, bioimaging, regenerative medicine, and additive manufacturing techniques. The increased surface-to-volume ratio of 2D nanomaterials facilitates better interactions with cells and biomolecules. Many 2D nanomaterials have been investigated for their potential in biomedical applications, including transition metal dichalcogenides (TMDs), layered double hydroxides (LDHs), layered silicates (nanoclays), 2D metal carbides and nitrides (MXenes), metal-organic frameworks (MOFs), covalent organic frameworks (COFs), and polymer nanosheets(Murali, Lokhande et al. 2021).

Inorganic, organic, or hybrid 2D nanomaterials make up the three main groups into which 2D nanomaterials may be roughly divided. Inorganic 2D nanomaterials include monolayers of carbon atoms (graphene and its analogs), transition metal dichalcogenides (TMDs), transition metal oxides (TMOs), 2D metal carbides and nitrides (MXenes), monoelemental 2D semiconductors, layered silicate (nanoclay), and layered double hydroxides (LDHs) (Murali, Lokhande et al. 2021).

TMDs are materials having a 2D layer and the general formula MX_2. Depending on their composition, they can be categorized as semiconductors, metals, semi-metals, or superconductors. TMDs have a wide variety of electronic characteristics that are advantageous for the regeneration of electrically active tissues due to their diversified chemical composition and structural phases. TMDs are incredibly strong and can withstand stresses of up to 10% before breaking. TMD's three-fold symmetry makes it simpler to design strains by using lower strains. The center transition metal layer (such as Mo, W, or Nb) of TMDs is sandwiched between two layers of chalcogenides (e.g., S, Se, Te), in contrast to graphene, which has a single layer of carbon atoms (Murali, Lokhande et al. 2021).

Chapter Two: Literature Review

Although graphene has amazing features, its use in the manufacturing of devices is constrained by its zero band gap, which causes graphene transistors to have a poor on-off current ratio (Liao, Lin et al. 2010). The TMD monolayers, particularly group-IV dichalcogenides (Coleman, Lotya et al. 2011, Hoi and Yarmohammadi 2018), are viewed as the perfect materials. Thus, group VI transition-metal dichalcogenides MX_2, M = Mo,W; X = S,Se (Fang, Chuang et al. 2012, Xiao, Liu et al. 2012, Geim and Grigorieva 2013, Li, Zhang et al. 2013, Lu, Yao et al. 2013), germanene (Sone, Yamagami et al. 2014), silicene (Dávila, Xian et al. 2014), and others with limited band gaps have been subjected to more research. When sliced into monolayers, MX_2 family of semiconductors form a fascinating class of materials (Tahir and Vasilopoulos 2016).

Due to their exceptional electrical, optoelectronic, and catalytic characteristics, TMD monolayers, particularly group-VIB Transition Metal Dichalcogenides TMDs ($MoSe_2$, MoS_2, WSe_2, and WS_2), are of great interest (Zong, Yan et al. 2008, Mak, Lee et al. 2010, Radisavljevic, Radenovic et al. 2011). Thickness (number of layers) and external factors as strain engineering, pressure, and electric or magnetic fields have a significant impact on the electronic characteristics of these materials (Muoi, Hieu et al. 2020). Many studies have recently concentrated on utilizing the effective low-energy Hamiltonian to examine the low-energy band structure and magneto-optical transport characteristics of Transition Metal Dichalcogenides TMDs and other buckling honeycomb lattices (Muoi, Hieu et al. 2020). These studies showed that the spin-splitting in the TMD monolayers' conduction band is significantly influenced by the external magnetic field, and that the TMD monolayers' strong spin-orbit interaction may make them useful for spintronic applications (Muoi, Hieu et al. 2020).

The thermodynamic quantities for four different TMD materials—MoS_2, WS_2, $MoSe_2$, and WSe_2—as functions of temperature and magnetic field have been investigated (Diffo, Fotue et al. 2021). The heat capacity has a peak structure as a function of temperature that, at low temperatures, represents the well-known Schottky anomaly (Diffo, Fotue et al. 2021). It has been shown that depending on the magnetic field, the environment can excite the system at a constant temperature for a certain amount of magnetic field, which is smaller for a temperature near to absolute zero than for room temperature (Diffo, Fotue et al. 2021).

Among the TMDs, WSe_2 has strong spin-orbit coupling (Tahir and Vasilopoulos 2016). Such a property as well as its high quality make for a fantastic spin and valley control system (Aivazian, Gong et al. 2015, Srivastava, Sidler et al. 2015). At room temperature, WSe_2 transistor has been proven to have a high-mobility (Movva, Rai et al. 2015). Even though, WSe_2 is a direct-band-gap semiconductor, the removal of the valley degeneracy makes it possible to control the electron valley index optically. This can be possible by introducing a magnetic field normal to the 2D layer (Aivazian, Gong et al. 2015, Srivastava, Sidler et al. 2015).

In a monolayer of WSe_2 and similar compounds, optical transitions in magnetic fields have been examined (Aivazian, Gong et al. 2015, Srivastava, Sidler et al. 2015). At the edge of the Brillouin zone, which is mostly made up of strongly localized d orbitals of the transition metal, direct optical transitions in a WSe_2 monolayer take place. As the emission of circularly polarized light arises from states with differing valley index, spin, and orbital magnetic moment, there are several potential contributions to the Zeeman splitting in a WSe_2 monolayer. These tests enable the identification of the various components to the Zeeman splitting since the valleys may be selectively addressed (Mitioglu, Plochocka et al. 2015). At zero magnetic field, a number of WSe_2 characteristics have been investigated (Aivazian, Gong et al. 2015, Srivastava, Sidler et al. 2015). Landau levels (LLs) are created in a limited magnetic field, and transitions between them cause the magneto-optical conductivity to exhibit certain absorption lines (Tahir and Vasilopoulos 2016). Also, the magneto-optical response in WSe_2 may be adjusted to operate between microwave and THz and visible frequencies (Tahir and Vasilopoulos 2016).

By investigation the magneto-optical transport characteristics of a WSe_2 monolayer in the presence of a perpendicular magnetic field, a periodic oscillation in conductivities with frequency caused by photon absorption corresponding to LL transitions triggered by the relevant selection rules were involved (Tahir and Vasilopoulos 2016). The conductivity peaks depend linearly on the applied magnetic field and represent the equally spaced LLs in each band due to the huge direct band gap of WSe_2 (Tahir and Vasilopoulos 2016). With transition occurring in the visible frequency range, the intraband and interband optical transitions in WSe_2 correspond to two entirely separate regimes (Tahir and Vasilopoulos 2016). The valley and spin splitting may be magnetically controlled. These discoveries broaden the understanding of the electrical characteristics of a 2D WSe_2 system leading to create spintronic and valleytronic optical devices (Tahir and Vasilopoulos 2016)].

In comparison to the other group-VIB TMDs, mentioned above, the WS_2 monolayer has the biggest natural band gap, and the spin-orbit interaction is a crucial term to understanding its electrical characteristics (Muoi, Hieu et al. 2020). For valleytronic and integrated spintronic applications, in particular, a huge spin splitting of 0.43 eV in the WS_2 monolayer caused by a loss of the inversion symmetry may be beneficial (Muoi, Hieu et al. 2020). On the basis of density functional theory (DFT), it was shown that WS_2 is kinetically stable and has a band gap that is significantly larger than that of bulk WS_2(Muoi, Hieu et al. 2020). Additionally, several methodologies have been developed and used to study the electrical characteristics of the WS_2 monolayer (Muoi, Hieu et al. 2020). Roldán and his team have examined the impact of the spin-orbit interaction on the electrical characteristics of the WS_2 monolayer by combining DFT with the tight-binding approximation (Muoi, Hieu et al. 2020).

Using the effective low-energy Hamiltonian, Muoi and his group investigated how the external electric and magnetic fields affected the low-energy bands and Landau levels of the monolayer WS_2. The band gap of the monolayer WS_2 grows linearly when the perpendicular electric field is applied. Additionally, the studies showed that the nanolayer WS_2's Landau levels are related to the applied magnetic field B. In addition, the Landau levels n as well as the magnetic field B affect the spin splitting energy. At high magnetic fields, the Zeeman fields and spin-orbit interaction in monolayer WS_2 resulted in a significant splitting energy being discovered in the valence band. These estimated findings may offer further helpful data for monolayer WS_2 applications in spintronic devices (Muoi, Hieu et al. 2020).

With regard to the monolayer of WS_2, the band gap and the intensity of the spin-orbit coupling are, respectively, 1.79 and 0.43 eV. It has a monolayer lattice constant of 3.197 Å. In the absence of an electric field, the monolayer of WS_2 band gap is 1.589 eV. The external electric field has a significant influence on the band gap of the monolayer of WS_2. The band gap of the monolayer increases linearly as the electric field is increased. Moreover, it has been noted that the band gap of the monolayer grows up to 1.79 eV in the case of no spin-orbit interaction when the electric field energy is equivalent to the magnitude of spin splitting. This behavior for monolayer WS_2 is different from silicone, whose energy gap will drop to zero as the electric field energy grows from zero to the magnitude of spin splitting and then increases as the electric field energy increases. Furthermore, when the electric field energy is higher, the size of spin splitting is greater (Muoi, Hieu et al. 2020).

In recent investigations, the exciton and trion g factors were extracted, the valley degeneracy was lifted, and the magneto-optical characteristics of single-layer diselenides were studied (Plechinger, Nagler et al. 2016). Recent studies on the high-field magnetooptics of transition metal disulfide monolayers have so far only focused on the study of CVD-grown materials with large linewidths or on the field-induced rotation of the linear polarization of excitonic photoluminescence (Plechinger, Nagler et al. 2016). This prevents a distinct examination of the behavior of various excitonic quasiparticles in magnetic fields, such as charge-neutral excitons and trions, which is crucial for comprehending the underlying causes for changes in the optical spectrum brought on by magnetic fields. High-quality mechanically exfoliated monolayer WS_2 was used for the low-temperature photoluminescence (PL) studies, which revealed incredibly crisp resonances emanating from many different excitonic quasiparticles and bringing the samples to high magnetic fields of up to 30 T. In the PL spectrum, it is possible to see charge-neutral excitons, singlet and triplet trions, and maybe phonon-related excitonic characteristics. Exciton and triplet trion g factors of 4.3 and two regimes (low and high magnetic field) with differing g factors for singlet trions were established. At 30 T, the excitons (singlet trions) exhibit a diamagnetic shift on the order of 1 meV–2 meV. A theoretical model and the extracted exciton radius of 25 Å agree quite well (Plechinger, Nagler et al. 2016).

In addition, the use of a magnetic field to create valley polarization was studied. The complicated interactions between various excitonic quasiparticles and the valley-orbit-splitted exciton and trion dispersions in the sample under study turn out to be quite significant, and in the case of excitons, they result in a predominance of the energetically unfavorable valley population. The combined impact of formation-rate-related and dispersion-related factors may be used to explain the singlet and triplet trion valley polarization (Plechinger, Nagler et al. 2016).

Two main consequences result from the application of a positive magnetic field. First, depending on the detecting helicity, all excitonic resonances vary in energy. Second, there is a large variation in the relative intensities of the different peaks (Plechinger, Nagler et al. 2016). Bright excitons come from states in the conduction and valence bands that have the same spin orientation, therefore the spin Zeeman effect does not influence the energy disparity between these bands, leaving exciton energies unaffected. Since the majority of the d orbitals in the conduction band states have m = 0, they lack an orbital magnetic moment. The degeneracy of the two branches at K = 0 is lifted in a magnetic field, and they become valley-polarized. This adds a new mechanism for brilliant exciton polarization, where the lowest energy state is predicted to emit light more effectively owing to thermal population (Plechinger, Nagler et al. 2016).

The TMD material WS_2 monolayer has a large natural band gap, also it has a spin-orbit interaction that is crucial to understand its electrical characteristics. Previously, it was suggested that the WS_2 is kinetically stable and has a band gap that is significantly larger than that of bulk WS_2 (Muoi, Hieu et al. 2020). Moreover, many techniques have been used to study the electrical characteristics of the WS_2 monolayer.

In this thesis, the effective Hamiltonian of a monolayer WS_2 in an electric field will be analyzed in order to get information about enhancing the energy band gap of the monolayer WS_2. The electronic properties such as the energy gap and the band structure of the monolayer in the presence of electric field will be considered. Using the utilized information other properties such as the density of states and Fermi energy may be discussed.

Also, the electronic properties will be considered after adding a magnetic field on the WS_2 monolayer. The added magnetic field will alter the electronic spectra and the Landau levels of the monolayer WS_2 will appear. Using the partition function and the statistical physics approaches the average energy, the specific heat capacity, the magnetization and magnetic susceptibility will be considered so that the uses of this material will be defined.

Analytical and computational methods will be used to carry this objective. For this, a MATLAB program will be utilized. The field of applications will be determined by analyzing the results.

The four chapters that make up this thesis each focus on a different aspect of the investigation. Chapter One that titled with Introduction gives a brief introduction to transition metal dichalcogenides and WS_2 monolayer, introduction and literature Survey, along with a review of the relevant literature and an analysis of the statement problem. The theories of this study, including the Dirac Hamiltonian of WS_2, Density of States Calculations, Fermi Energy Calculations, Thermal Properties Calculations, and Magnetic Properties Calculations, are stated in Chapter Two which is titled with Theoretical Background. The primary computational results on the electrical, thermal, and magnetic characteristics of the WS2 monolayer are presented in Chapter Three that is titled with Results and Discussion. Finally, Chapter Four, Conclusions, provides a summary of the key findings as well as possible future research topics.

Chapter Three: Methodology

The group-VI transition metal dichalcogenides in a monolayer configuration was examined. The material has a much stronger spin-orbit coupling effect than graphene (Kane and Mele 2005), which has a significant impact on the electrical structures of transition metal dichalcogenides. The Kane–Mele type, which is provided by (Tabert, Carbotte et al. 2015, Muoi, Hieu et al. 2019), can be used to characterize the system's effective low-energy Hamiltonian in the absence of an electric field, as follows (Muoi, Hieu et al. 2020):

$$\mathcal{H} = \hbar v_F\left(\eta\sigma_x k_x + \sigma_y k_y\right) + [\Delta + \eta s(\lambda_c - \lambda_v)]\sigma_z + (\lambda_c + \lambda_v)\eta s\mathbf{I} \qquad (2.1)$$

Where;

v_F is the fermi velocity which is $6.65 \times 10^5 \mathrm{m/s}$ (Muoi, Hieu et al.2020),

2Δ is the energy gap of the material in the case of excluding the effect of spin $-$ orbit coupling, which is equal to 1.79 ev,

$\eta = \pm 1$ correspond respectively to the two valleys K and K$'$. A schematic geometry of WS_2 monolayer is shown in Fig.2.1.

$s = \pm 1$ for electrons of spin up and spin down, respectively,

$\boldsymbol{k}$ is the 2D wave vector,

λ_c is the spin $-$ orbit coupling of conduction band.

λ_v is the spin $-$ orbit coupling of valance band.

$\boldsymbol{I}$ is the unit matrix and

$\sigma_{x,y,z}$ is the Pauli matrices.

$$\sigma_x = \begin{pmatrix} 0 & 1 \\ 1 & 0 \end{pmatrix}, \sigma_y = \begin{pmatrix} 0 & -i \\ i & 0 \end{pmatrix}, \sigma_z = \begin{pmatrix} 1 & 0 \\ 0 & -1 \end{pmatrix}.$$

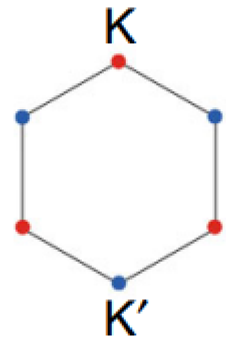

Fig.3.1: Schematic of the WS_2 monolayer.

The spin-orbit coupling effect has been incorporated into the Kane-Mele Hamiltonian (2.1) through the parameters λ_c and λ_v, where the spin-orbit coupling strength is represented by $2(\lambda_c + \lambda_v)$ (Muoi, Hieu et al. 2020).

By substituting the Pauli matrices into equation (2.1), the Hamiltonian is rewritten in the matrix form as:

$$\mathcal{H}_0 = \begin{pmatrix} \Delta + (\lambda_c - \lambda_v)\eta s & \hbar v_F(\eta k_x - ik_y) \\ \hbar v_F(\eta k_x + ik_y) & -\Delta - (\lambda_c - \lambda_v)\eta s \end{pmatrix} + (\lambda_c + \lambda_v)\eta s\mathbf{I} \tag{2.2}$$

By diagonalization of the Hamiltonian (2.2) of $det|\mathcal{H}_0 - E_0| = 0$, the low-energy spectrum of the WS_2 can be obtained as the following:

$$E_0 = \gamma\left(v_F^2\hbar^2k^2 + \Delta_{\eta s}^2\right)^{1/2} + \lambda\eta s \tag{2.3}$$

Where;

$\gamma = \pm 1$ stands respectively for the conduction band and the valence band,

k is the 2D wave vector, and

$\Delta_{\eta s} = \Delta + (\lambda_c - \lambda_v)\eta s$.

In the case the 2D surface of the monolayer subject to a perpendicular electric field E_z, the system's Hamiltonian becomes:

$$\mathcal{H}_E = \mathcal{H}_0 + \frac{1}{2}\Delta_z \sigma_z \tag{2.4}$$

Where;

$\Delta_z = E_z d,$

$\text{with d is the distance between the W and S atoms in the sub} - \text{lattice}.$

Likewise, the matrix form of the Hamiltonian (2.4) can be written as:

$$\mathcal{H}_E = \begin{pmatrix} \Delta_{\eta s} + \frac{1}{2}\Delta_z & \hbar v_F(\eta k_x - i k_y) \\ \hbar v_F(\eta k_x + i k_y) & -\Delta_{\eta s} - \frac{1}{2}\Delta_z \end{pmatrix} + (\lambda_c + \lambda_v)\eta s \mathbf{I} \tag{2.5}$$

Again, by diagonalization of equation (2.5), the energy eigenvalues of the WS_2 under an electric field are:

$$E_E = \gamma \left(v_F^2 \hbar^2 k^2 + \left(\Delta_{\eta s} + \frac{1}{2}\Delta_z \right)^2 \right)^{1/2} + (\lambda_c + \lambda_v)\eta s \tag{2.6}$$

The 2-dimension canonical momentum is $\boldsymbol{\pi} = P + e\,\boldsymbol{A}$ with the vector potential $\boldsymbol{A} = (0, Bx, 0)$. When an external magnetic field B is applied along the z-axis. The effective low-energy Hamiltonian (2.1) can be rewritten as (Tahir and Vasilopoulos 2016):

$$\mathcal{H}^{s\eta} = \mathcal{H}_0 + sM_z - \eta M_v \tag{2.7}$$

Where;

$\mathrm{M_z} = {}^{\mathrm{g'\mu_B B}}\!/_{2}$ is the Zeeman term, with

$\mathrm{g'} = \mathrm{g'_e} + \mathrm{g'_s}$ is the Landee'factor, with $\mathrm{g'_e} = 2$ and $\mathrm{g'_s} = 0.84$ and

$\mathrm{\mu_B}$ is the Bohr magneton.

$\mathrm{M_v} = {}^{\mathrm{g_v \mu_B B}}\!/_{2}$ is the valley term, with $\mathrm{g_v} = 4.96$ (Muoi, Hieu et al. 2019)

The magnetic field altered the momentum operators in the presence of the perpendicular magnetic field, by Peierls substituting as follows (Muoi, Hieu et al. 2020):

$$\hbar k_i \longrightarrow \hbar k_i + eA_i \qquad (2.8)$$

where;

e is the elementary charge, and we used it in the unit of $c = 1$.

Then, the Hamiltonian $\mathcal{H}_0$ in equation 2.7 becoms $\mathcal{H}_0^{s\eta}$ as follows:

$$\mathcal{H}_0^{s\eta} = \begin{pmatrix} \Delta + 2\eta s\lambda_c & \hbar v_F\left[\eta k_x - i\left(p_y + eBx\right)\right] \\ \hbar v_F\left[\eta p_x + i\left(k_y + eBx\right)\right] & -\Delta + 2\eta s\lambda_v \end{pmatrix} + (\lambda_c + \lambda_v)\eta s\mathbf{I} \qquad (2.9)$$

By diagonalization, the energy was obtained:

$$E_0^{s\eta} = \gamma\left(\Delta_{s\eta}^2 + 2Bn\eta v_F^2 e\hbar\right)^{1/2} + \eta\ (\lambda_c + \lambda_v) \qquad (2.10)$$

Finally, the eigenvalues of the Hamiltonian in equation (2.8) can be expressed as:

$$E_0^{s\eta} = E_0 + sM_z - \eta M_v$$

$$E_n^{s\eta} = \gamma\left(\Delta_{s\eta}^2 + 2Bn\eta v_F^2 e\hbar\right)^{1/2} + \eta\ (\lambda_c + \lambda_v) + sM_z - \eta M_v \qquad (2.11)$$

$or;$

$$E_n^{s\eta} = s\eta(\lambda_c + \lambda_v) + sM_z + \gamma\ E_n^{s\eta} \qquad (2.12)$$

Where;

$E_n^{s\eta} = \left(\Delta_{s\eta}^2 + n\hbar^2{\omega_c}^2\right)^{1/2}, with$

$\omega_c = \left(2eB/\hbar\right)^{1/2}$ is the cyclotron frequency,

n is the Landau levels, and

$\gamma = \pm 1$ refers to the electron and hole states; respectively.

The distribution of energy states that a monolayer material's electrons can access is described by its density of states (DOS). Because there are more electronic states near the band boundaries, the DOS usually exhibits a larger density at lower energies. Because monolayer materials' electrical structures frequently produce densely packed energy levels near the Fermi level, this high density is the outcome. The density of states DOS can be expressed as (Gammag and Villagonzalo 2012):

$$DOS(E) = \frac{eB_z}{h}\sum_n \left(\frac{1}{2\pi}\right)^{1/2} \frac{1}{\Gamma} exp\left[-\frac{(E-E_n^{\pm})^2}{2\Gamma^2}\right] \tag{2.13}$$

Where;

Γ is the broadening parameter.

The fermi energy can be invistaged through (Tahir and Vasilopoulos 2016):

$$f(E) = \left(\frac{\exp\,(E-\mu)}{k_B T} + 1\right)^{-1} \tag{2.14}$$

With k_B is the Boltzmann constant.

Also, the density of electron (n_e) is given through (Tahir and Vasilopoulos 2016):

$$n_e = \int_0^{\infty} dE\ DOS(E) f(E) + \int_{-\infty}^{0} dE\ DOS(E)[1 - f(E)] \tag{2.15}$$

The thermodynamic properties of WS_2 monolayer can be calcualted using

the partition function Z through the following formulae (Sedehi and Khordad 2021, Arora, Gupta et al. 2023):

$$\bar{E} = -\frac{\partial\ logZ}{\partial\beta}, \tag{2.16}$$

Where;

$$Z = \sum_n e^{-\beta E_n}$$

$\overline{\mathrm{E}}$ is the mean energy,

$\beta = \frac{1}{k_B T}$, with k_B is the Boltzmann constant, and

E_i are the eigen − energies found at different energy levels.

Understanding the thermal properties and behavior of a monolayer, or single layer of atoms or molecules, requires an understanding of its specific heat capacity. Monolayers have distinct thermal properties because of their decreased dimensionality and the greater impact of surface effects than bulk materials. The material composition, how layers interact, and outside factors like temperature and pressure can all have a substantial impact on the specific heat capacity. For example, it has been demonstrated that monolayers of materials such as transition metal dichalcogenides or graphene have large specific heat capacity, which can be explained by their significant phonon contributions and bonding.

$$C_v = \frac{\partial \bar{E}}{\partial T} \tag{2.17}$$

Where;

C_v is the specific heat capacity (Khordad and Sedehi 2018).

The degree of disorder or unpredictability in a single layer of atoms or molecules is expressed as the monolayer's entropy, and this value is crucial in defining the thermodynamic properties and stability of the monolayer. Entropy in monolayers can be affected by the configuration of atoms, the intensity of interatomic interactions, and external variables like pressure and temperature. Due to their lower dimensionality, monolayers frequently exhibit different entropy behavior than bulk materials, which results in special mechanical and thermal properties.

$$S = K_B \log Z - K_B \beta \frac{\partial \, logZ}{\partial \beta}, \tag{2.18}$$

Where;

S is the entropy.

With potential applications in magnetic refrigeration and thermal management, the magnetocaloric effect (MCE) in monolayers—a fascinating phenomena where a change in magnetic field generates a temperature change in a material—is being studied extensively. Because of their decreased dimensionality and distinct magnetic properties—which frequently result from strong spin interactions and weaker symmetry when compared to their bulk counterparts—monolayers can exhibit much higher MCEs. Certain two-dimensional magnetic materials and transition metal dichalcogenides, for example, have prominent MCEs that enable more effective heat exchange under different magnetic field conditions. This property not only provides information about basic magnetic behavior at the nanoscale, but it also creates opportunities for the advancement of cooling devices that consume less energy.

The magnetocaloric effect can be caclculated through (Kosogor and L'vov 2023):

$$\Delta S = S(B \neq 0, T) - S(B = 0, T) \tag{2.19}$$

A monolayer's magnetization, or net magnetic moment per unit area, is a crucial component of its magnetic characteristics and has significant ramifications for a range of nanotechnology and spintronics applications. The arrangement of atoms and the interactions between their electronic spins typically control the magnetic behavior of monolayers, which can result in unusual phenomena not found in bulk materials. For example, the reduced dimensionality and enhanced surface-to-volume ratio can lead to different magnetic ordering and anisotropy in monolayers of ferromagnetic materials or transition metal dichalcogenides. This magnetization allows for customizable magnetic qualities that can be used in devices like memory storage and magnetic sensors. It can also be sensitive to external influences like temperature and the strength of a magnetic field.

The magnetization M of WS_2 monolayer was calculated using (Elsaid, Ali et al. 2019):

$$M = -\frac{\partial \bar{E}}{\partial B} \tag{2.20}$$

One important measure of a material's ability to become magnetized in response to an external magnetic field is its magnetic susceptibility in a monolayer. Because monolayers are less dimensional than bulk materials, their magnetic susceptibility can behave differently, frequently displaying increased or anisotropic responses. This is especially noteworthy for materials such as ferromagnetic monolayers and transition metal dichalcogenides, where susceptibility can be greatly influenced by interactions between spins and the geometry of the monolayer. Magnetic susceptibility is a dynamic property that can vary according to factors including temperature, tension, and external magnetic fields.

The magnetic susceptibility of WS_2 monolayer χ was calculated using (Alia, Elsaid et al. 2019):

$$\chi = \frac{\partial M}{\partial B} \tag{2.21}$$

Chapter Four: Results

This chapter examined the response of the WS_2 monolayer to temperature fluctuations, changing band gap values, and various magnetic field strengths. Energy spectra, density of states, Fermi-energy calculations, average energy calculations, specific heat capacity, entropy, entropy variations, magnetization, and magnetic susceptibility are among the important parameters that are the focus of the analysis. These characteristics offer crucial information about the behavior of the WS_2 monolayer in various external environments.

4.1 Simulation Approach

MATLAB, a potent computing environment well-known for its skills in numerical analysis, data visualization, and algorithm creation, is used in this thesis to construct the simulation approach. With the help of MATLAB's comprehensive toolkit and functionalities, researchers may more easily model complicated systems and produce intricate simulations that are suited to particular research topics. This study intends to investigate and evaluate a variety of scenarios pertinent to the research objectives by utilizing MATLAB's intuitive interface and powerful computing capabilities. MATLAB is a vital tool in the quest for significant insights and conclusions throughout this study since it allows for the real-time visualization of findings and the manipulation of parameters, which improves comprehension of system behavior.

Initially, the band structure of WS_2 monolayer in the absence of an electric field was obtained by programming Equation 2.3 with the values provided in Chapter 2. Following the addition of an external electric field, Equation 2.6 was coded to examine how the electric field affected the energy gap.

Equation 2.11 was then programmed using the values provided in Chapter 2 to examine the impact of the magnetic field on the energy. Additionally, the density of the levels and the Fermi energy, as well as their relationship to temperature and magnetic field, were determined by programming Equations 2.13 and 2.14.

The research of thermodynamic properties became the main focus after the electrical properties were finished. After programming a partition function, the average energy was determined by programming Equation 2.16 using the general definition of the derivative. Equation 2.17 was then programmed to get the specific heat capacity, using the derivative of the average energy with respect to temperature.

Equation 2.18 was programmed using MATLAB to investigate the entropy of the WS_2 monolayer, taking note that any derivative was implemented in MATLAB using the general definition of the derivative. Following the examination of thermodynamic properties, attention turned to using Equation 2.19 to program in order to investigate the phenomena of the magnetocaloric effect.

By programming Equation 2.20, the magnetic characteristics of the WS_2 monolayer were examined at the final stage of the thesis. This allowed for the determination of the magnetization by finding the derivative of the average energy with respect to the magnetic field strength. Equation 2.21 was programmed by deriving the magnetization with respect to the magnetic field strength in order to determine the magnetic susceptibility.

In summary, the efficiency and accuracy of the analysis have been much improved by the use of MATLAB throughout the computations. A greater comprehension of the behavior of the system was made possible by the methodical derivation of essential electric, thermodynamic, and magnetic properties through the programming of key equations. The versatility of MATLAB enhanced the insights by enabling real-time viewing of results in addition to the simple execution of intricate mathematical processes. All things considered, MATLAB's incorporation into the thesis was quite helpful in handling the complex calculations required to investigate the relevant physical processes.

4.2 Electronic Properties

It is known that the monolayer WS_2 in the case of no spin – orbit interaction has a band gap of 1.79 eV (Muoi, Hieu et al. 2020). Also, the strength of the spin orbit coupling and the lattice constant of the monolayer are respectively 0.43 eV and 3.197 A^o. Using equation 2.1, the band structure of WS_2 monolayer when the applied electric field is zero was investigated.

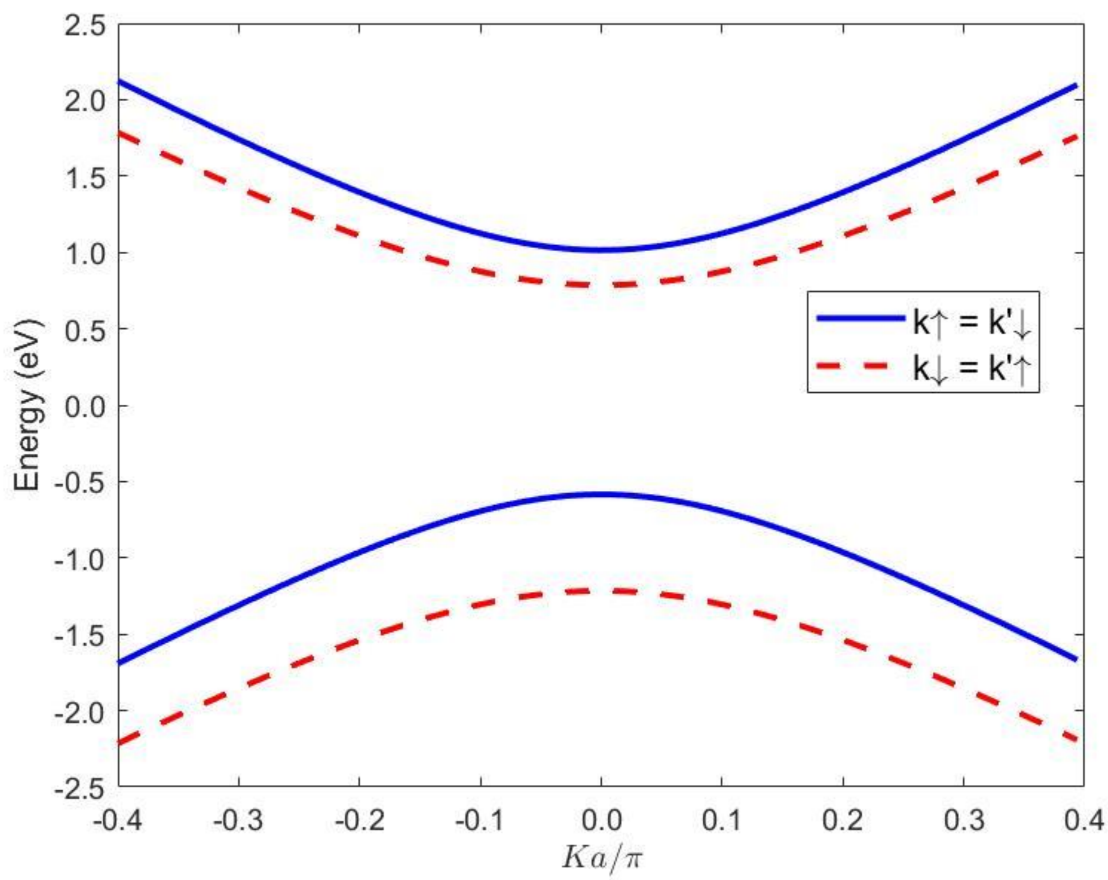

Fig.4.1: The band structure of WS_2 monolayer without electric field.

Fig.4.1 shows the low energy spectrum of WS_2 monolayer for the K and K` valleys without electric field ($\Delta z = 0$). It is evident that the bands corresponding to spin-up at the

K valley (K↑) and spin-down at the K′ valley (K′↓) are the same, and the bands corresponding to spin-down at the K valley (K↓) and the spin-up bands at the K′ valley (K′ ↑) are the same. Moreover, the monolayer WS_2 bands are spin split. From Fig.4.1 the band gap of WS_2 monolayer when the electric field is zero can be determined to be 1.5892 eV in consistence with Do Muoi research (Muoi, Hieu et al. 2020).

Fig.4. 2 illustrates how the monolayer WS_2's low-energy bands and band gap are affected by the external electric field. The figure shows that spin configurations have considerable effects on the valence band. In contrast, there is very little variation between spin-up and spin-down configurations' subbands in the conduction band, particularly in the middle of the Brillouin zone. Additionally, our calculations show that the external electric field has a significant influence on the band gap of the monolayer WS_2.

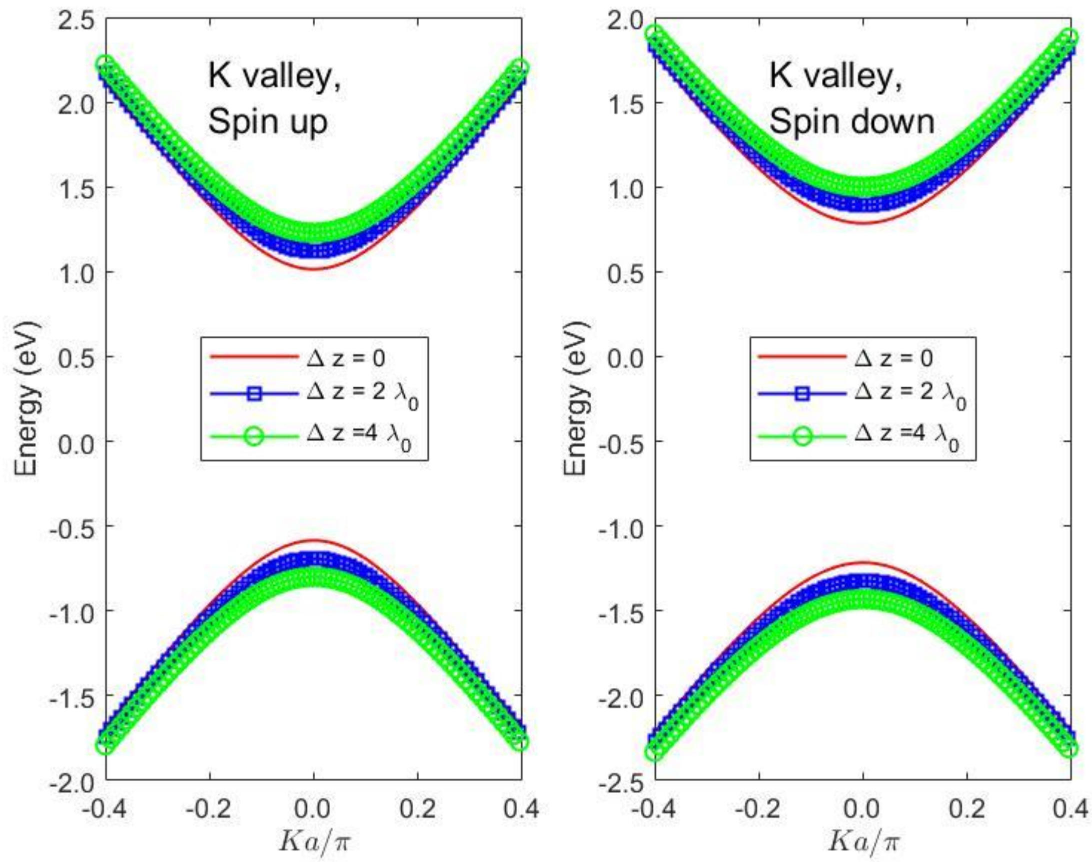

Fig.4.2: The band structure of WS_2 monolayer with electric field for K valley with spin up and spin down.

As illustrated in Fig.4.3, the band gap of the monolayer grows linearly with increasing electric field. Specifically, in the absence of spin-orbit interaction, the band gap of the monolayer grows to $2\Delta = 1.79$ eV when the electric field energy Δz equals the size of spin splitting $2\lambda_0(\lambda_0 = \lambda_c - \lambda_v)$. Compared to silicone (Tabert, Carbotte et al. 2015), whose energy gap will decrease to 0 when the electric field energy increases from 0 to the size of spin splitting, and whose band gap will increase as the electric field energy increases (the larger the size of spin splitting, the higher the electric field energy),This result is different for monolayer WS_2. Spin splitting energy is independent of the external electric field in the absence of an external field, having values of 0.43 eV in the valance band and zero in conduction band. These results are in consistence with Do Muoi research (Muoi, Hieu et al. 2020).

It is evident that a monolayer material's band gap can be greatly impacted by the application of an additional electric field, which can change the material's electrical characteristics. The band gap may change as a result of the Stark effect, a phenomenon brought on by the introduction of an electric field. This may cause the valence and conduction bands to shift, so changing the energy differential between them. Generally, the way the band structure of the monolayer interacts with the electric field can have a significant impact on how it is used in devices, especially in areas like photonics, optoelectronics, and nanoelectronics.

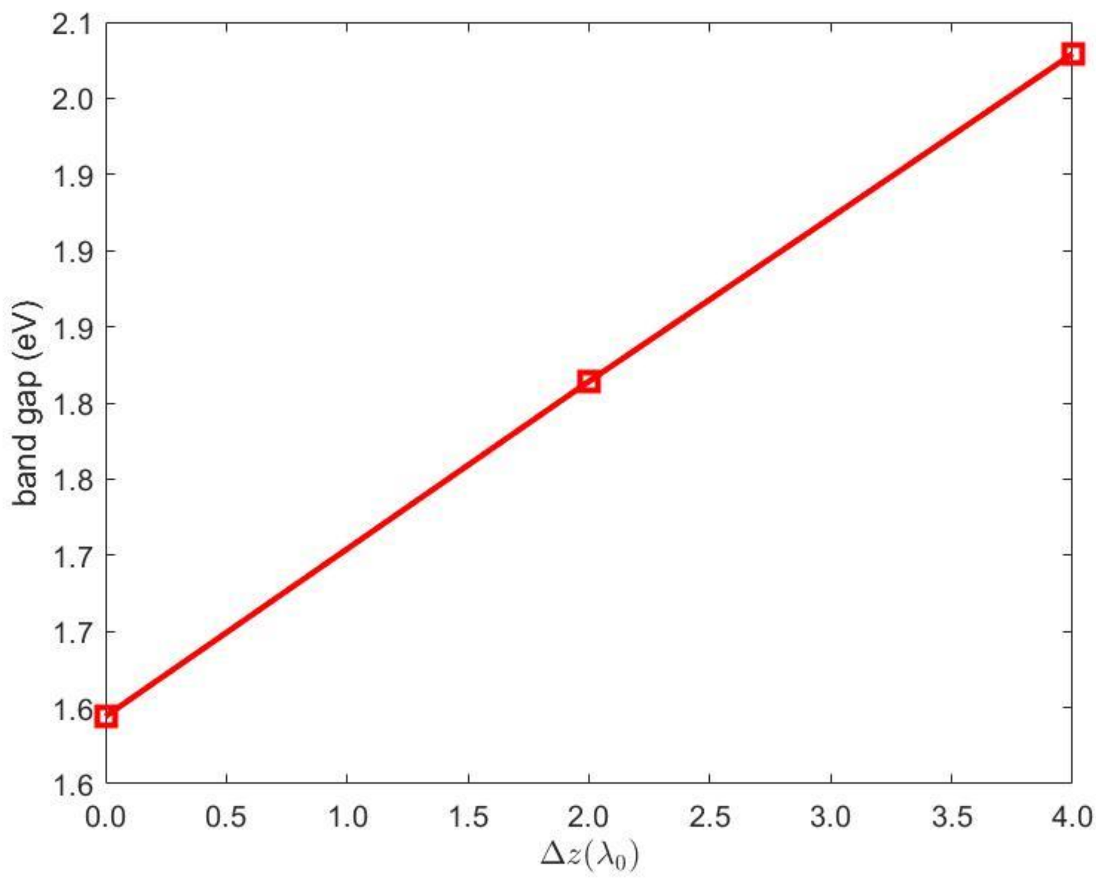

Fig.4.3: Dependence of the band gap on the energy of electric field.

The dependency of the monolayer WS_2's Landau levels on magnetic field B is given by Equation (2.12). The energy $E_n^{s\eta,\gamma}$ is evidently proportional to B Compared to silicene, where the energy is proportional to $\sqrt{B}$, this result for the monolayer WS_2 is different (Tabert, Carbotte et al. 2015). Figures 4 and 5 display the monolayer WS_2's Landau levels in the magnetic field for conduction band for the case $M_z = M_v = 0$.

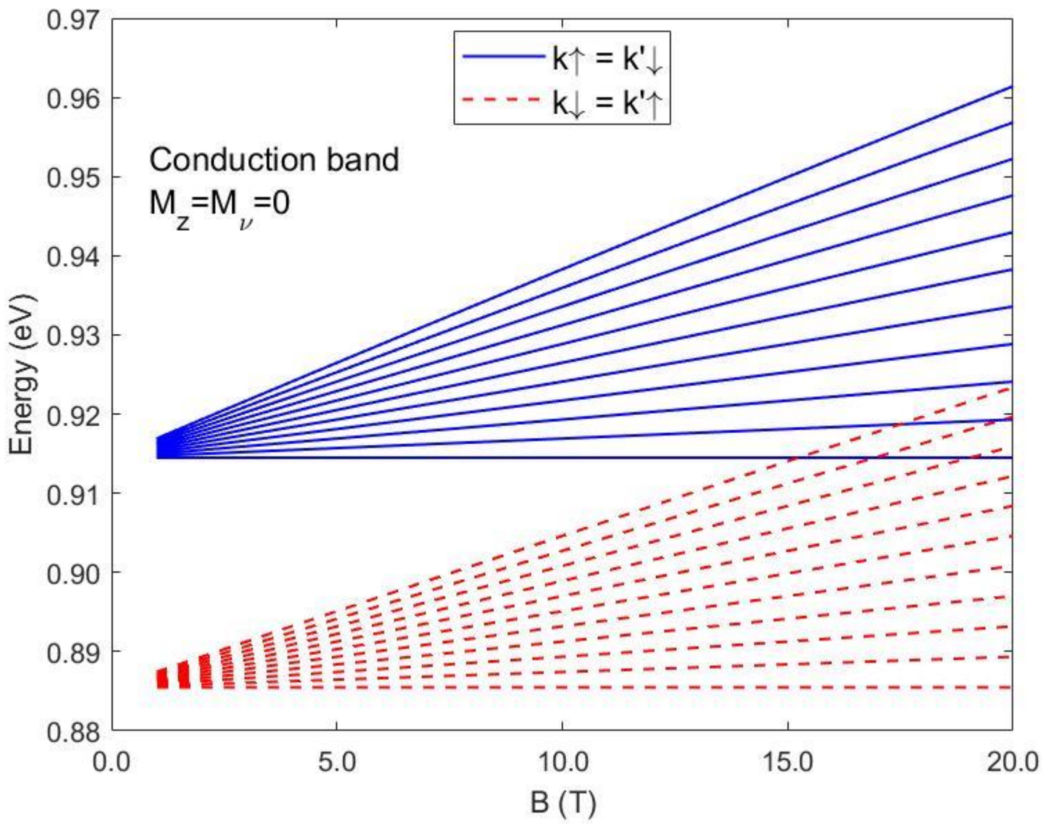

Fig.4.4: The band structure of WS_2 monolayer for conduction band of K valley and K′ valley when $M_z = M_v = 0$.

As seen in Fig.4.4 and Fig.4.5, the bands of the monolayer WS_2 are relatively simple when $M_z = M_v = 0.$, while the bands in the K′ valley with spin down (up) match with the bands in the K valley with spin up (down).

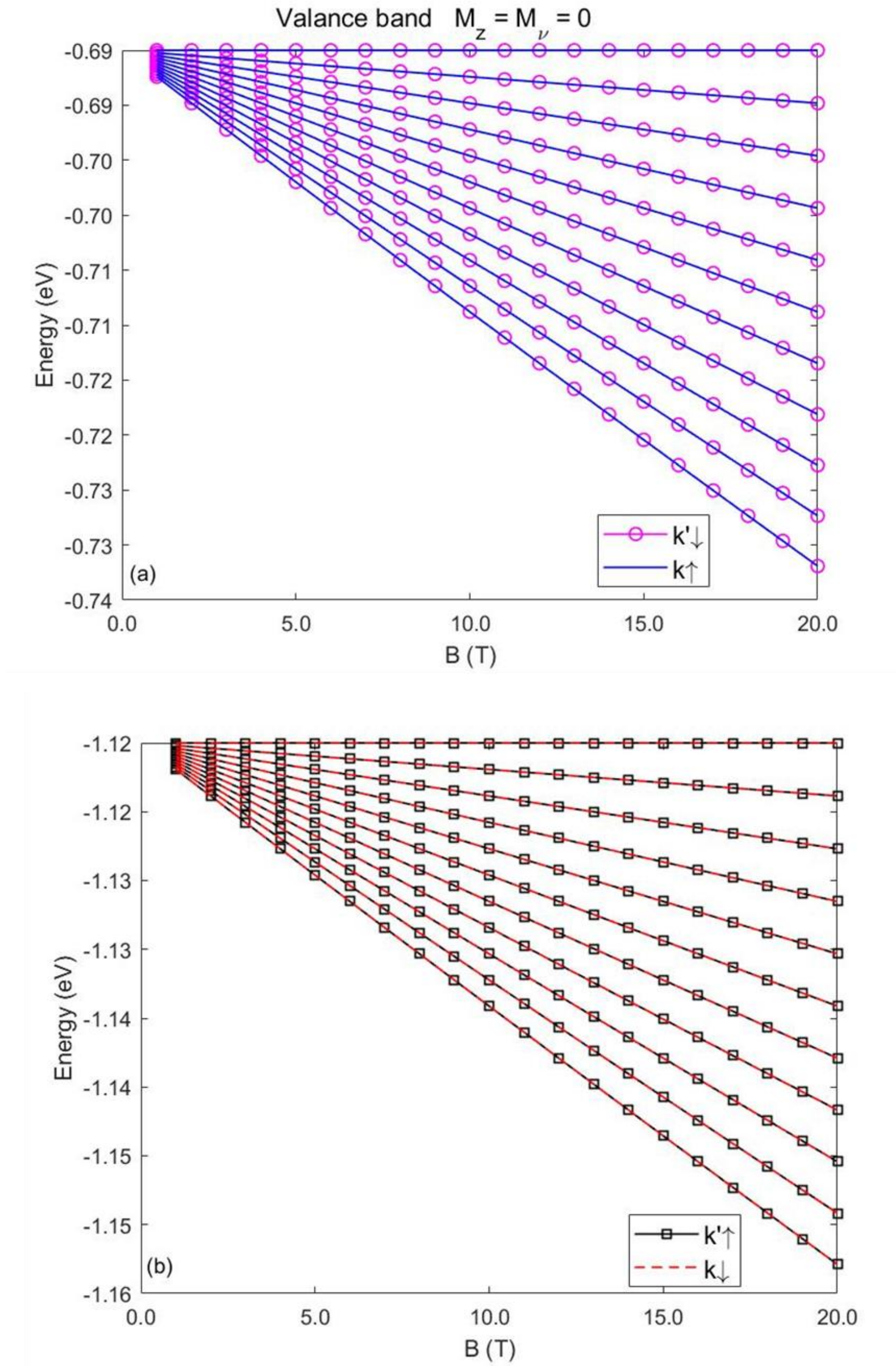

Fig.4.5: The band structure of WS_2 monolayer for valance band of K valley and K′ valley when $M_z = M_v = 0$.

On the other hand, as Fig.4.6 and 3.7 illustrate, in the situation of $M_z = M_\nu \neq 0.$, the band structure is substantially dependent on the spin configurations. For instance, in the figures, it can be observed that, in the case of spin down, energy is rapidly decreased when the magnetic field increases, whereas for the spin up electrons, this reduction is slower. This occurs at the K valley in the conduction band with the Landau level n = 0. In the presence of a magnetic field, this causes a change in the spin splitting energy in the conduction band.

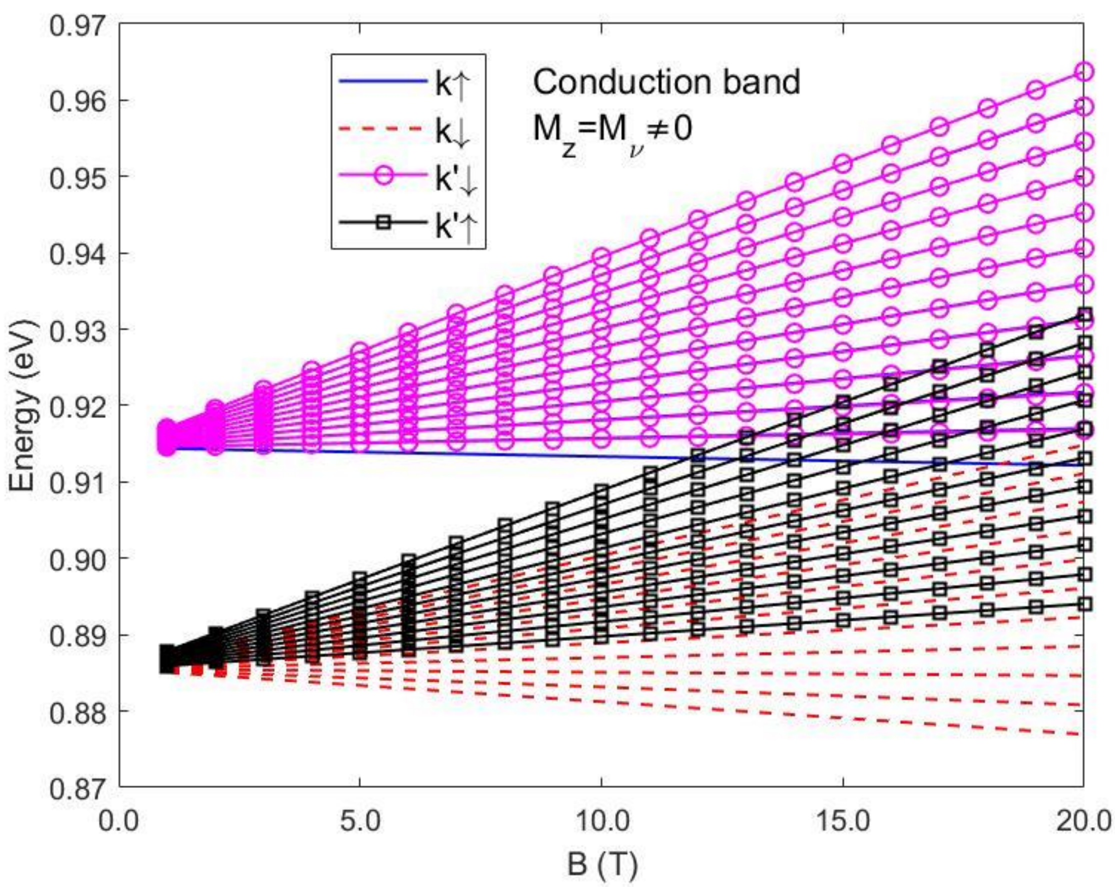

Fig.4.6: The band structure of WS_2 monolayer for conduction band of K valley and K′ valley when $M_z = M_\nu \neq 0$

In the case of $M_z = M_\nu \neq 0$, the splitting energy has been significantly changed by applying the magnetic field. The Figures illustrate how the spin splitting energy at the monolayer WS_2's valence and conduction bands varies with the external magnetic field B at various Landau level values when $M_z = M_v \neq 0$. First, by concentrating on Fig.4.6 where an increase in the magnetic field causes a linear rise in the splitting energy at the conduction band. It is evident that splitting energy is dependent on both the Landau level n and the magnetic field. When n > 1, however, the splitting energy in the K and K′ valleys is heavily dependent on the magnetic field. The splitting energy difference between the K and K′ valleys for the same value of n is very substantial for the conduction band.

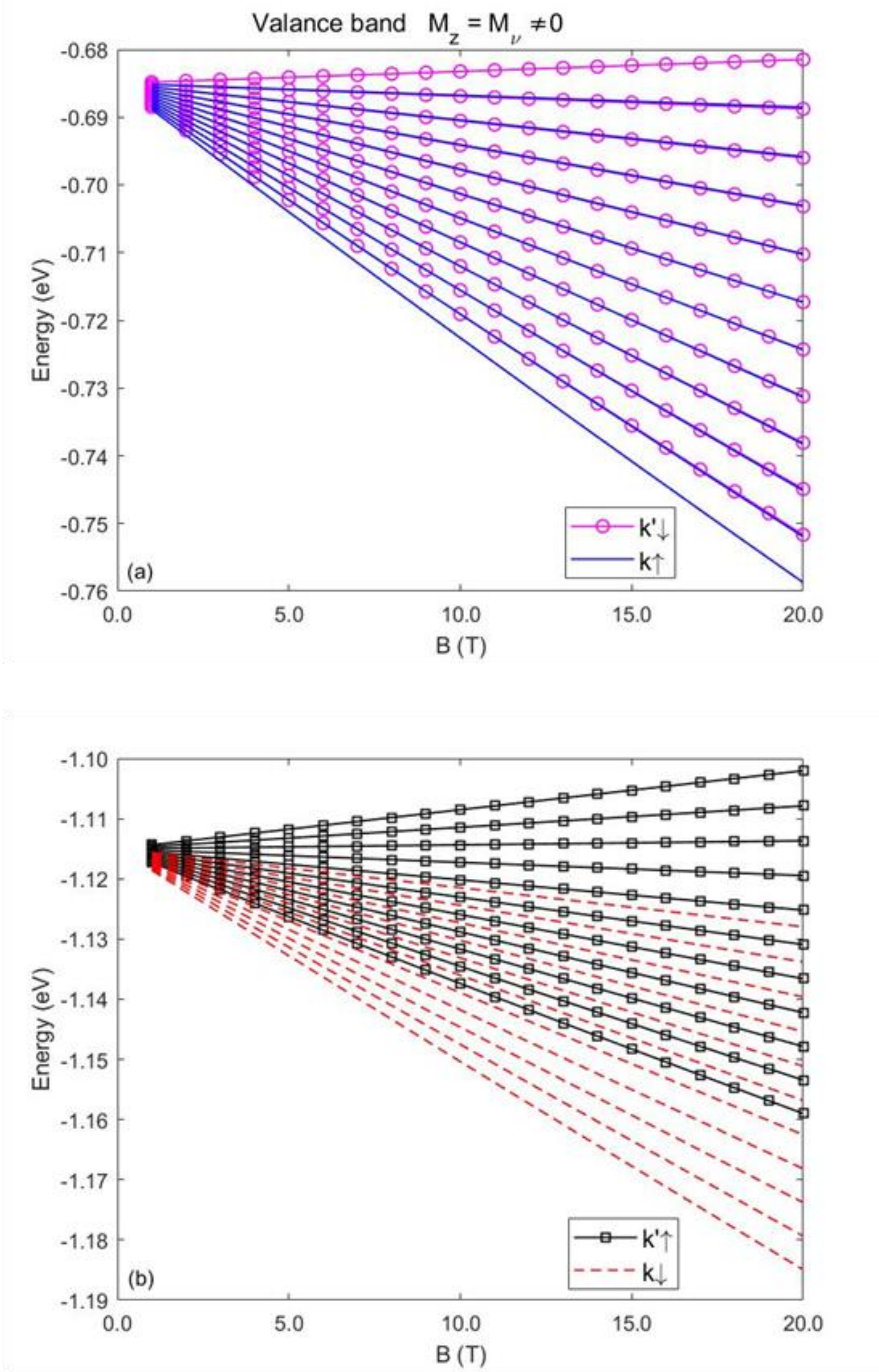

Fig.4.7: The band structure of WS_2 monolayer valance band of K valley and K′ valley when $M_z = M_\nu \neq 0$

As seen in Fig.4.7, the spin splitting energy for the valence band is relatively large. The Landau level n and magnetic field have a significant influence on the spin splitting energy. It's interesting to note that the splitting energy in the valence band for the K valley increases for only the n = 0 case when the magnetic field B was raised, but drops for the $n \geq 1$ case. External magnetic field B lowers the splitting energy in the valence band for the K′ valley.

The density of states tends to decrease with increasing energy, particularly beyond the band boundaries, indicating a decrease in the number of accessible electronic states. Understanding this trend, which affects phenomena like conductivity and optical absorption in monolayer structures, is essential to comprehending the material's electrical characteristics (Li, Tao et al. 2017).

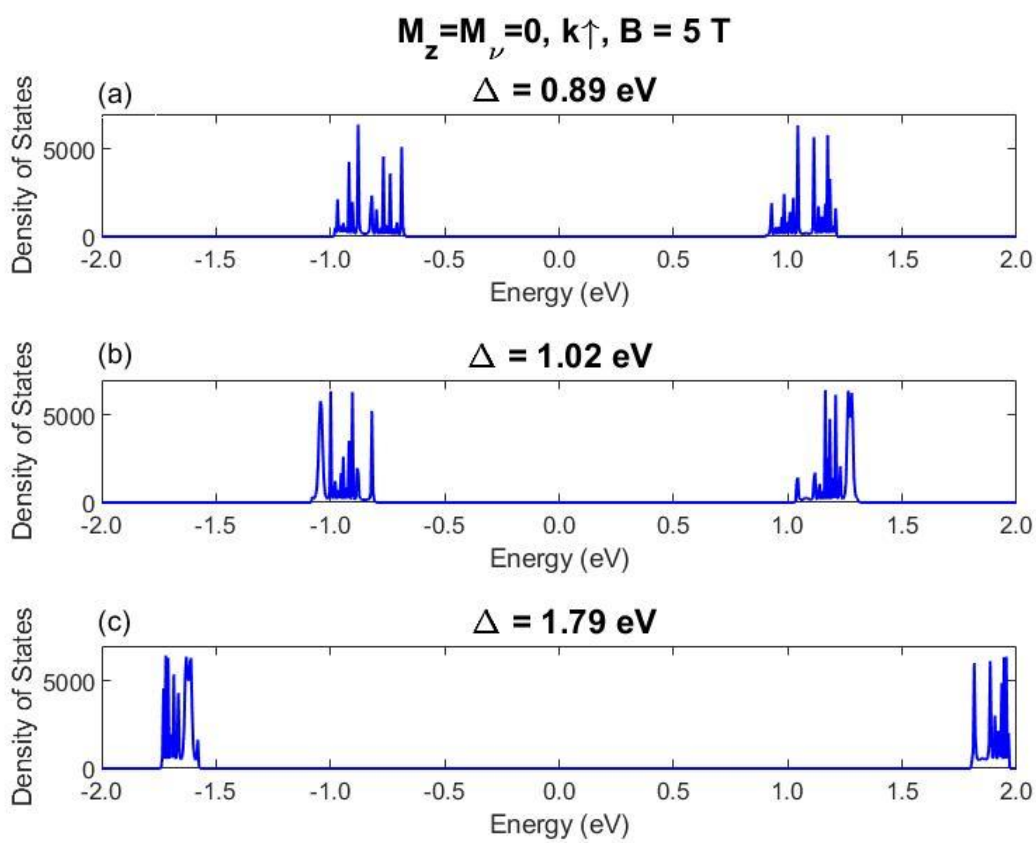

Fig.4.8: The DOS for spin up k valley in the absence of Zeeman term for the three values of Δ at a magnetic strength of 5T.

The density of states (DOS) for spin up k valley in the absence of Zeeman term for the three values of Δ at a magnetic field strength of 5T is plotted in Fig.4.8. As it is seen, by increasing the value of Δ the distance between peaks is increased. As was noted in the first part of this chapter, increasing the electric field led to increasing the energy gap Δ, and thus these results confirm that quantum confinement effects can be produced by the electric field, which can result in discrete energy levels and change the DOS in this structure.

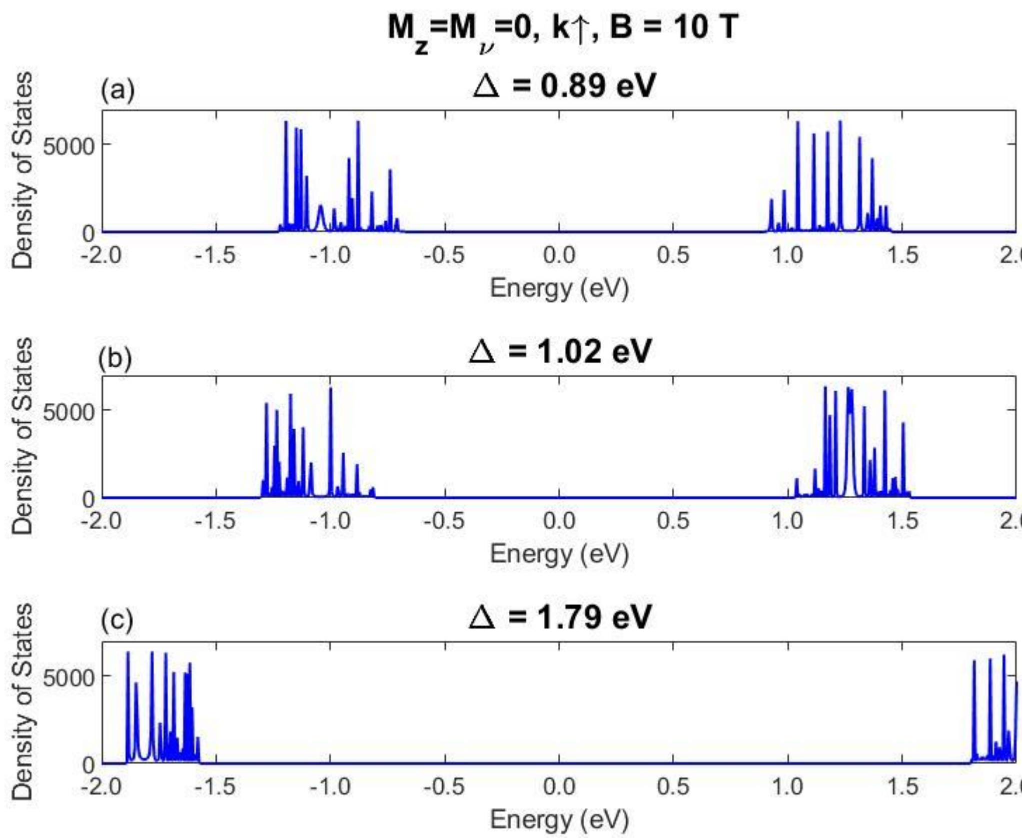

Fig.4.9: The DOS for spin up k valley in the absence of Zeeman term for the three values of Δ at a magnetic strength of 10T.

The effect of increasing the magnetic field strength is studied and plotted in Fig.4.9, which represents the density of states (DOS) for spin up k valley in the absence of Zeeman term for the three values of Δ at a magnetic strength of 10T. As it is expected, the gap between peaks increases by increasing the magnetic field, thus, the magnetic field alters the shape of the density of states by shifting the peaks toward higher energy. Also, by increasing the magnetic field strength, the peaks were split and more peaks were formed. Moreover, with high strengths of magnetic field the DOS reflects an oscillatory behavior (Nasir, Khan et al. 2009).

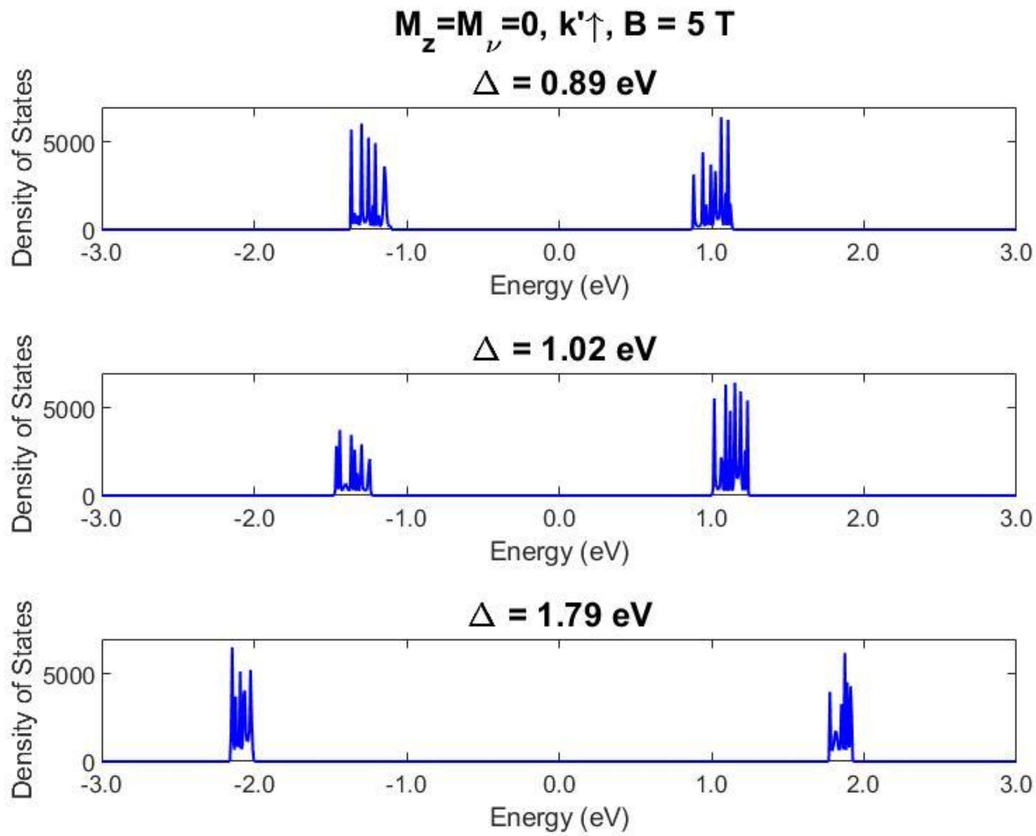

Fig.4.10: The DOS for spin up K′ valley in the absence of Zeeman term for the three values of Δ at a magnetic strength of 5T.

Same procedures were done on the K′ valley, The density of states (DOS) for spin up K′ valley in the absence of Zeeman term for the three values of Δ at a magnetic strength of 5T is plotted in Fig.4.10. the gap between peaks also increased by increases the Δ values through increasing the applied electric field. According to the positive part of energy axis, the peaks of K′ valley have the same position as the K valley with more splitting peaks.

Whereas, for the negative part of energy axis, the peaks of K′ valley were shifted toward more negative energy compared with peaks of K valley.

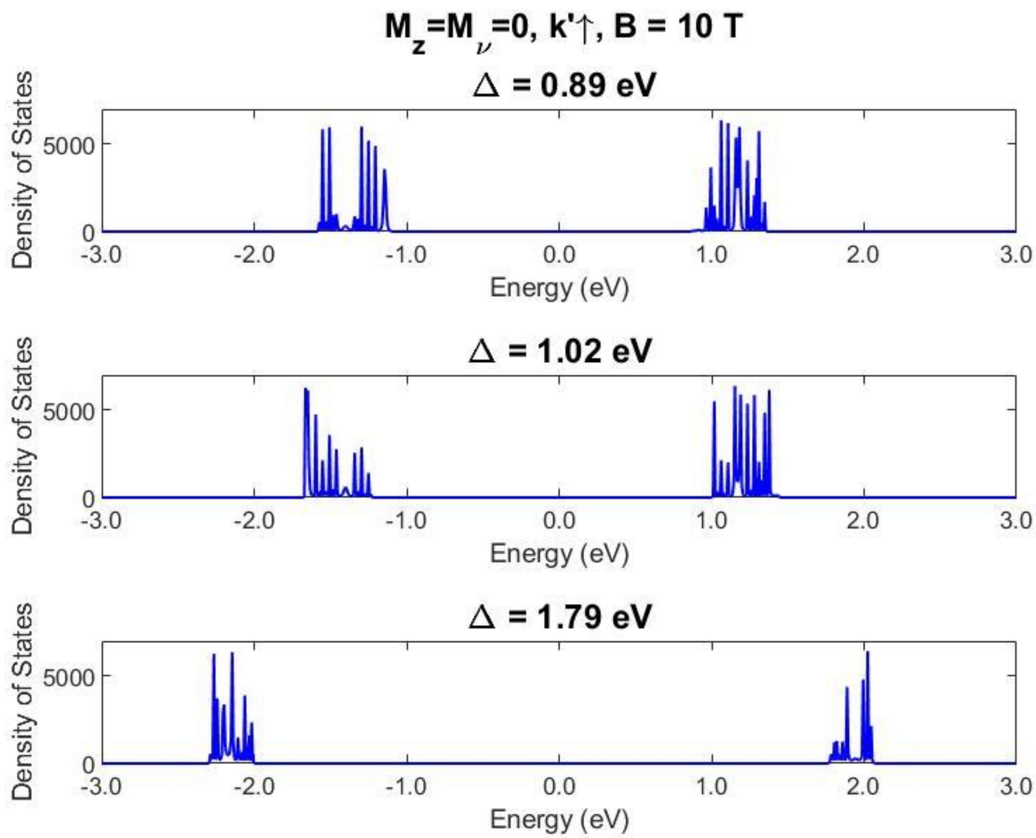

Fig.4.11: The DOS for spin up K′ valley in the absence of Zeeman term for the three values of Δ at a magnetic strength of 10T.

The DOS for spin up K′ valley in the absence of Zeeman term for the three values of Δ at a magnetic strength of 10T is shown in Fig.4.11. Higher magnetic field strength causes a more splitting of the DOS peaks of K′ valley.

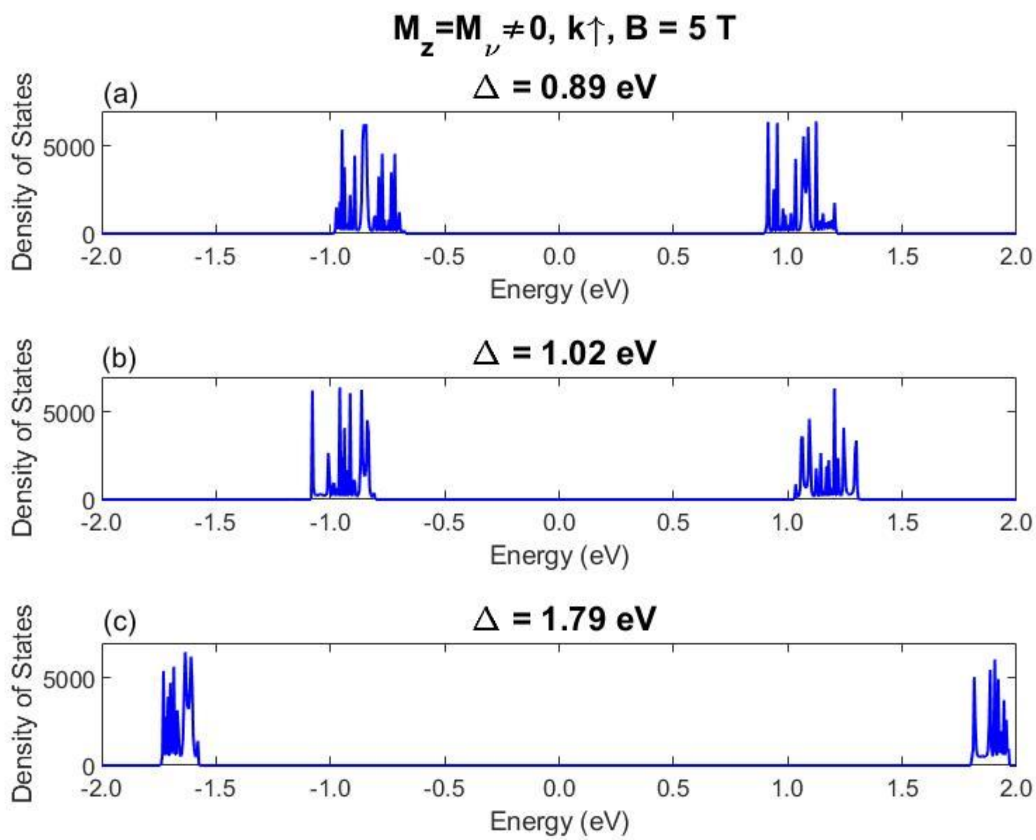

Fig.4.12: The DOS for spin up K valley when $M_z = M_\nu \neq 0$ for the three values of Δ at a magnetic strength of 5T.

Now, the effect of Zeeman term on the electronic structure of WS_2 monolayer will be studied. The DOS for spin up K valley when $M_z = M_\nu \neq 0$ for the three values of Δ at a magnetic strength of 5T is plotted in Fig.4.12. As it is shown, The original degenerate energy levels split into several levels corresponding to distinct spin states as a result of the Zeeman effect.

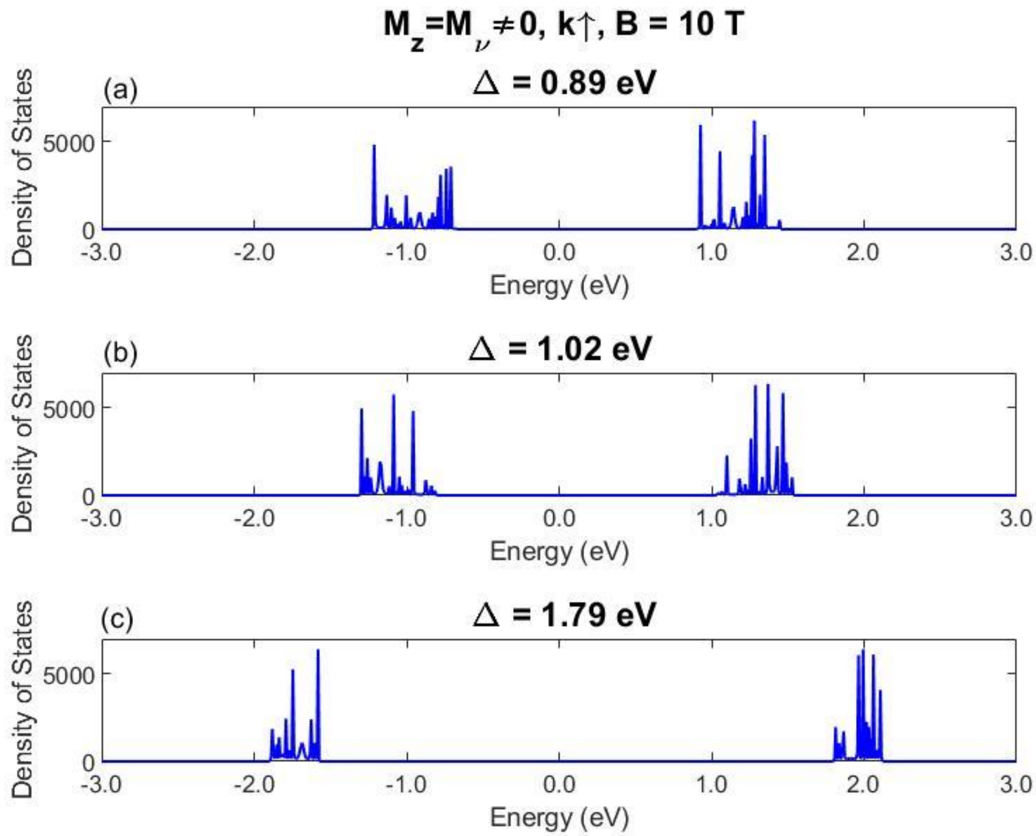

Fig.4.13: The DOS for spin up K valley when $M_z = M_\nu \neq 0$ for the three values of Δ at a magnetic strength of 10T.

The density of states for spin up K valley when $M_z = M_\nu \neq 0$ for the three values of Δ at a magnetic strength of 10T is plotted in Fig13. Higher magnetic field strength causes a more splitting of the energy levels.

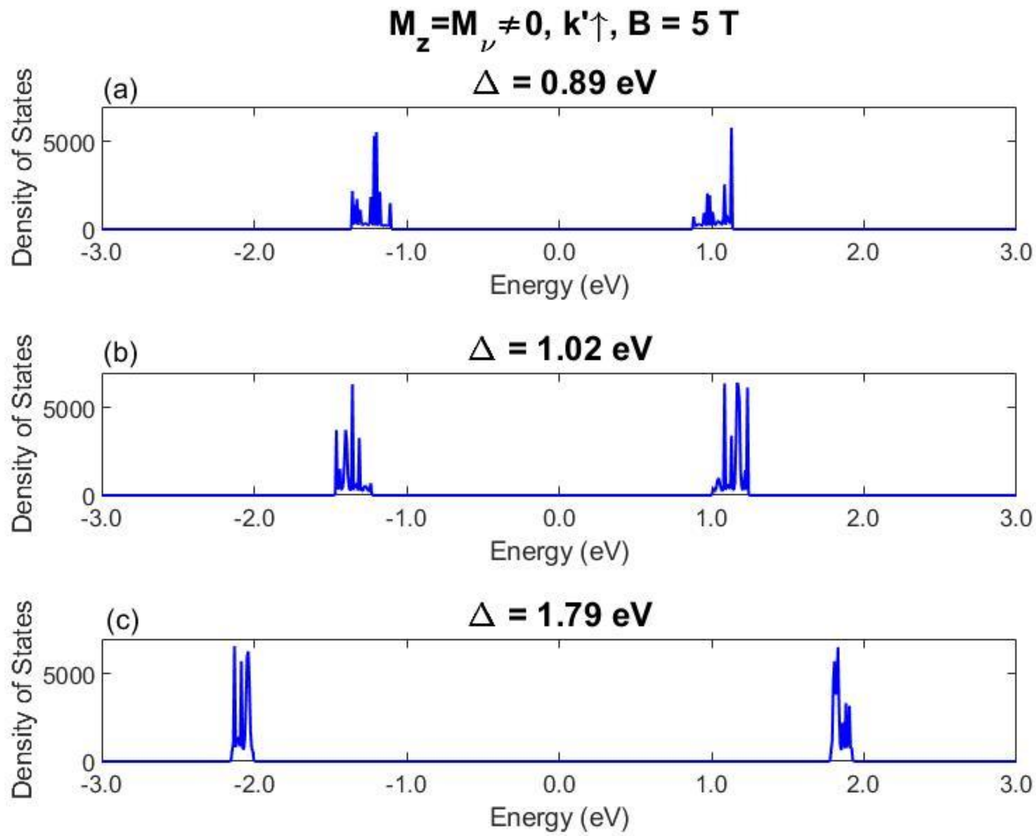

Fig.4.14: The DOS for spin up K′ valley when $M_z = M_\nu \neq 0$ for the three values of Δ at a magnetic strength of 5T.

The DOS of spin up K′ valley when $M_z = M_\nu \neq 0$ for the three values of Δ at a magnetic strength of 5T is shown in Fig.4.14. As it is seen, the Zeeman term affects the DOS spectrum by showing more spin splitting energy levels.

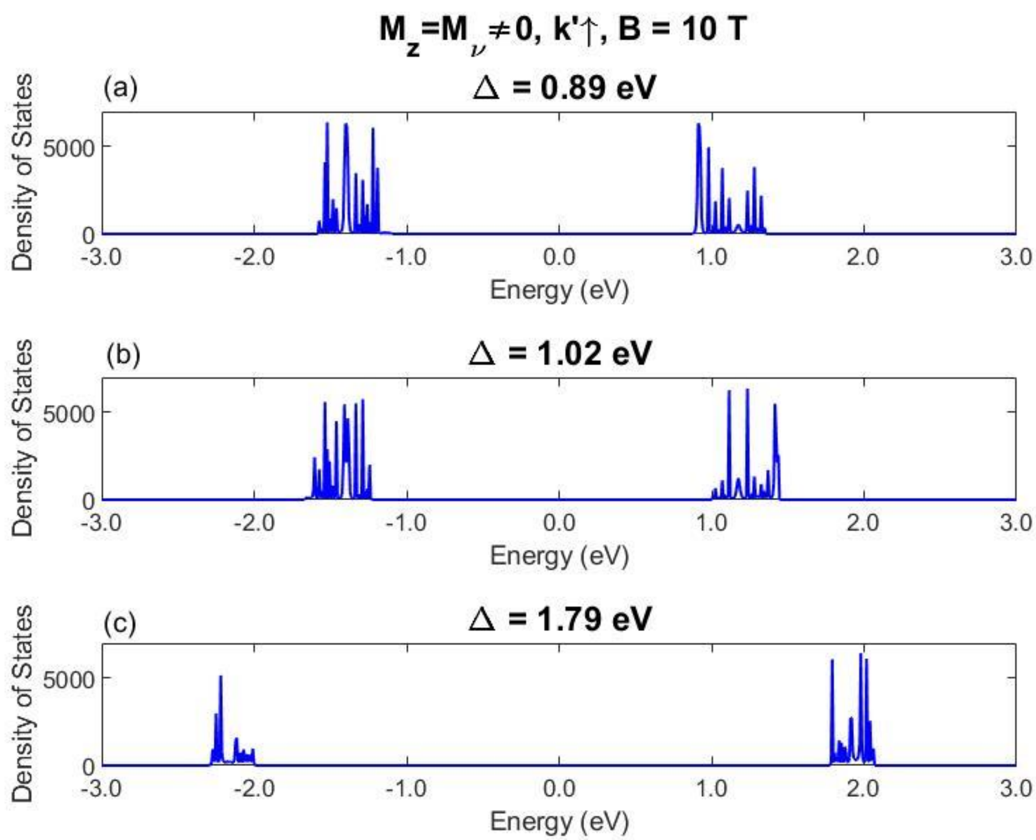

Fig.4.15: The DOS for spin up K′ valley when $M_z = M_\nu \neq 0$ for the three values of Δ at a magnetic strength of 10T.

The density of states for spin up K′ valley when $\mathrm{M_z} = \mathrm{M_\nu} \neq 0$ for the three values of Δ at amagnetic strength of 10T. As it is seen, at higher magnetic field strength and a large band gap the density of the peaks on the density of states decreases.

Fig.4.16 is focusing on the positive part of energy axis of the density of states for k valley at 10T when a) $M_z = M_\nu = 0$ and b) $M_z = M_\nu \neq 0$. As it is seen, Zeeman term affects the oscillatory behavior of the density of states spectrum.

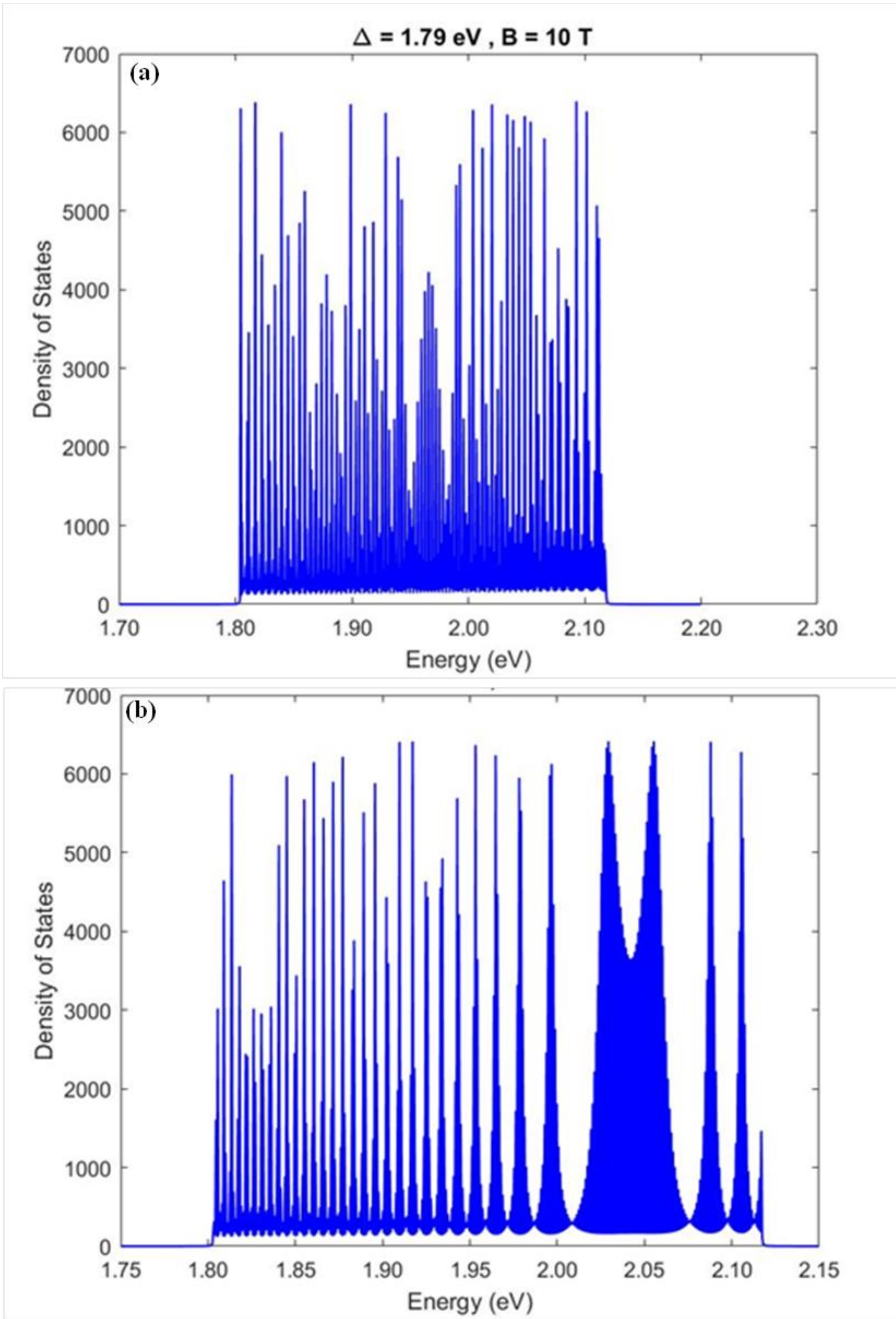

Fig.4.16: The positive part of energy axis of the density of states for k valley at 10T when a) $M_z = M_\nu = 0$ and b) $M_z = M_\nu \neq 0$.

To Investigate more about the electronic structure of WS_2 monolayer, the Fermi level for the WS_2 TMD monolayer versus the strength of magnetic field will be discussed at different temperatures and concentrations.

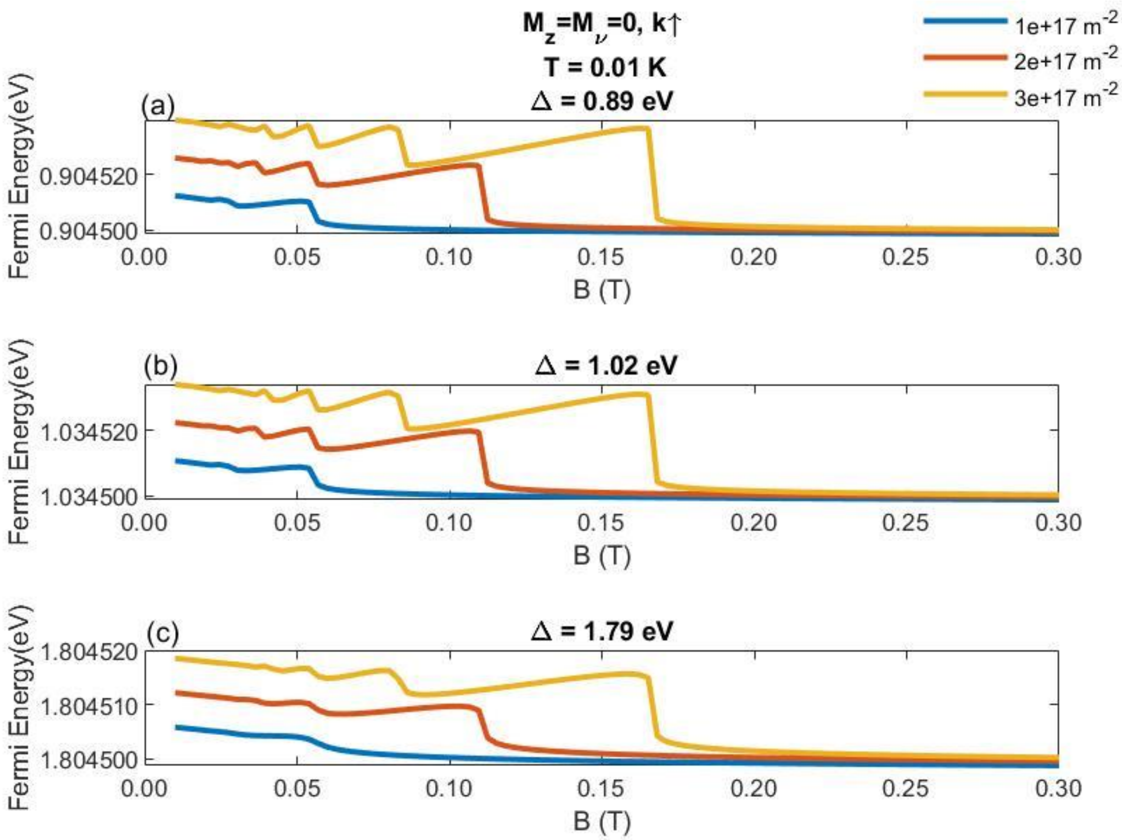

Fig.4.17: Fermi energy for K valley of WS_2 monolayer versus strength of magnetic field when $M_z = M_\nu = 0$ for the three values of Δ and three different concentration at 0.01 K.

Fermi energy versus magnetic field strength shows how the Fermi level energy alter in response to varying the magnetic field strength. Fermi energy for K valley of WS_2 monolayer versus strength of magnetic field when $M_z = M_\nu = 0$ for the three values of Δ and three different concentration at 0.01 K is shown in Fig.4.17. As it is shown, Fermi energy slightly increases as the concentration of electrons increases. Also, an oscillation of Fermi energy is appeared below 0.2T for the three values of Δ. Moreover, the magnitude of Fermi energy increased when the value of the band gap is increased.

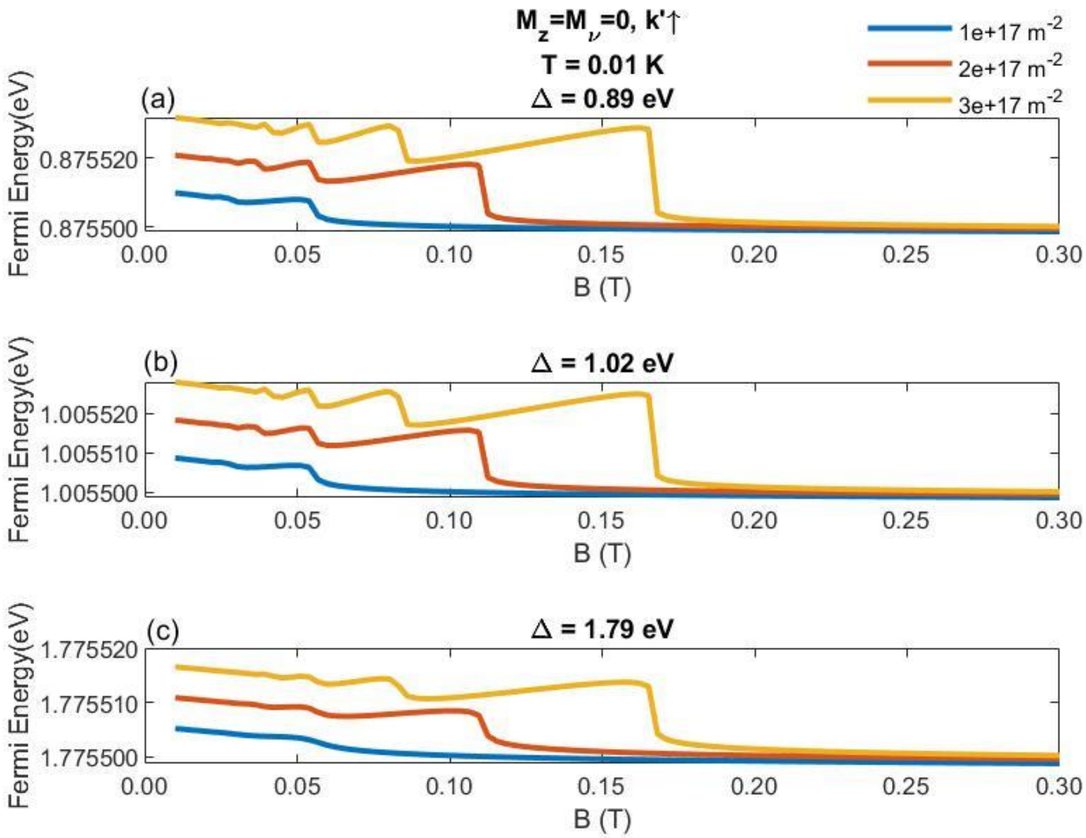

Fig.4.18: Fermi energy for K′ valley of WS_2 monolayer versus strength of magnetic field when $M_z = M_\nu = 0$ for the three values of Δ and three different concentration at 0.01 K.

The Fermi energy for K′ valley of WS_2 monolayer versus strength of magnetic field when $M_z = M_\nu = 0$ for the three values of Δ and three different concentration at 0.01 K is investigated in Fig.4.18. From the figure the same results were extracted, that is, increasing the electron concentration leads to slightly increasing of the value of Fermi energy. In addition, by increasing the value of band gap using an applied electric field will increase the value of Fermi energy. Moreover, the oscillatory behavior appears below 0.3T. By comparing the Fermi energy between K valley and K′ valley it is shown that Fermi energy acquire higher value in the K valley compared with K′ valley.

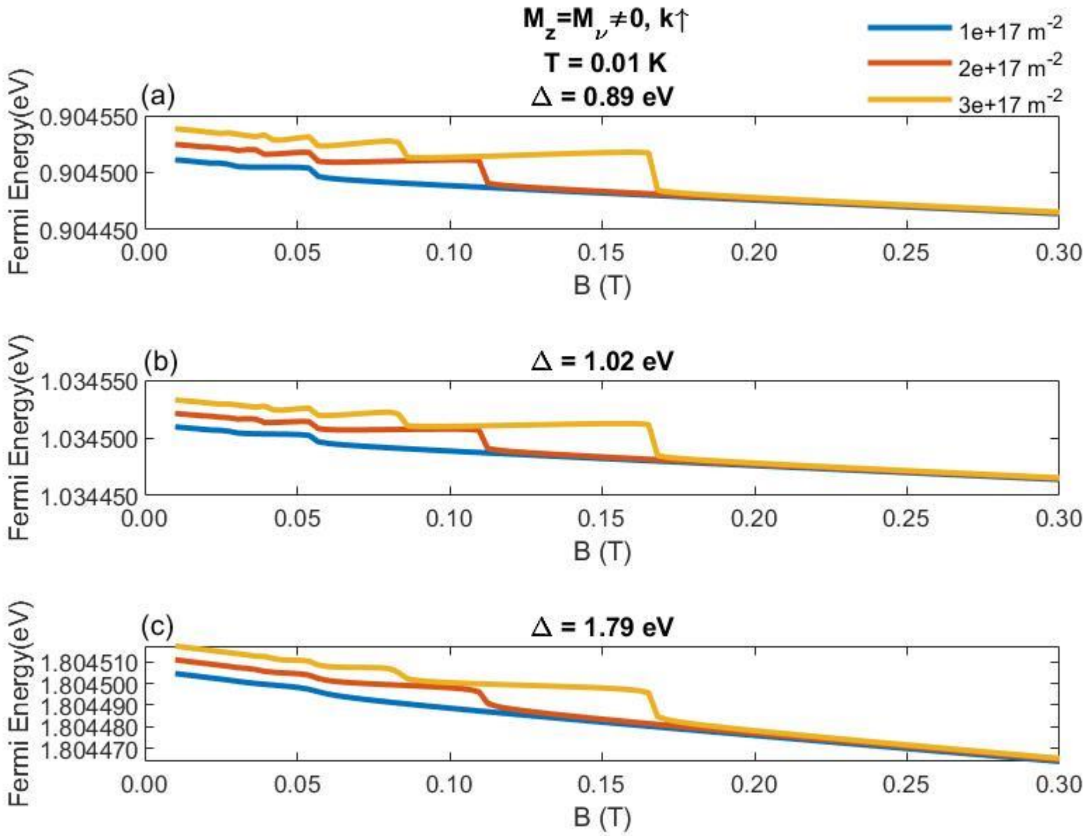

Fig.4.19: Fermi energy for K valley of WS_2 monolayer versus strength of magnetic field when $M_z = M_\nu \neq 0$ for the three values of Δ and three different concentration at 0.01 K.

The Fermi energy for K valley of WS_2 monolayer versus strength of magnetic field when $M_z = M_\nu \neq 0$ for the three values of Δ and three different concentration at 0.01 K is plotted in Fig.4.19. At this temperature the effect of Zeeman term is shown, the value of Fermi energy is slightly shifted toward higher energy. In addition, by adding Zeeman term the oscillatory behavior starts to die at band gap of 1.79 eV.

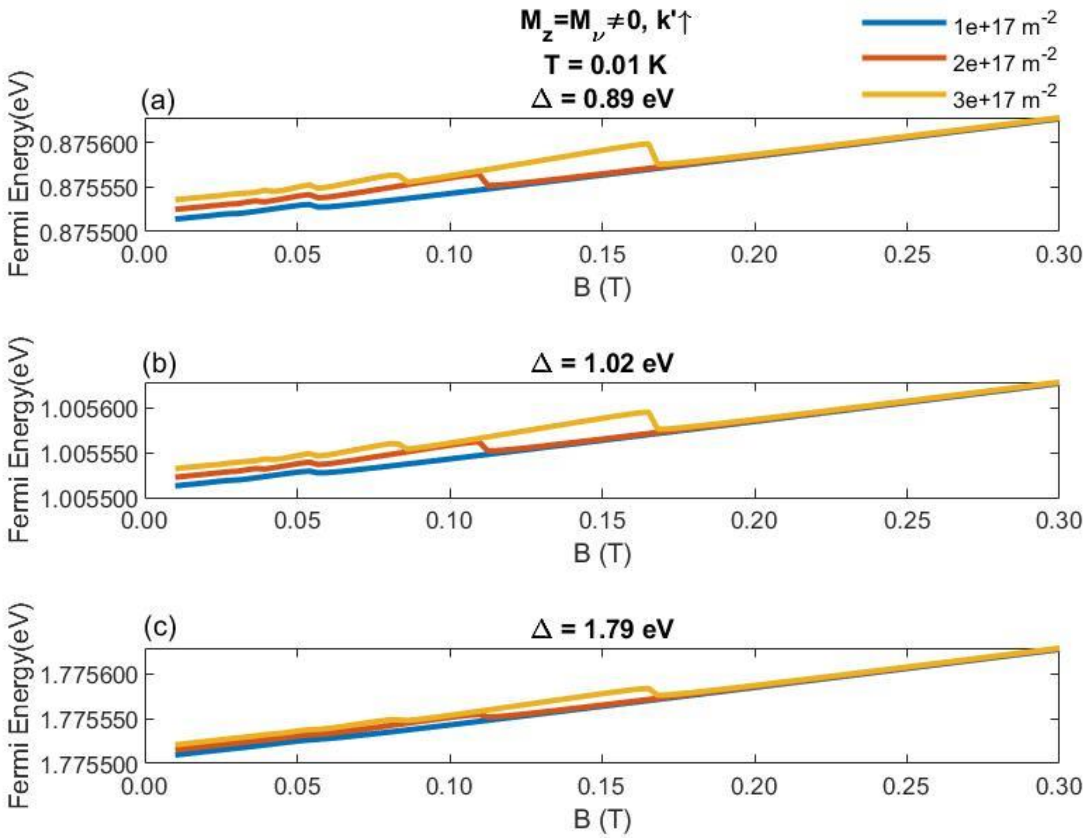

Fig.4.20: Fermi energy for K′ valley of WS_2 monolayer versus strength of magnetic field when $M_z = M_\nu \neq 0$ for the three values of Δ and three different concentration at 0.01 K.

The Fermi energy for K′ valley of WS_2 monolayer versus strength of magnetic field when $M_z = M_\nu \neq 0$ for the three values of Δ and three different concentration at 0.01 K is shown in Fig.4.20. As it is seen when the Zeeman term is added for the K′ valley, the oscillatory behavior will disappear.

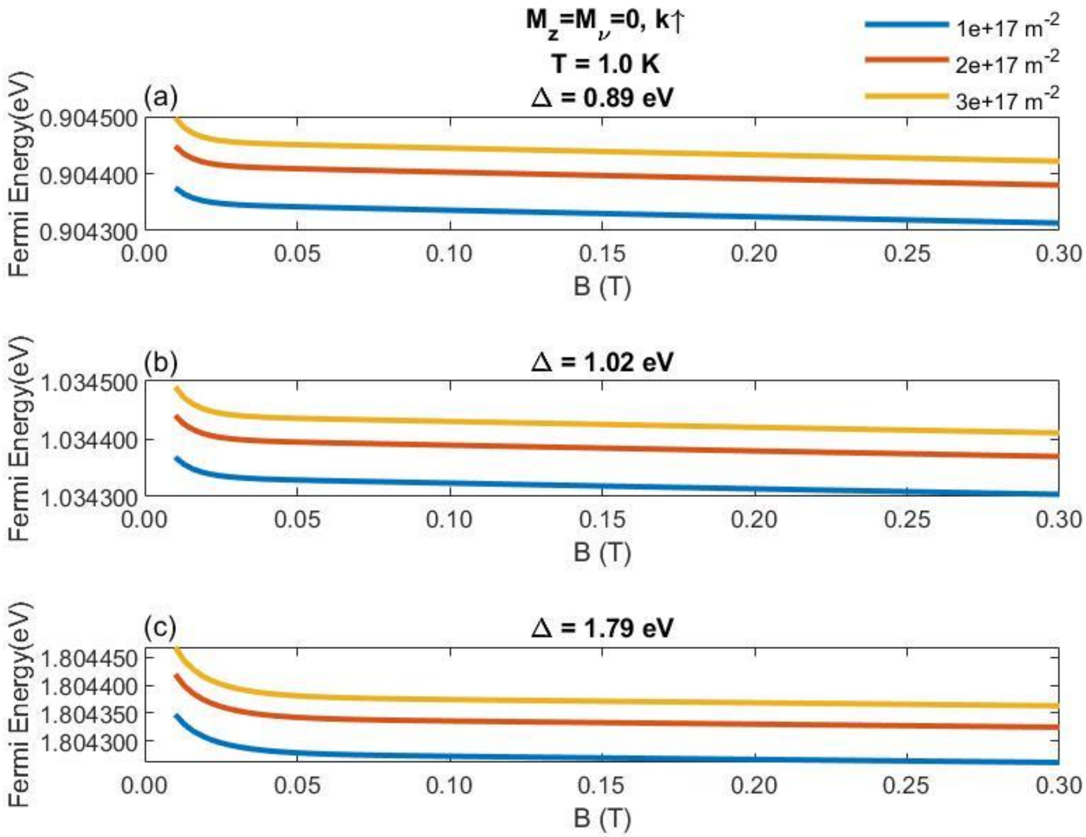

Fig.4.21: Fermi energy for K valley of WS_2 monolayer versus strength of magnetic field when $M_z = M_\nu = 0$ for the three values of Δ and three different concentration at 1.00 K.

At temperature of 1.00K the Fermi energy for K valley of WS_2 monolayer versus the strength of magnetic field when $M_z = M_\nu = 0$ for the three values of Δ and three different concentration was plotted in Fig.4.21. As it is seen the oscillatory behavior disappeared and the Fermi level has constant position equals the given band gap. In addition, increasing the electron concentration shifts the Fermi level toward higher energy.

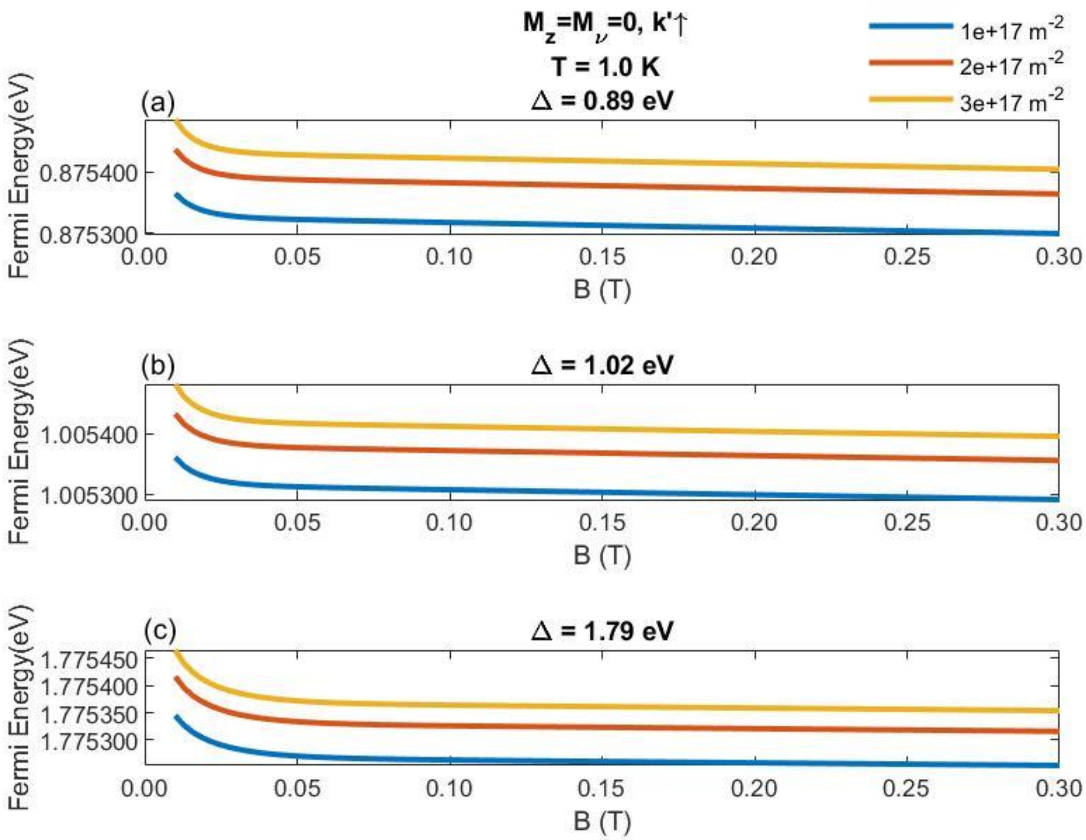

Fig.4.22: Fermi energy for K′ valley of WS_2 monolayer versus strength of magnetic field when $M_z = M_\nu = 0$ for the three values of Δ and three different concentrations at 1.00 K.

At temperature of 1.00K the Fermi energy for K′ valley of WS_2 monolayer versus the strength of magnetic field when $M_z = M_\nu = 0$ for the three values of Δ and three different concentration was plotted in Fig.4.22. Fermi level acquire lower energy value for K′ valley compared with K valley. As for the K valley, the oscillatory behavior disappears at this temperature.

4.3: Thermal Properties

Convergence of the energy function implies that the system reaches a state where the energy is minimized or stabilized, indicating a balanced configuration; this state is often sought after in studies of self-assembly, surface adsorption, or molecular packing, where understanding the energy landscape helps to predict and control the behavior and properties of the monolayer. The convergence of an energy function in the context of a monolayer typically refers to the stability and equilibrium of the system as described by the energy functional (ELSAYED).

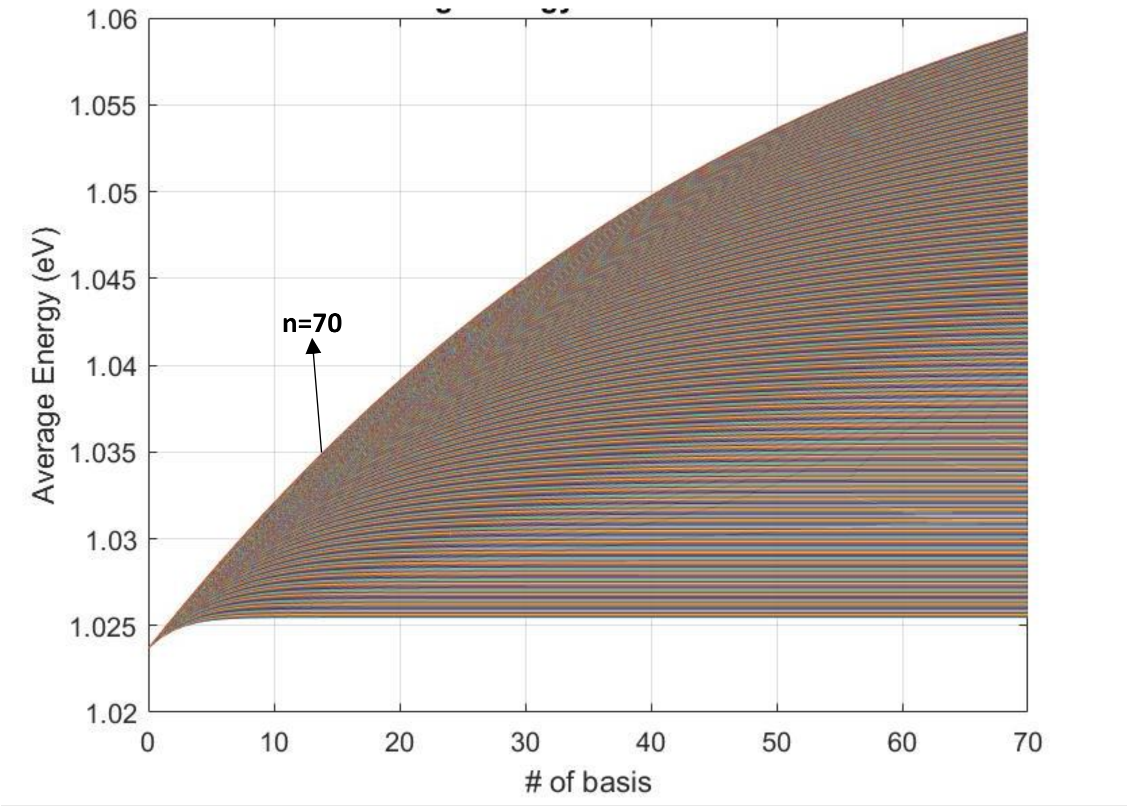

Fig.4.23: Average energy of WS_2 monolayer versus number of basis.

Understanding the monolayer system's structural transitions, functional characteristics, and thermodynamic stability is essential for a variety of applications, including materials science and nanotechnology (Lv, Robinson et al. 2015). This can be achieved by examining the convergence of the energy function. Figure 3.23 illustrates the average energy of the WS_2 monolayer in the presence of magnetic field versus the number of basis. As it is seen from the figure the convergence of average energy function is achieved when the number of basis is around 70.

Statistical mechanics dictates that a monolayer material's average energy changes with temperature. Higher temperatures result in a rise in thermal energy and kinetic energy for the atoms and electrons in the monolayer (Peng, Zhang et al. 2016). The distribution of this thermal energy among the electronic states and vibrational modes of the material raises the system's average energy. On the other hand, as temperatures drop, thermal excitations lose their significance and the average energy drops as well (Lubchenko and Wolynes 2003). Phase transitions, thermal conductivity, and the material's reaction to external stimuli are just a few of the phenomena that are influenced by the relationship between average energy and temperature in a given set of conditions (Peng, Zhang et al. 2016) (Lubchenko and Wolynes 2003).

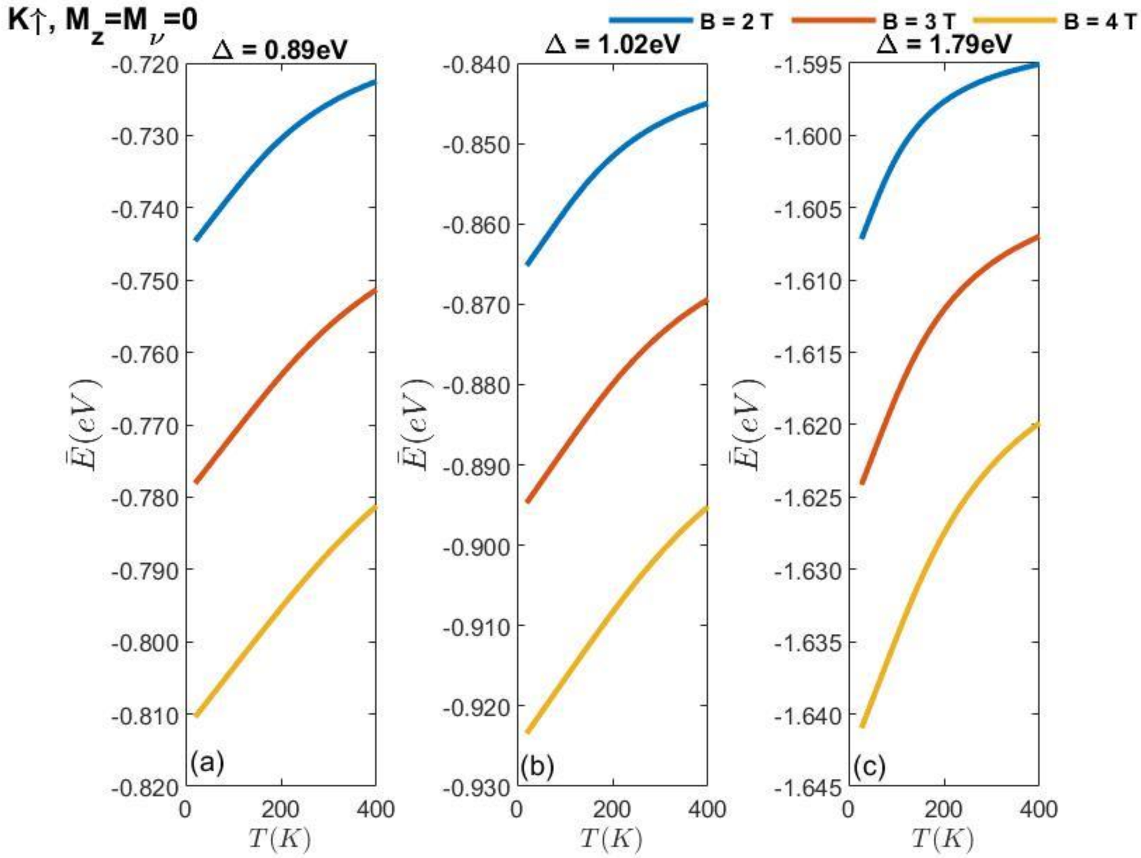

Fig.4.24: Average energy for the K valley of WS_2 monolayer versus temperature at three strengths of magnetic field and for three values of band gaps when $M_z = M_\nu = 0$.

The average energy of spin up K valley of WS_2 monolayer versus temperature at three strengths of magnetic field and for three values of band gaps when $M_z = M_\nu = 0$ was investigated and plotted in Fig.4.24. As it is shown, the average energy increases with rising temperature and then starts to stabilize. Moreover, increasing the magnetic field causes the average energy to decrease, exhibiting the same trend. In addition, the value of average energy can be increased by increasing the value of band gap. That because the valence band and conduction band are farther apart when the band gap is greater. This will have an impact on the overall energy distribution of charge carriers because the average energy of the electrons in the conduction band will be higher than that of the electrons in the valence band.

There exist multiple impacts of increasing the magnetic field strength on the average energy of a monolayer material. First, the Zeeman effect allows for the splitting of spin state energy levels upon the introduction of a magnetic field. The average energy of spin-polarized states increases as a result, particularly in materials with strong spin-orbit coupling. Landau levels can also occur for two-dimensional materials under intense magnetic fields. The average energy of the carriers in the monolayer is impacted by this quantization of energy levels, which can also change the density of states.

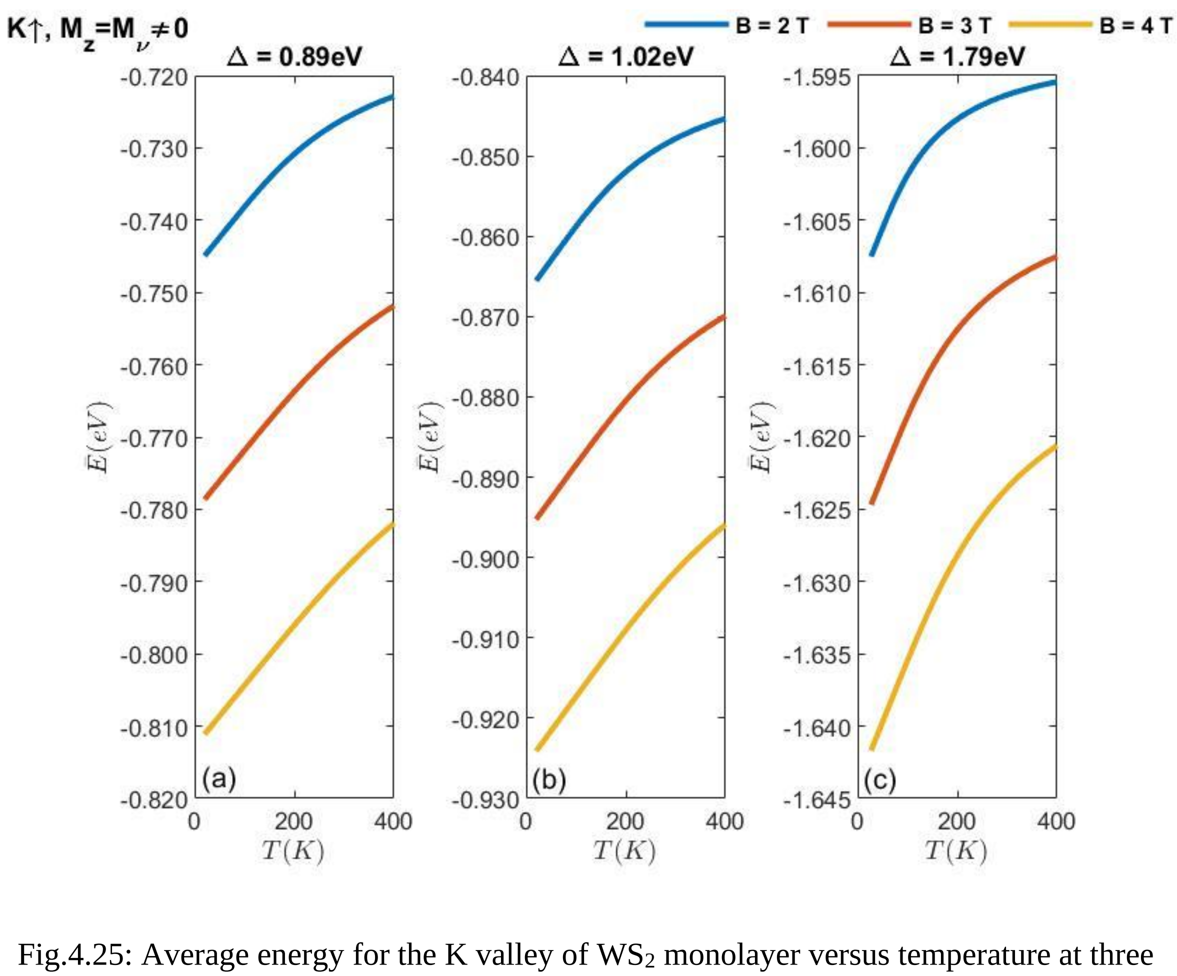

Fig.4.25: Average energy for the K valley of WS_2 monolayer versus temperature at three strengths of magnetic field and for three values of band gaps when $M_z = M_\nu \neq 0$.

When $M_z = M_\nu \neq 0$, the average energy for the K valley of WS_2 monolayer versus temperature at three strengths of magnetic field and for three values of band gaps is investigated in Fig.4.25. Same behavior of the previous figure is obtained. Also, Zeeman term is found to increase the average energy with small amount.

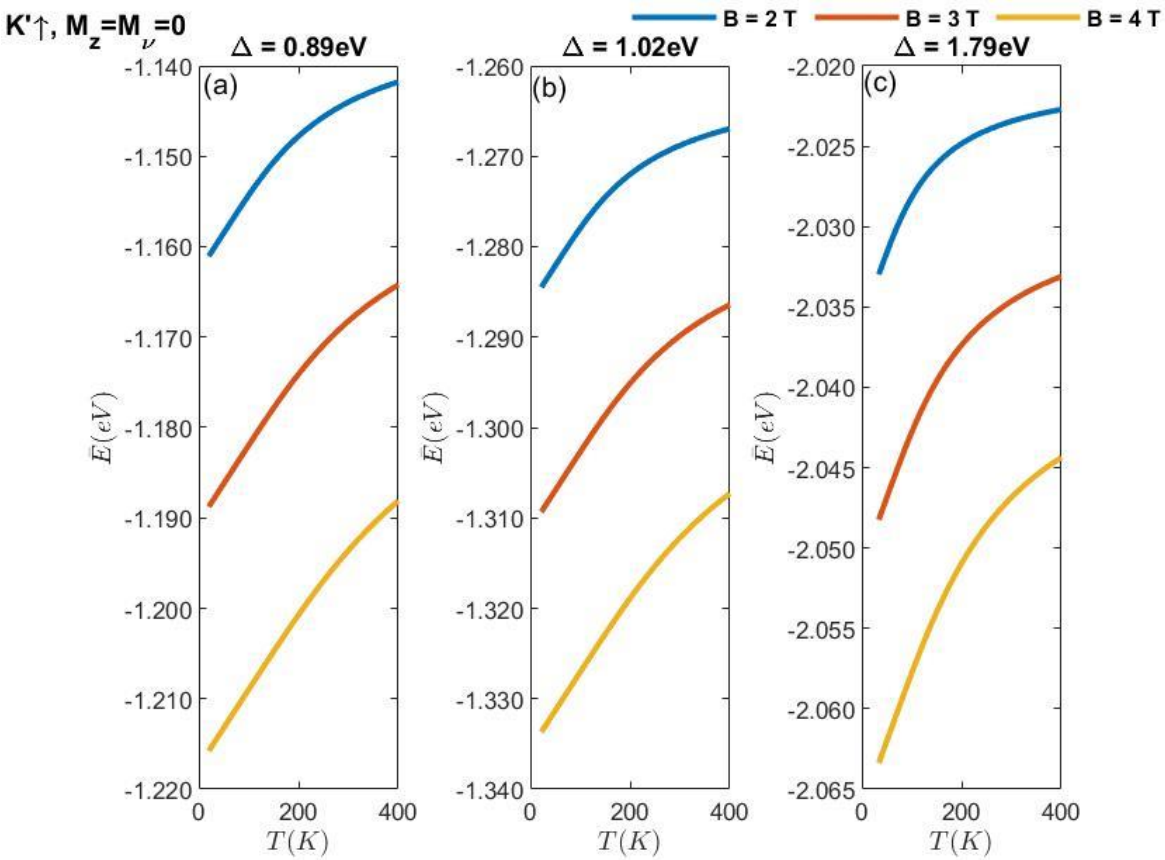

Fig.4.26: Average energy for the K′ valley of WS_2 monolayer versus temperature at three strengths of magnetic field and for three values of band gaps when $M_z = M_\nu = 0$.

The average energy for the K′ valley of WS_2 monolayer versus temperature at three strengths of magnetic field and for three values of band gaps when $M_z = M_\nu = 0$ is investigated in Fig.4.26. As it is seen, the average energy increases by increasing the value of band gap. In addition, increasing the strength of the magnetic field leads to have more negative of the average energy.

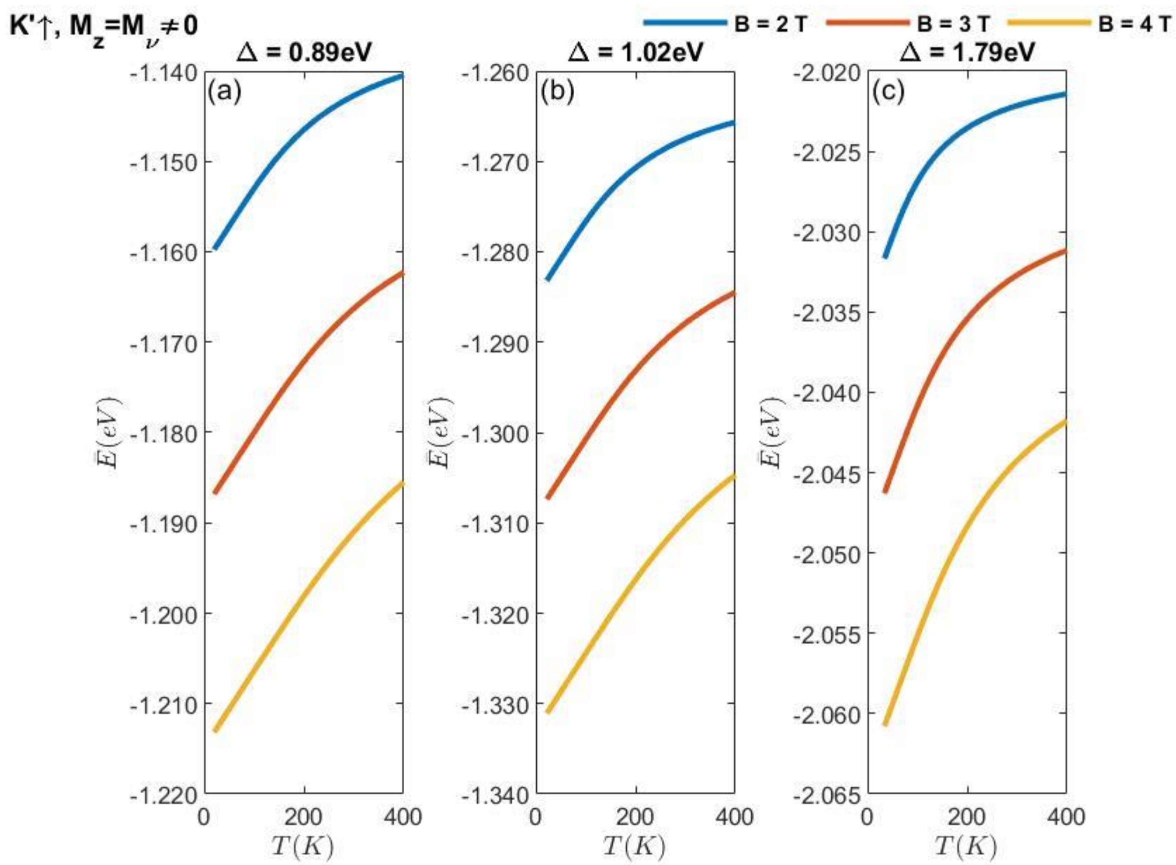

Fig.4.27: Average energy for the K′ valley of WS_2 monolayer versus temperature at three strengths of magnetic field and for three values of band gaps when $M_z = M_\nu \neq 0$.

When $M_z = M_\nu \neq 0$, the average energy for the K' valley of WS_2 monolayer versus temperature at three strengths of magnetic field and for three values of band gaps is investigated in Fig.4.27. it is shown that by adding the Zeeman term to the energy function, the average energy will increase by small quantity.

The quantity of heat needed to alter a monolayer's temperature per unit mass when it is in the presence of a magnetic field is known as the monolayer's specific heat capacity (Kosterlitz and Thouless 1978, Elsaid, Abdelkareem et al. 2021). Magnetic fields in such systems can significantly affect the energy levels and interactions of the constituents of the monolayer, changing their thermal behavior (Gibertini, Koperski et al. 2019). The monolayer's specific heat capacity, which reflects its capability to retain or release heat as temperature varies, describes how it reacts to thermal energy inputs (Li, Tian et al. 2020).

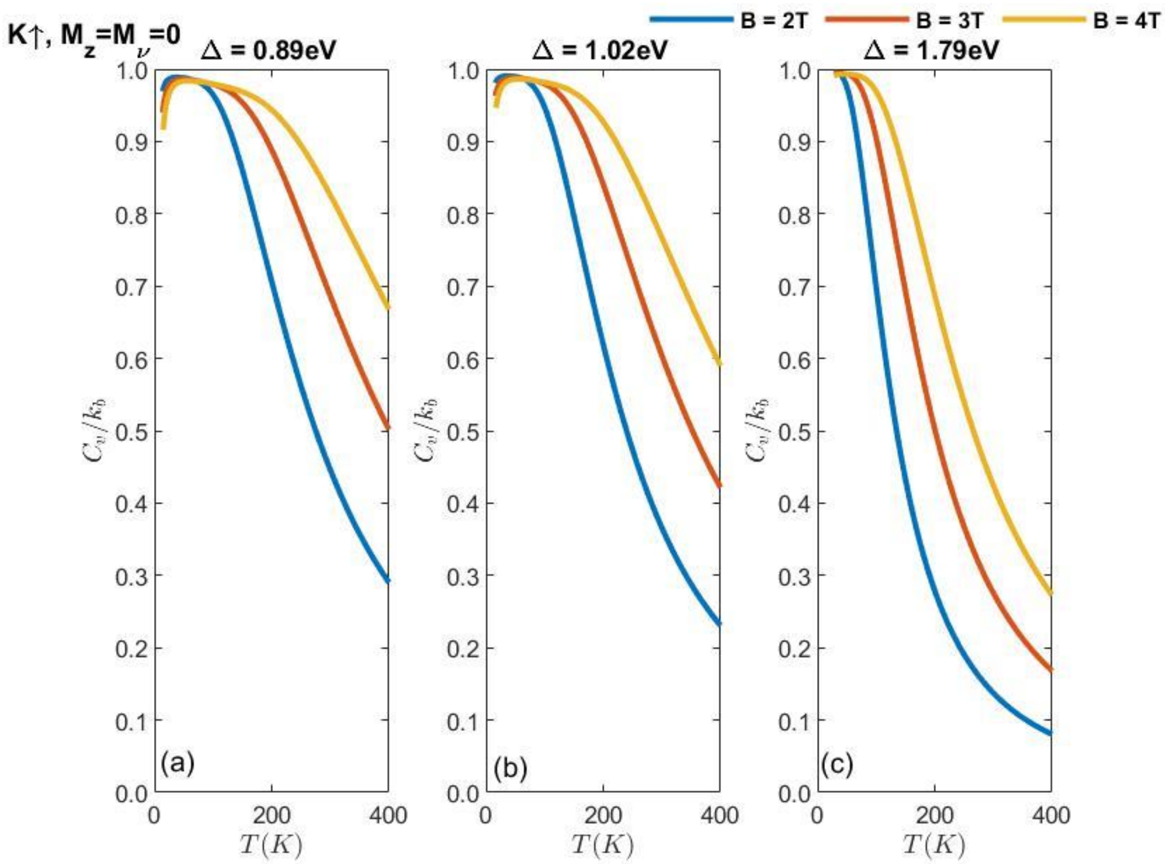

Fig.4.28: Specific heat capacity for the K valley of WS_2 monolayer versus temperature at three strengths of magnetic field and for three values of band gaps when $M_z = M_\nu = 0$.

Due to spin interactions, variations in the vibrational modes of the monolayer constituents, or magnetic ordering effects, the specific heat capacity in magnetic fields may show anomalies or dependence on field intensity (Brahim 2023). Comprehending these interdependencies is critical for applications in quantum devices, spintronics, and magnetic materials, where stability and performance are maximized by exact control over thermal characteristics in magnetic fields (Kim 2014, Liu, Zeng et al. 2020). Fig.4.28 shows the variation of specific heat capacity for the K valley of WS_2 monolayer divided by Boltzmann constant versus temperature for different values of magnetic field and band gaps when $M_z = M_\nu = 0$.

The heat capacity is shown to rise gradually as temperature rises to a peak, after which it starts to fall and eventually achieves a constant value. At low temperature, the specific heat capacity has a higher value of its peak when the magnetic field strength is low. However, at high temperature the specific heat capacity increases with increasing the magnetic field strength. It is shown that the peak position remains constant. The prominent Schottky anomaly, which manifests across a narrow temperature range, is the anomalous peak shown in figures (Kim 2014, Yahyah, Elsaid et al. 2019). By increasing the Δ value the effect of increasing the magnetic field strength will be minimized.

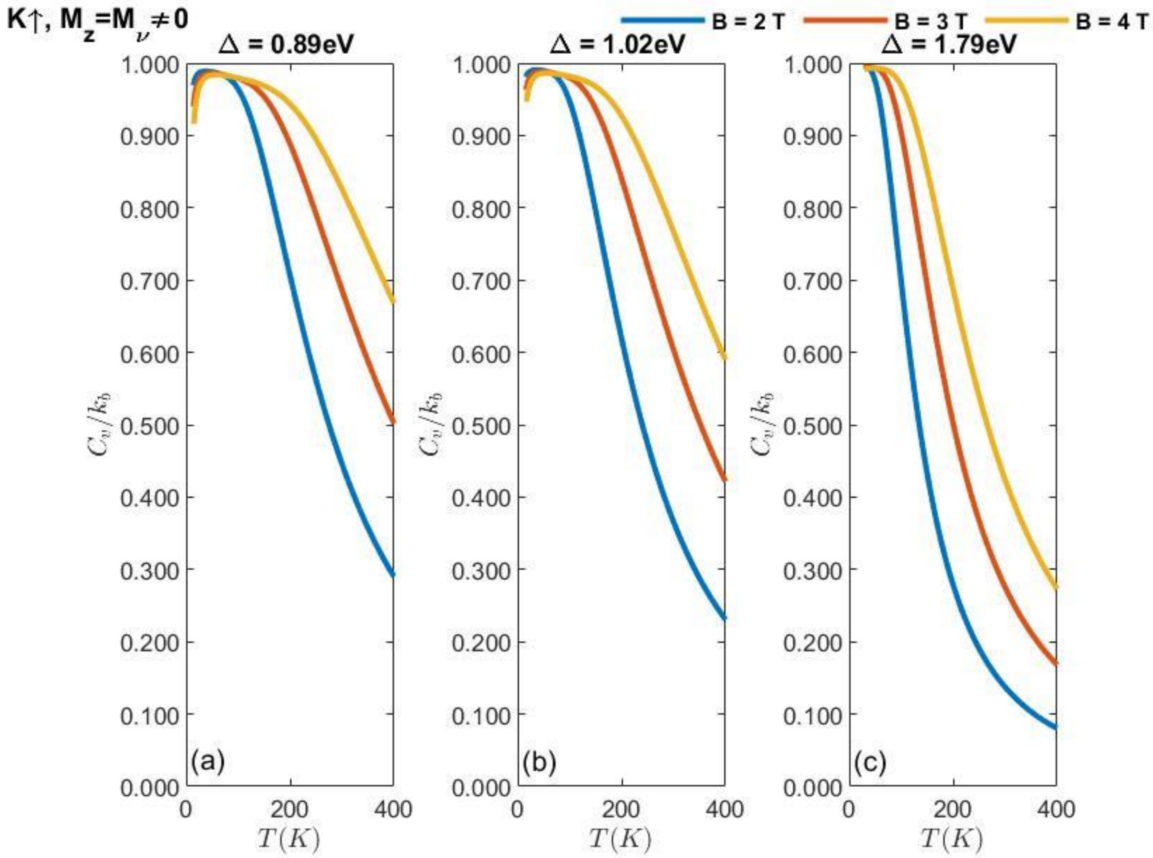

Fig.4.29: Specific heat capacity for the K valley of WS_2 monolayer versus temperature at three strengths of magnetic field and for three values of band gaps when $M_z = M_\nu \neq 0$.

The specific heat capacity for the K valley of WS_2 monolayer versus temperature at three strengths of magnetic field and for three values of band gaps when $M_z = M_\nu \neq 0$ is plotted in Fig.4.29. The prominent Schottky anomaly is appeared at low temperatures with a higher value at a lower magnetic field strength. The specific heat decreases as the temperature increases at high temperature. In addition, by considering the effect of Zeeman term, the specific heat capacity alters with small amount in a range of 10^{-4},thus this increment isn't obvious through the figure.

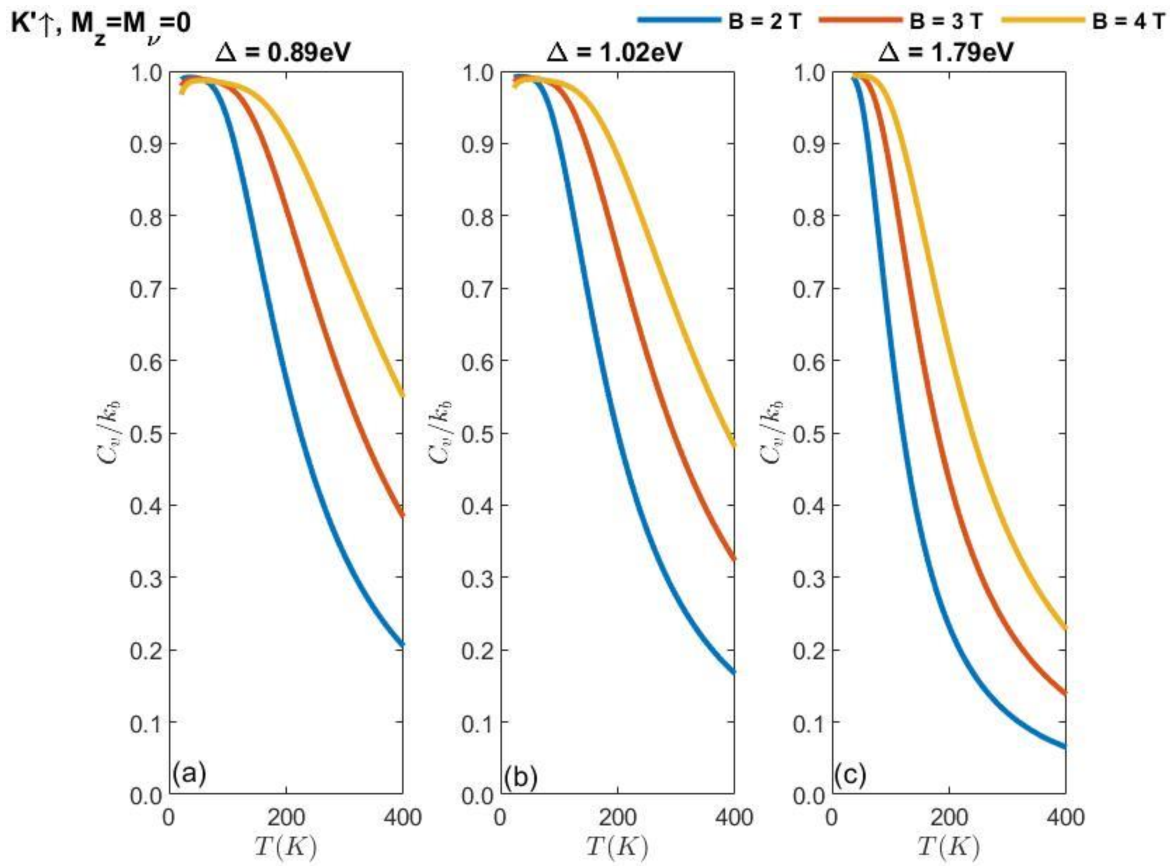

Fig.4.30: Specific heat capacity for the K′ valley of WS_2 monolayer versus temperature at three strengths of magnetic field and for three values of band gaps when $\mathrm{M_z} = \mathrm{M_\nu} = 0$.

The specific heat capacity for the K′ valley of WS_2 monolayer versus temperature at three strengths of magnetic field and for three values of band gaps when $\mathrm{M_z} = \mathrm{M_\nu} = 0$ is plotted in Fig.4.30. As it is shown, the value of the peak of specific heat capacity decreases in tiny amount by increasing magnetic field strength. Also, the specific heat capacity for the K′ valley decreasing with increasing temperature at different strengths of magnetic field.

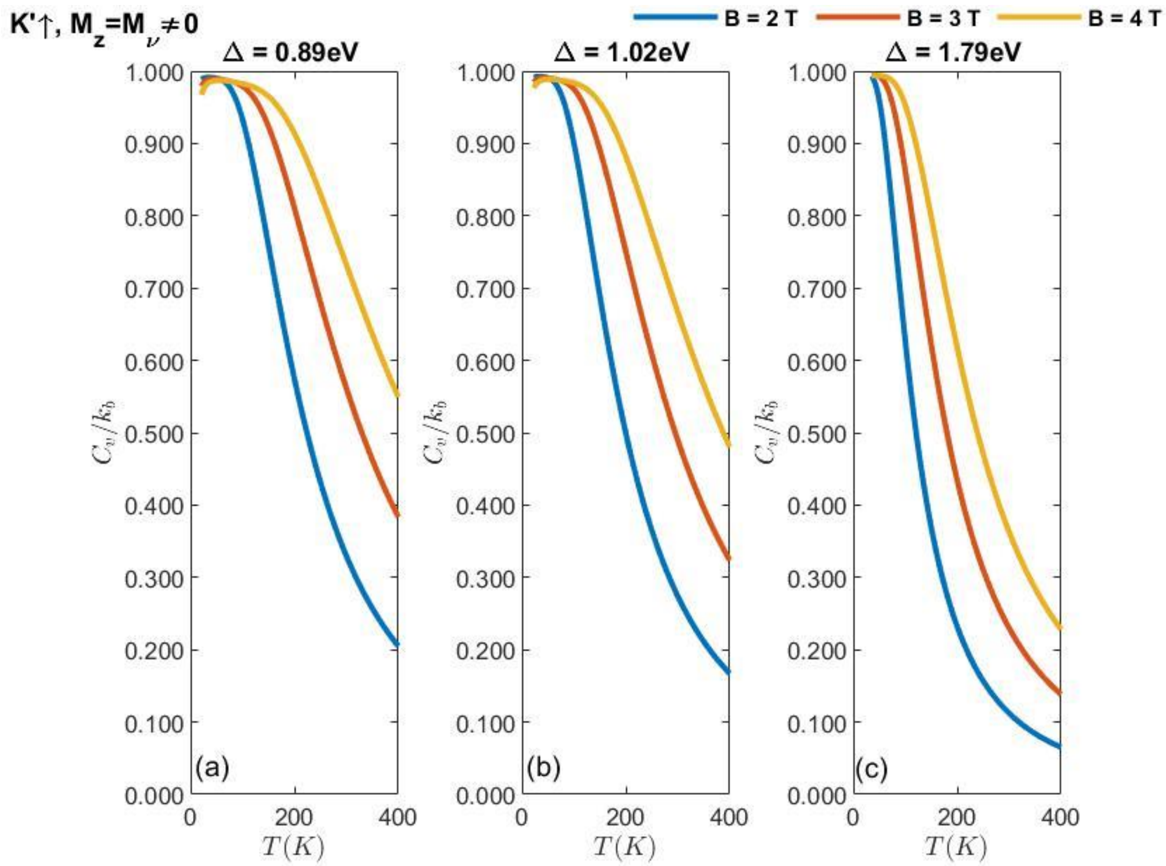

Fig.4.31: Specific heat capacity for the K′ valley of WS_2 monolayer versus temperature at three strengths of magnetic field and for three values of band gaps when $M_z = M_\nu \neq 0$.

When $M_z = M_\nu \neq 0$ the Specific heat capacity for the K′ valley of WS_2 monolayer versus temperature at three strengths of magnetic field and for three values of band gaps is plotted in Fig.4.31. As it is seen, Zeeman term change the magnitude of the specific heat capacity with tiny amount, maintaining the same behavior of previous figures.

In order to investigate more about Schottky anomaly, the variation of specific heat capacity with magnetic field strength will be studied. In specific heat capacity versus magnetic field strength figures, this Schottky anomaly is clearly visible; whereas, the peak in specific heat capacity versus temperature figures is not very well developed. This conclusion is consistent with the observation made by YARMOHAMMADI (Yarmohammadi 2016), that the heat capacity exhibits a peak structure at low temperatures;

in their instance, the peak structure is particularly noticeable. The heat capacity shows consistent behavior at high temperatures as well as were found here.

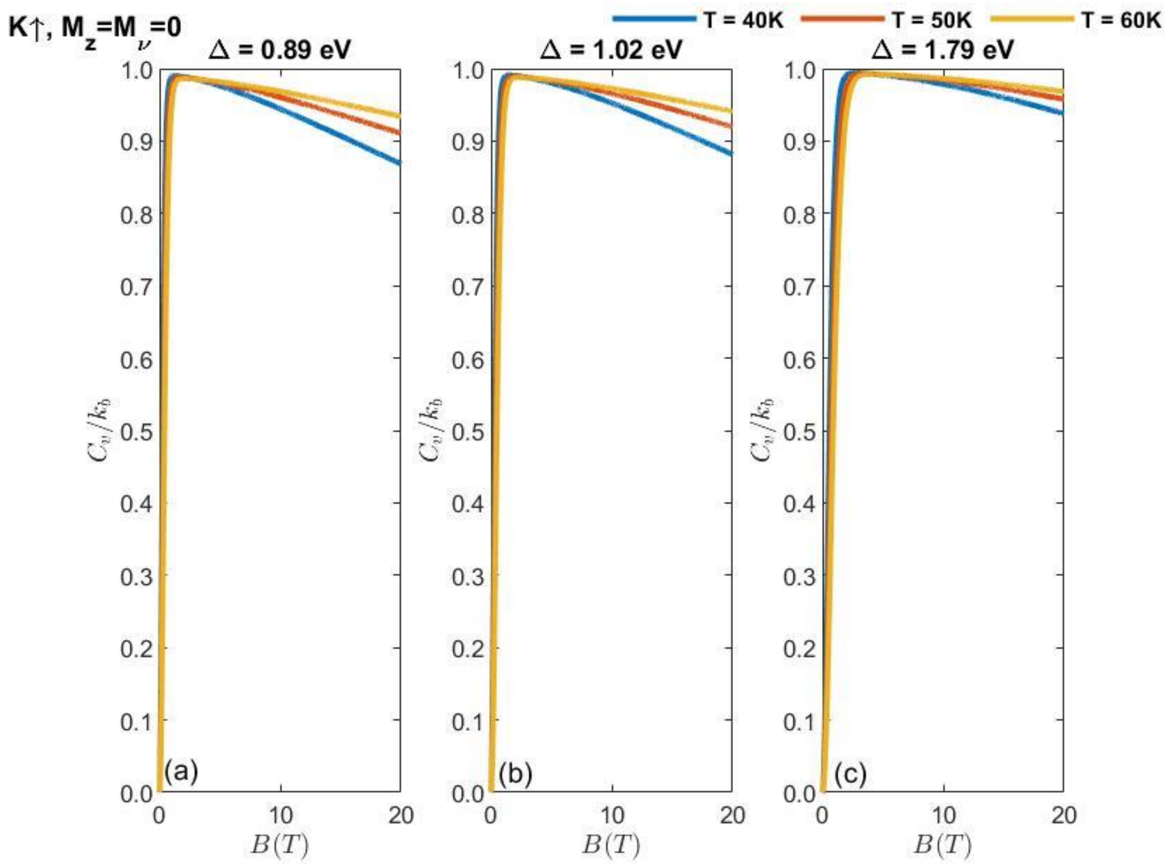

Fig.4.32: Specific heat capacity for the K valley of WS_2 monolayer versus magnetic field strength at three different temperature and for three values of band gaps when

$$M_z = M_\nu = 0 .$$

The heat capacity for the K valley of WS_2 monolayer is depicted in Fig.4.32 as a function of the magnetic field at three different temperature and for three values of band gaps when $M_z = M_\nu = 0$. It has been noted that as the magnetic field increases, the heat capacity rises extremely quickly, peaks, and then lowers right away (Deatsch and Evans 2014). Only at a specific magnetic field value will the environment be able to most effectively excite the system thermodynamically. Another reason is that, at a constant temperature, the system absorbs energy from the magnetic field up to a certain point, after which it absorbs substantially less energy, leading to a sudden decrease in the system's heat capacity (Gopal 2012). The magnetic field serves as a scaling parameter that allows the heat capacity to be calibrated again (Diffo, Fotue et al. 2021).

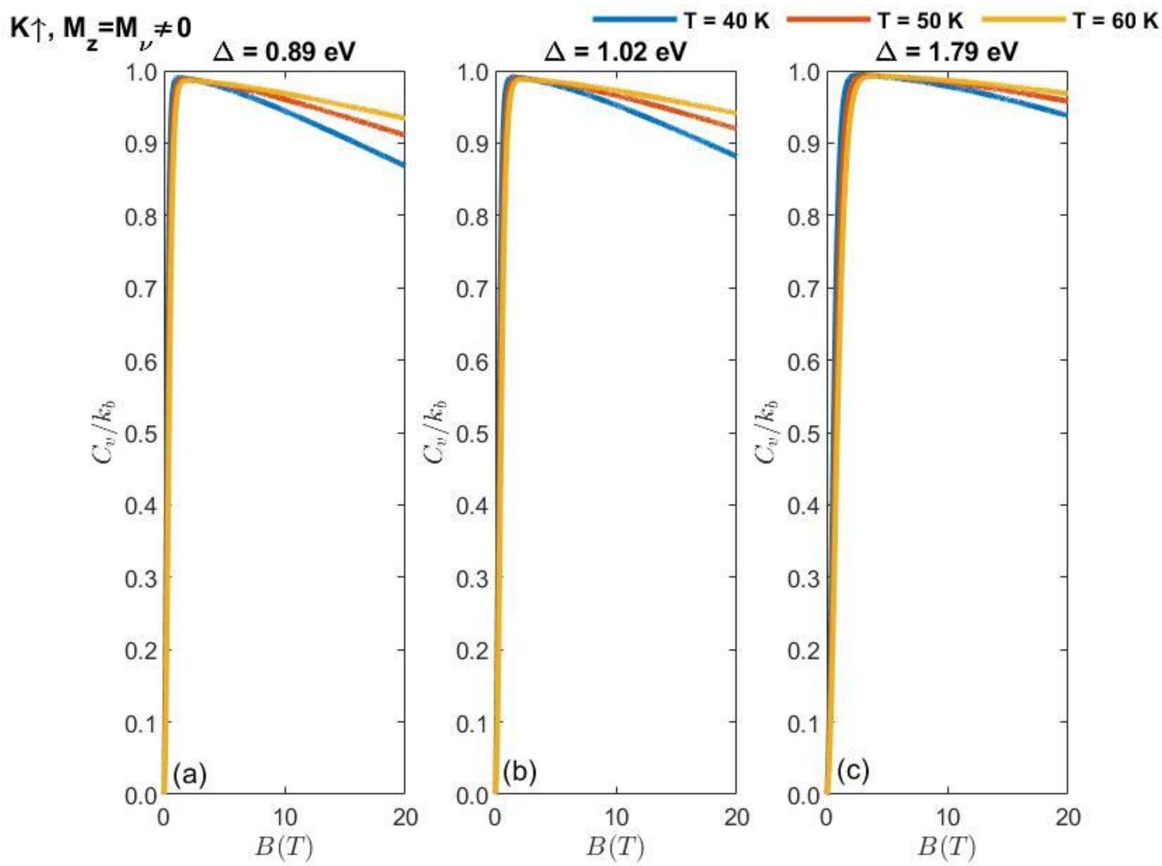

Fig.4.33: Specific heat capacity for the K valley of WS_2 monolayer versus magnetic field strength at three different temperature and for three values of band gaps when $M_z = M_\nu \neq 0$.

When $M_z = M_\nu \neq 0$, the specific heat capacity for the K valley of WS_2 monolayer versus magnetic field strength at three different temperature and for three values of band gaps is investigated in Fig.4.33. As it is seen the specific heat capacity increases with increasing the magnetic field strength until reaching the Schottky peak. At each specific band gap, the Schottky peak shifted toward higher magnetic field strength when the temperature increases. Also, the magnitude of the specific heat slightly decreased at Schottky peak by increasing temperature. In addition, increasing the band gap by applied electric field shifted the Schottky peak toward higher magnetic field strength. Moreover, the magnitude of specific heat capacity at Schottky peak slightly decreased with increasing band gap.

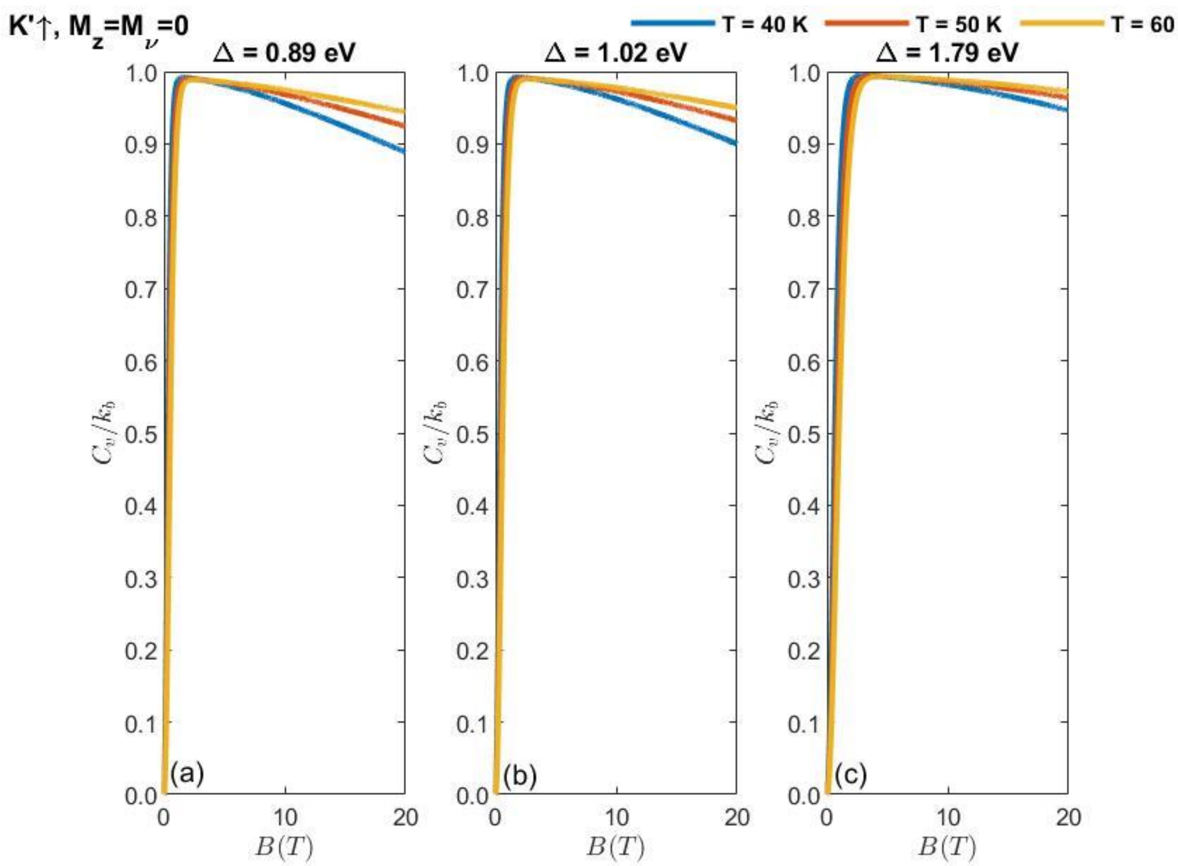

Fig.4.34: Specific heat capacity for the K′ valley of WS_2 monolayer versus magnetic field strength at three different temperature and for three values of band gaps when

$$M_z = M_\nu = 0 .$$

When $M_z = M_\nu = 0$, the specific heat capacity for the K′ valley of WS_2 monolayer versus magnetic field strength at three different temperature and for three values of band gaps was investigated in Fig.4.34. The specific heat capacity increases with increasing magnetic field strength until reaching the peak. After that, the specific heat capacity decreases with increasing magnetic field.

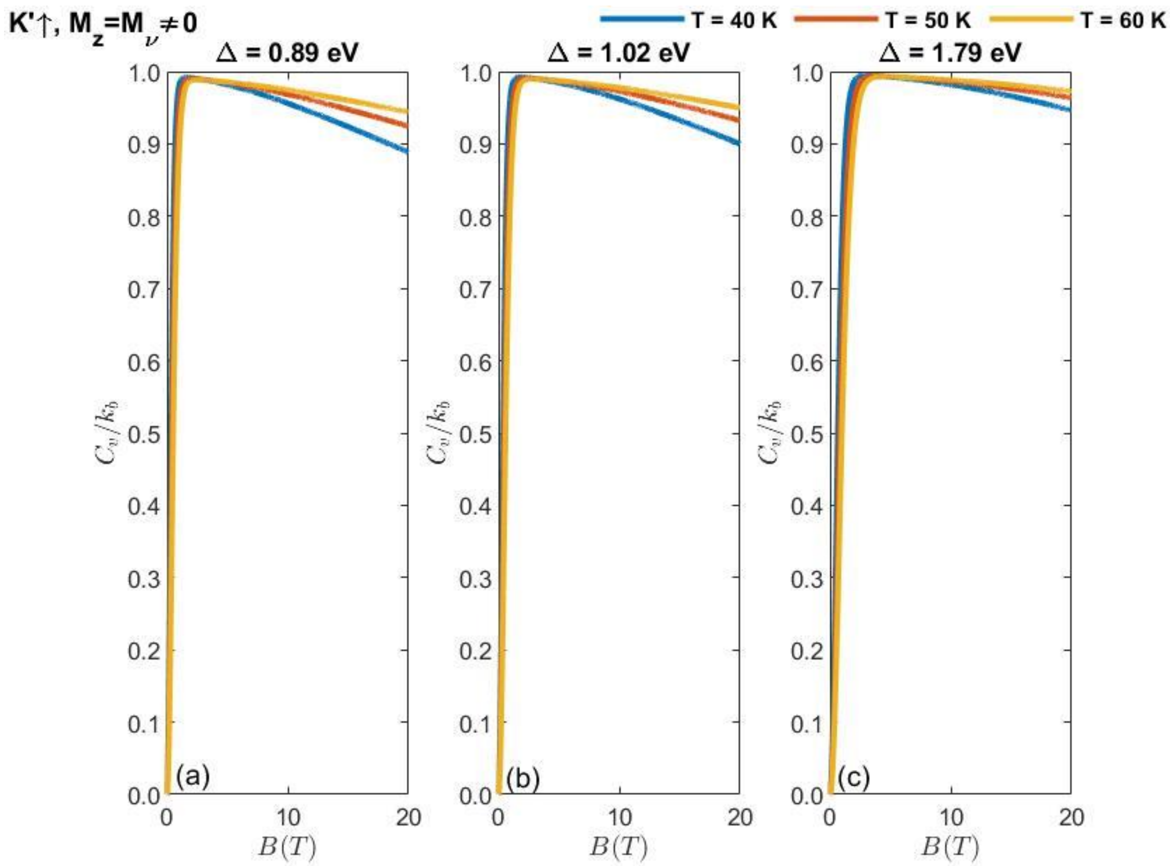

Fig.4.35: Specific heat capacity for the K′ valley of WS_2 monolayer versus magnetic field strength at three different temperature and for three values of band gaps when $M_z = M_\nu \neq 0$.

When $M_z = M_\nu \neq 0$, the specific heat capacity for the K′ valley of WS_2 monolayer versus magnetic field strength at three different temperature and for three values of band gaps is studied in Fig.4.35. As it is noticed for K valley the Schottky peak is appeared below magnetic field strength of 5.0 T.

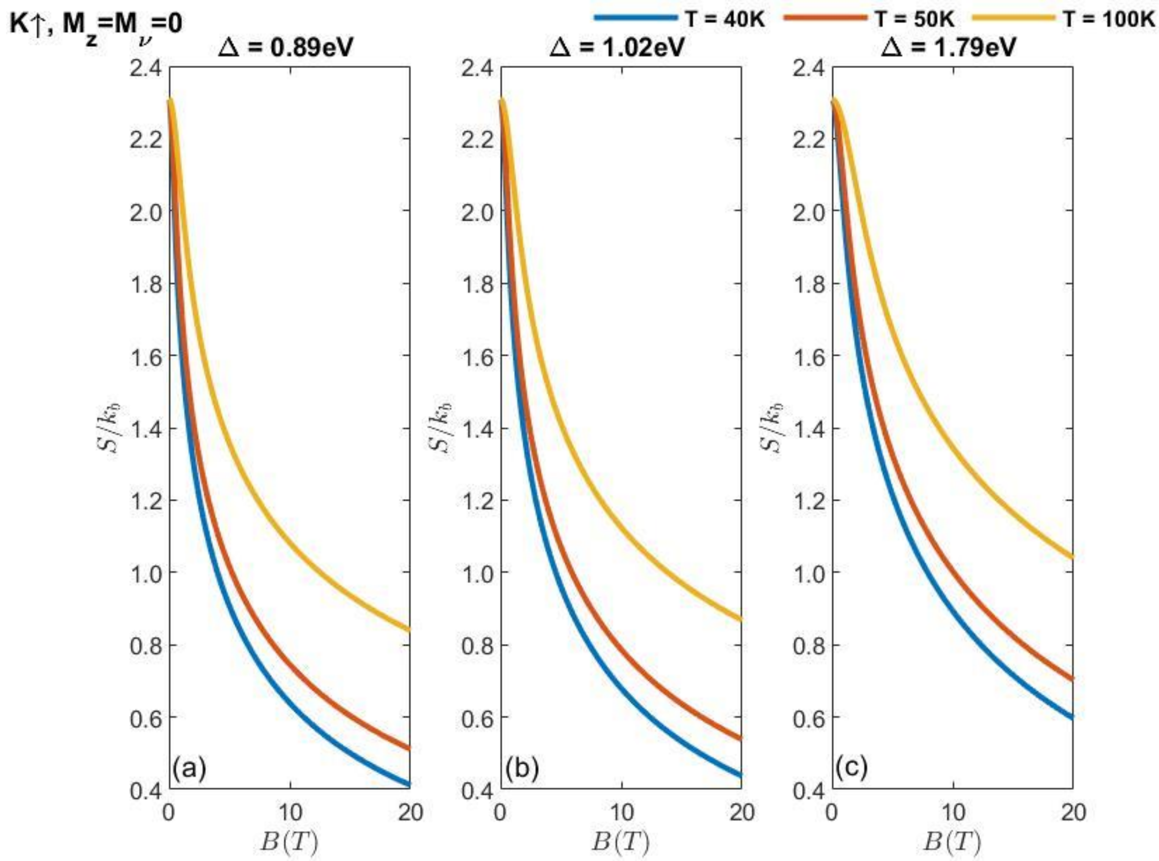

Fig.4.36: Entropy for the K valley of WS_2 monolayer versus magnetic field strength at three different temperature and for three values of band gaps when $M_z = M_\nu = 0$.

For the WS_2 monolayer, the entropy as a function of the strength of the magnetic field (B) at three distinct temperature values was plotted in Fig.4.36. Values at temperatures equal to 40, 50, and 100K have been examined. It is found that changing of the entropy with the magnetic field for high temperatures, such as T of 100K, is less than the changing at low temperatures of 40 and 50K. That is, as the magnetic field increases at relatively low temperatures of 40 and 50K, the entropy rapidly decreases, while at 100K the entropy is slowly decreasing with increasing the magnetic field.

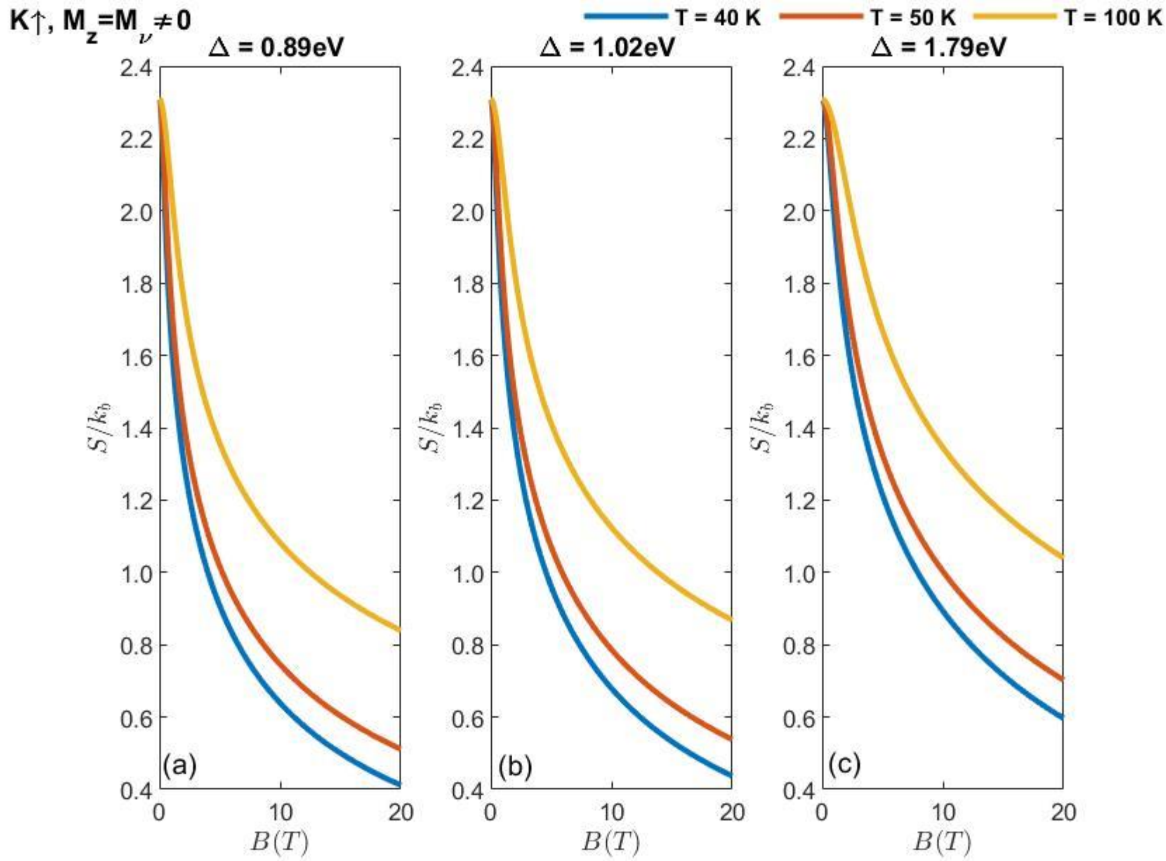

Fig.4.37: Entropy for the K valley of WS_2 monolayer versus magnetic field strength at three different temperature and for three values of band gaps when $M_z = M_\nu \neq 0$.

The Entropy for the K valley of WS_2 monolayer versus magnetic field strength at three different temperature and for three values of band gaps when $M_z = M_\nu \neq 0$ was plotted in Fig.4.37. As it seen, the entropy decreases with increasing magnetic field strength. Also, the entropy increases with increasing temperature. However, changing the band gap plays insignificant role on the entropy.

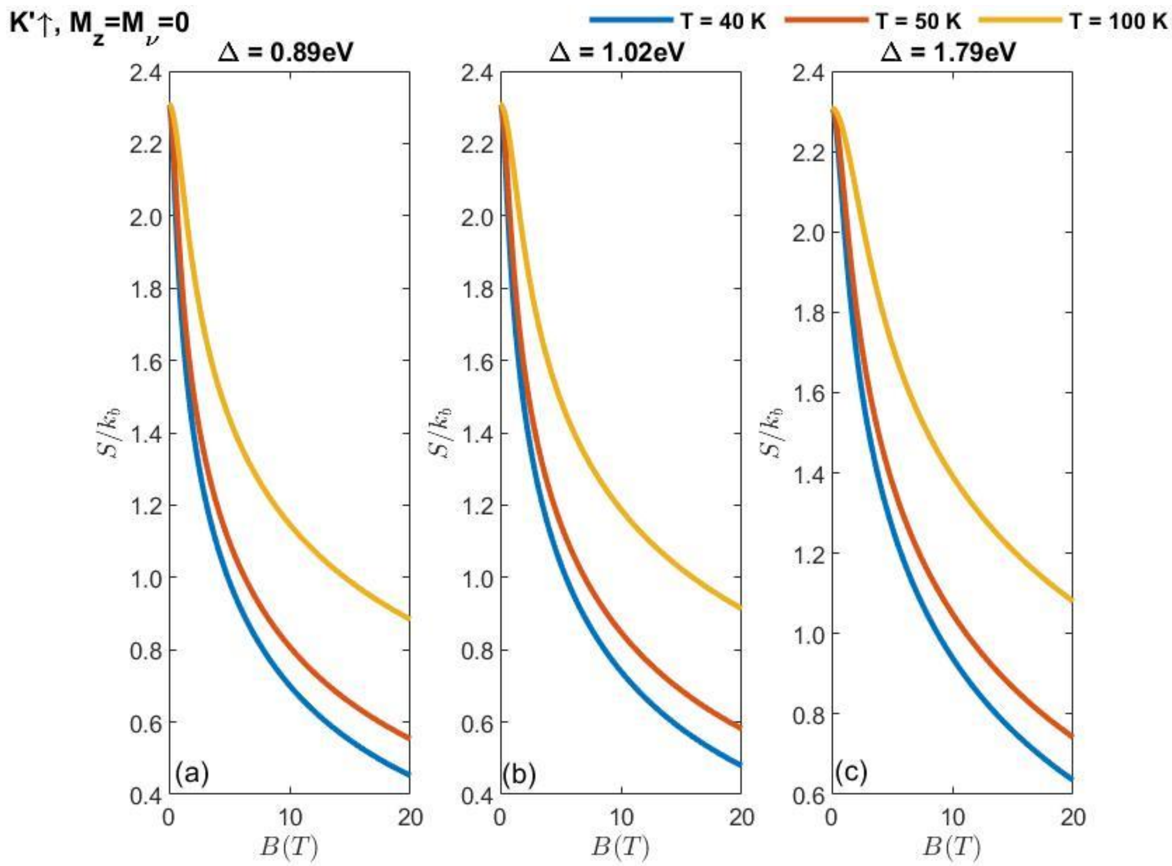

Fig.4.38: Entropy for the K′ valley of WS_2 monolayer versus magnetic field strength at three different temperature and for three values of band gaps when $M_z = M_\nu = 0$.

The entropy for the K′ valley of WS_2 monolayer versus magnetic field strength at three different temperature and for three values of band gaps when $M_z = M_\nu = 0$ is plotted in Fig.4.38. As it is seen, the entropy changes as the magnetic field changes more slowly at higher temperatures, so the effect of the magnetic field on the entropy appears more clearly at lower temperatures.

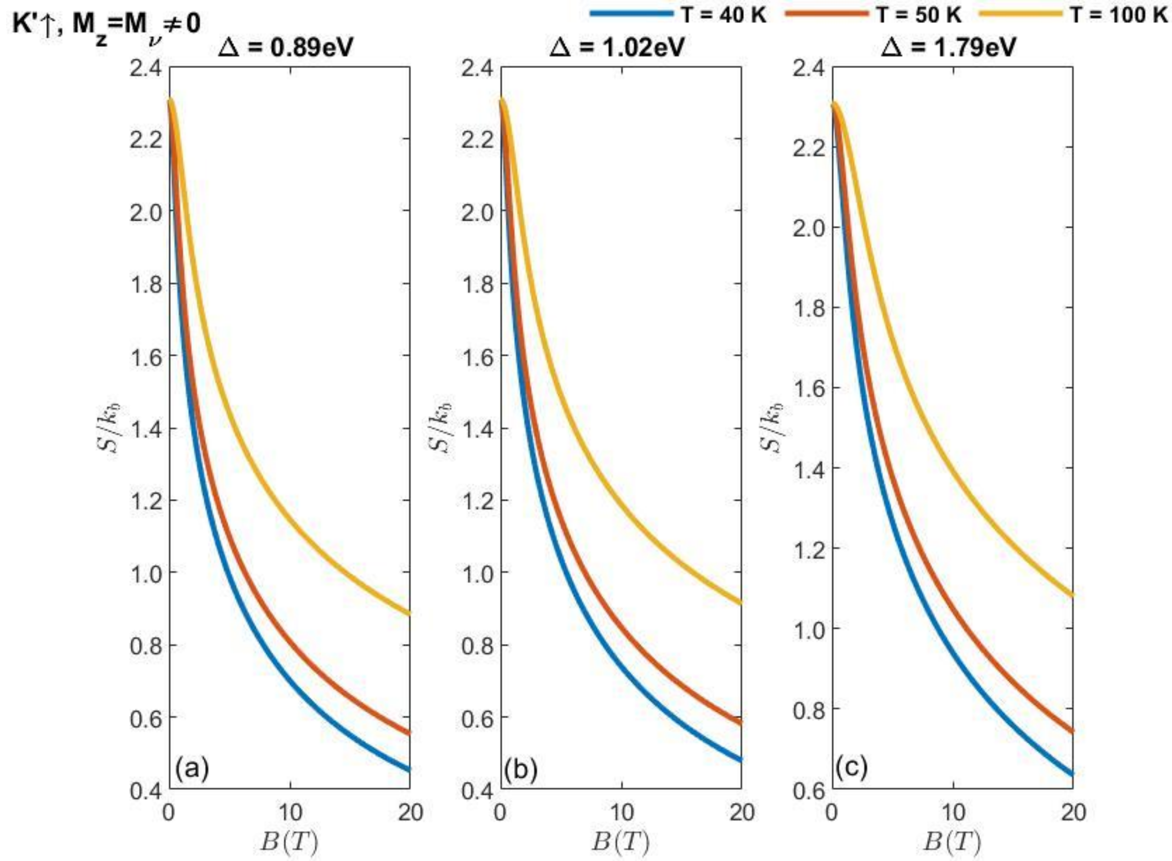

Fig.4.39: Entropy for the K′ valley of WS_2 monolayer versus magnetic field strength at three different temperature and for three values of band gaps when $M_z = M_\nu \neq 0$.

When $M_z = M_\nu \neq 0$, the entropy for the K′ valley of WS_2 monolayer versus magnetic field strength at three different temperature and for three values of band gaps is studied in Fig.4.39. The entropy decreases with increasing the strength of magnetic field. One possible explanation for the observed pattern is that, at higher temperatures, confinement with thermodynamic disorder may result in kinetic energy counterbalancing the order provided by the magnetic field in the system (Sheikholeslami and Ganji 2015). At lower temperatures, on the other hand, magnetic energy is more prevalent, and as the magnetic field increases, entropy decreases. Thus, for lower temperatures, it can be said that the magnetic field lowers disorder in the system; yet, for higher temperatures, the magnetic field has no apparent effect (Nersesyan, Tsvelik et al. 1995, Diffo, Fotue et al. 2021).

Within the system, magnetic and thermal energy are in conflict with one another. Since the energy levels in relation to this TMD are discrete, the entropy can be stated to rely on the distribution of energy levels (Lu 2018, Uechi, Uechi et al. 2023). Thus, for lower temperatures, it can be said that the magnetic field lowers disorder in the system; nonetheless, for higher temperatures, the magnetic field has no discernible effect. This result is consistent with reference (Boyacioglu and Chatterjee 2012, Gumber, Kumar et al. 2015). Consequently, the system's entropy is very susceptible to changes in temperature and magnetic field. Since an increase in the magnetic field in the system minimizes the disorder, it has been shown that it is a crucial factor for particle confinement (Diffo, Fotue et al. 2021).

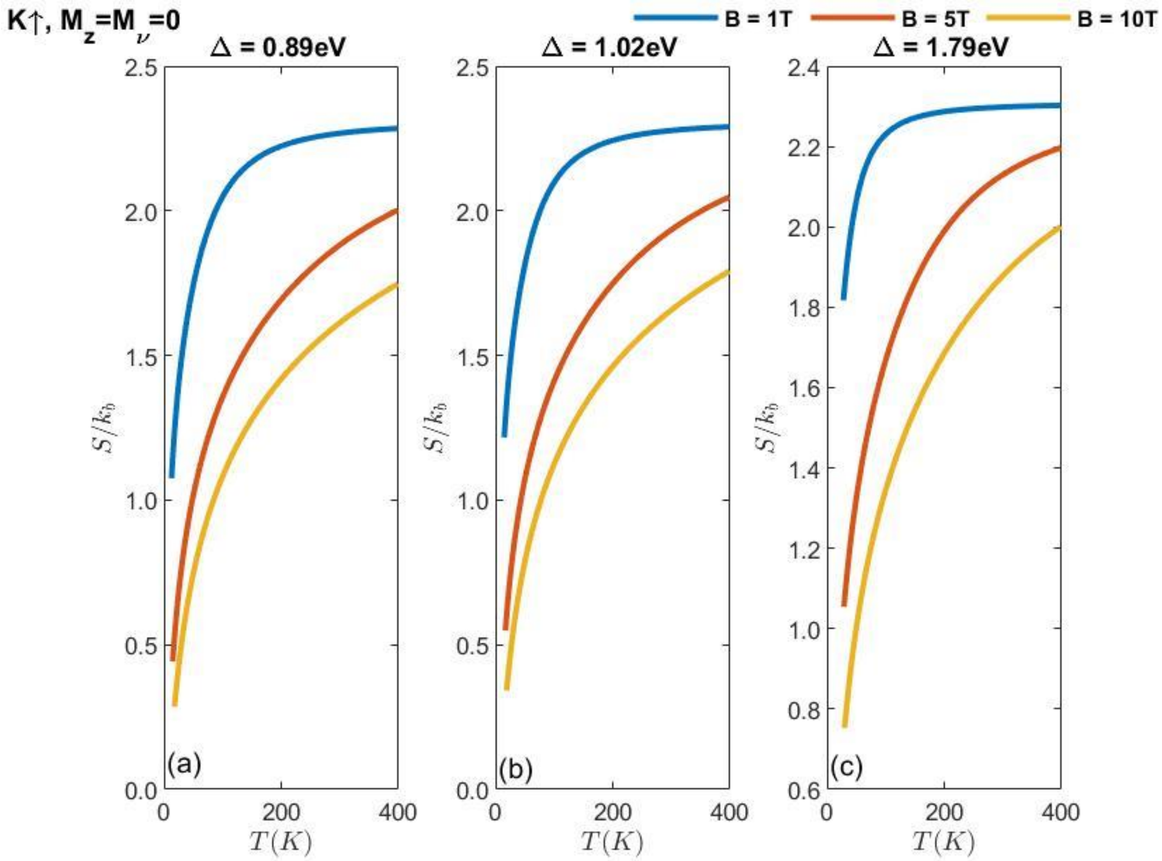

Fig.4.40: Entropy for the K valley of WS_2 monolayer versus temperature at three strengths of magnetic field and for three values of band gaps when $M_z = M_\nu = 0$.

The entropy for the K valley of WS_2 monolayer is displayed against temperature (T) for three different magnetic field strength in Fig.4.40. It has been taken into account values at B equals 1, 5, and 10T in this instance. At higher temperatures, the entropy behaves differently than it does at lower temperatures. It was found that the entropy increases gradually at a fixed magnetic field value before showing a shoulder where it increases quickly at lower temperatures and becomes independent of the magnetic field at higher temperatures. It is observed that as the magnetic field drops, the shoulder becomes more noticeable (Marcos, Planes et al. 2002). This suggests that at low temperatures, the entropy is reliant on the magnetic field and independent at high temperatures. This outcome is consistent with the entropy result that was found before (Diffo, Fotue et al. 2021).

According to physical principles, information loss decreases at low magnetic field strengths and then stabilizes at high magnetic field strengths. Furthermore, this study suggests that the temperature and magnetic field are important variables for information control (Leslie-Pelecky and Rieke 1996).

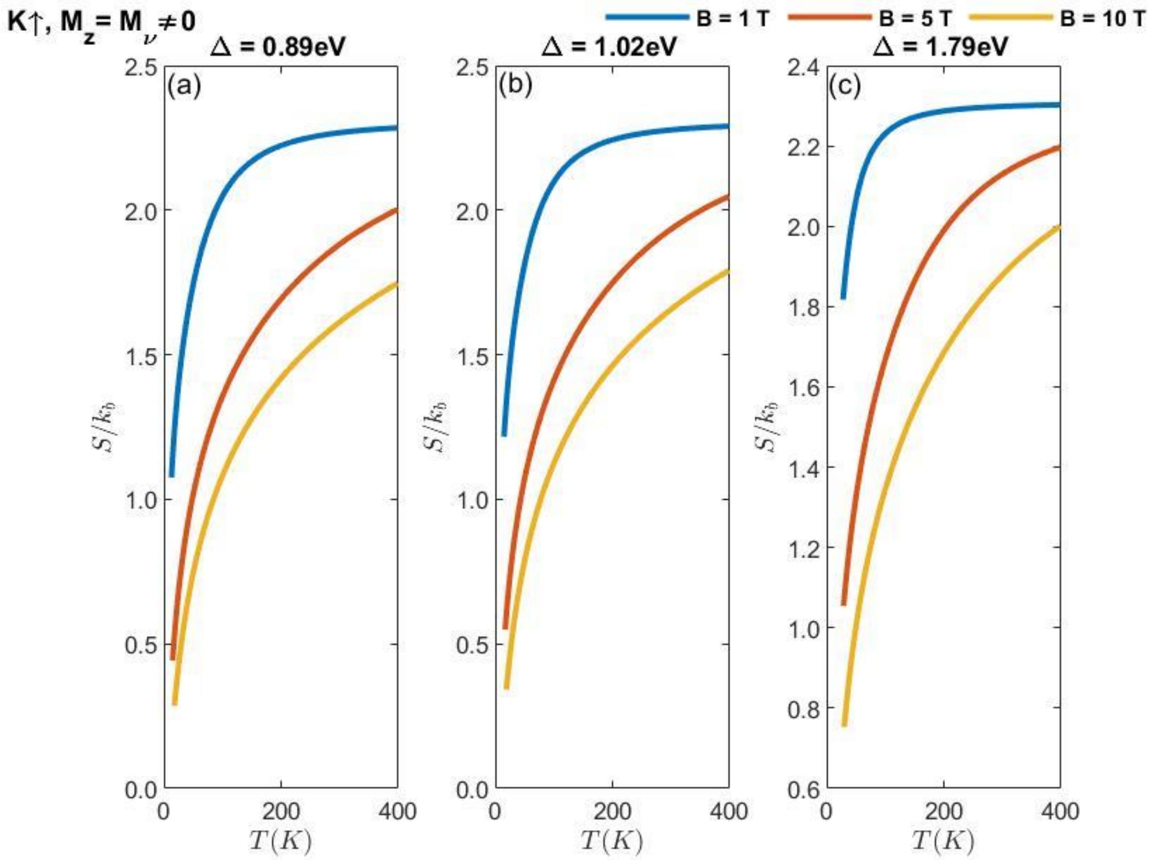

Fig.4.41: Entropy for the K valley of WS_2 monolayer versus temperature at three strengths of magnetic field and for three values of band gaps when $M_z = M_\nu \neq 0$.

The entropy for the K valley of WS_2 monolayer versus temperature at three strengths of magnetic field and for three values of band gaps when $M_z = M_\nu \neq 0$ is discussed in Fig.4.41. It became apparent that the entropy increases gradually at a fixed magnetic field value before exhibiting a shoulder at lower temperatures where it increases rapidly and at higher temperatures where it is independent of the magnetic field. It is found that the shoulder is more pronounced at lower magnetic fields.

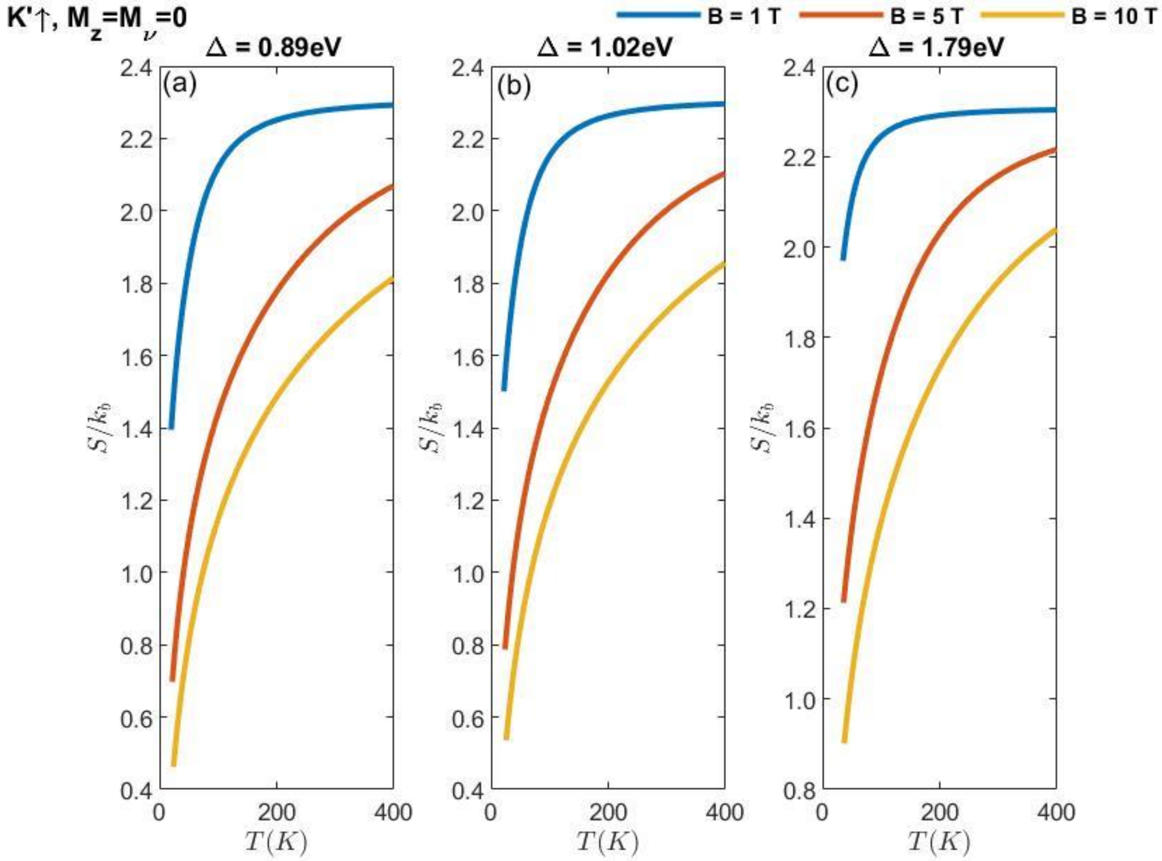

Fig.4.42: Entropy for the K′ valley of WS_2 monolayer versus temperature at three strengths of magnetic field and for three values of band gaps when $M_z = M_\nu = 0$.

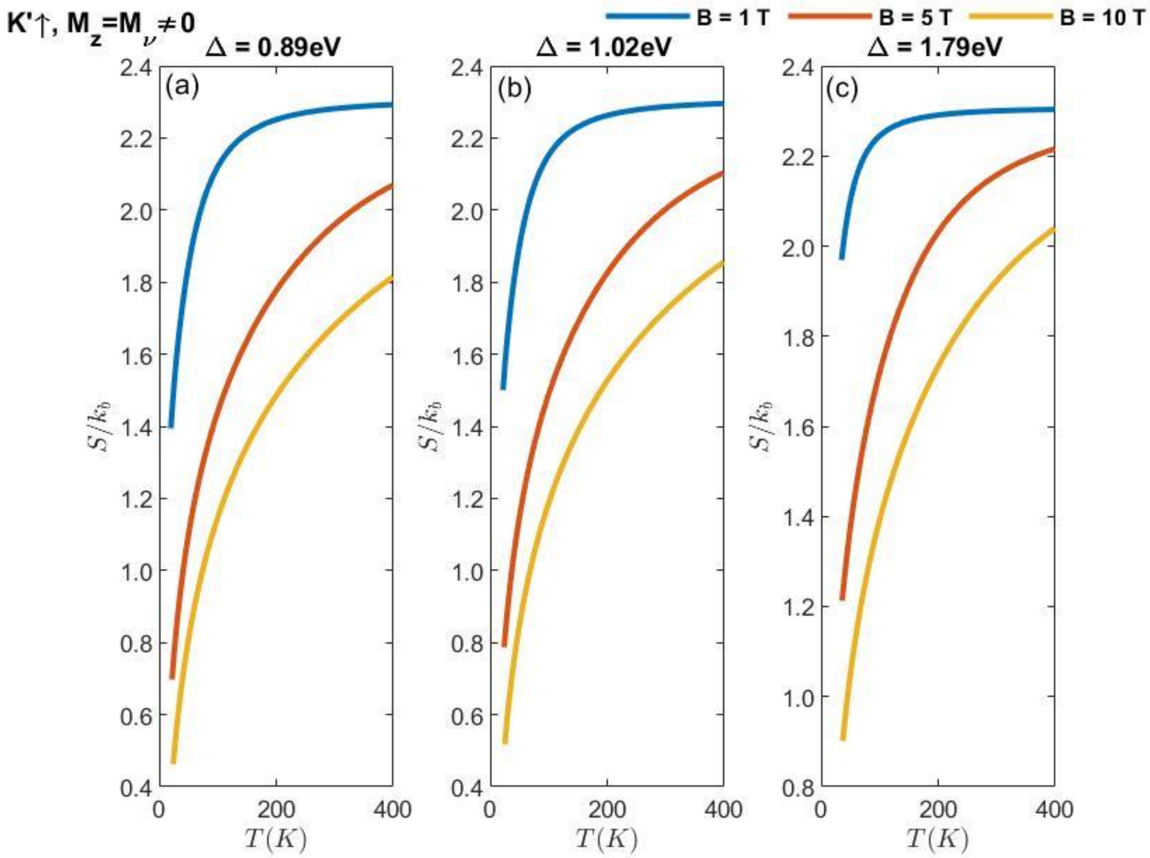

Fig.4.43: Entropy for the K′ valley of WS_2 monolayer versus temperature at three strengths of magnetic field and for three values of band gaps when $M_z = M_\nu \neq 0$.

In the absence and presence of Zeeman term, the entropy for the K′ valley of WS_2 monolayer versus temperature at three strengths of magnetic field and for three values of band gaps was investigated in Fig.4.42 and Fig.4.43. At low temperature, the entropy increases with increasing temperature, and at high temperature the entropy seems to be constant.

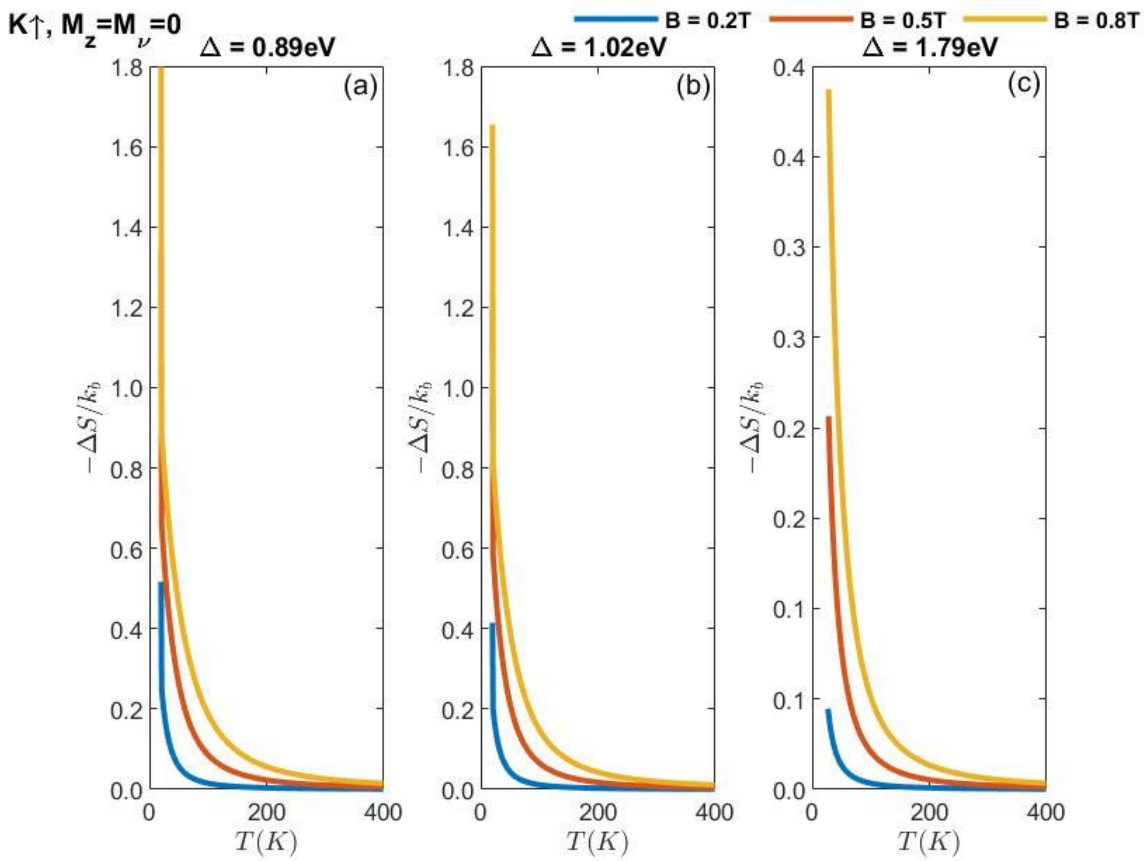

Fig.4.44: MCE for the K valley of WS_2 monolayer versus temperature at three strengths of magnetic field and for three values of band gaps when $M_z = M_\nu = 0$.

The phenomenon known as the Magnetocaloric Effect (MCE) occurs when a magnetic substance is exposed to a fluctuating magnetic field and experiences a change in temperature. The coupling between the material's thermal and magnetic properties is what causes this phenomenon (Rehn, Li et al. 2018, Wei, Liao et al. 2020, Cortés, Peña et al. 2022).

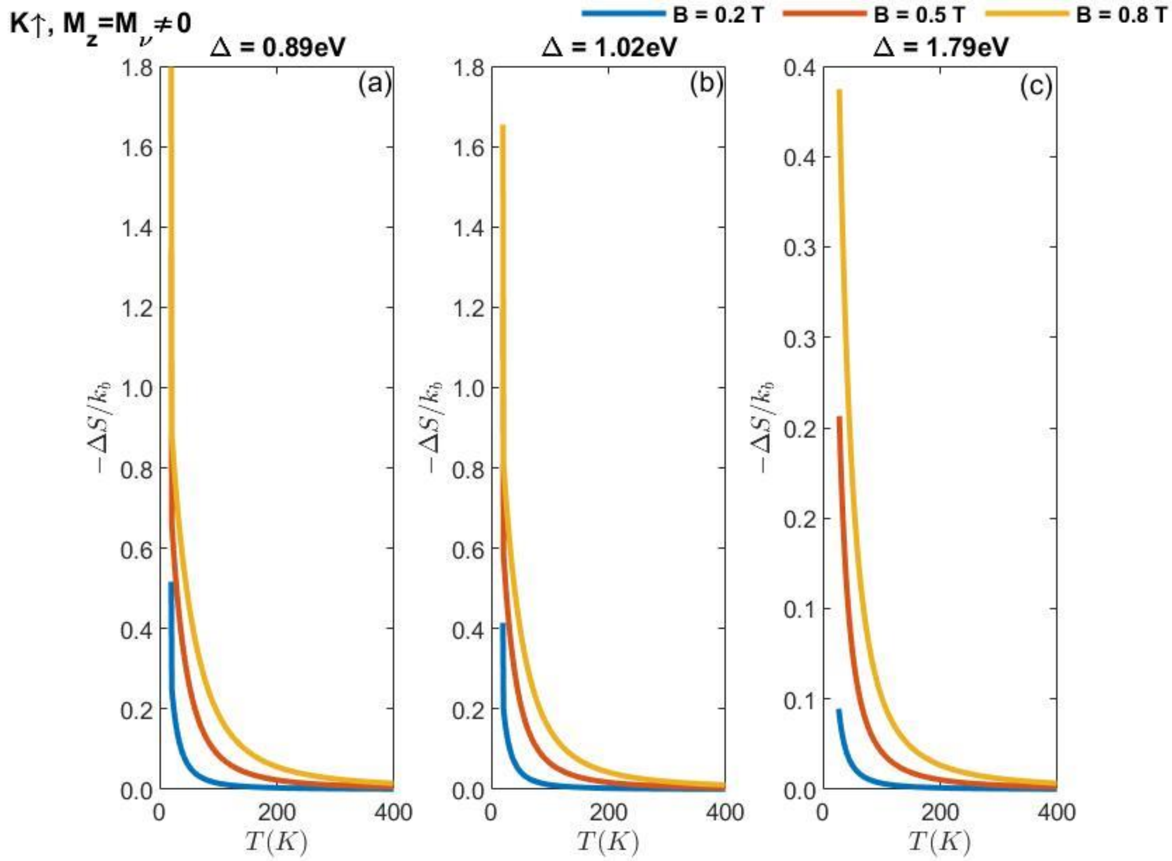

Fig.4.45: MCE for the K valley of WS_2 monolayer versus temperature at three strengths of magnetic field and for three values of band gaps when $\mathrm{M_z} = \mathrm{M_\nu} \neq 0$.

Fig44. and Fig.4.45 show the magnetocaloric Effect (MCE) for the K valley of WS_2 monolayer at three strengths of magnetic field. Their special electrical and magnetic properties cause the Magnetocaloric Effect (MCE) to show interesting fluctuations with temperature. Because of their clearly defined electronic band structures and the susceptibility of magnetic ordering to external magnetic fields, monolayers frequently exhibit strong MCE at lower temperatures. Temperature variations have the ability to modify the magnetic interactions in a material, which could lead to a decrease in the MCE's magnitude. Understanding the particular temperature dependency of MCE in monolayers is important for understanding their prospective uses in solid-state cooling and magnetic refrigeration, where it is critical to optimize performance over a wide temperature range (Bulatova 2014).

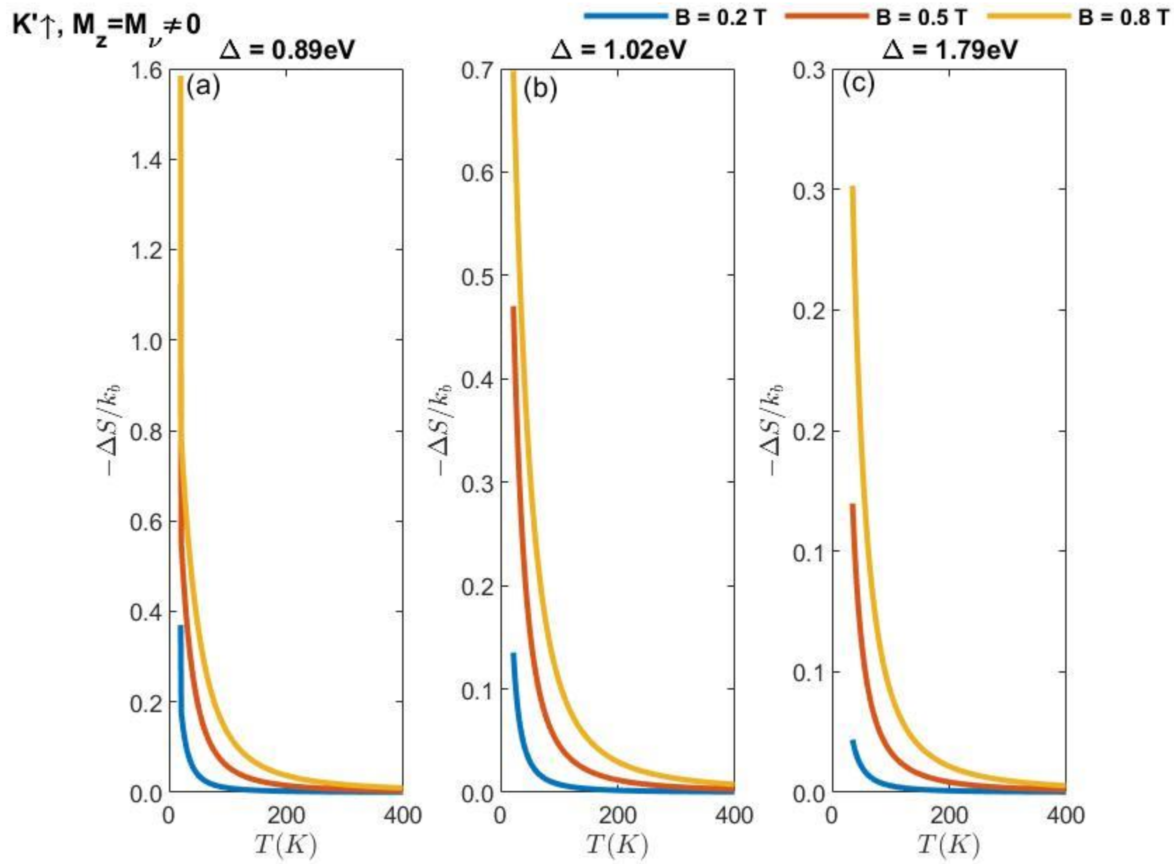

Fig.4.46: MCE for the K′ valley of WS_2 monolayer versus temperature at three strengths of magnetic field and for three values of band gaps when $M_z = M_\nu = 0$.

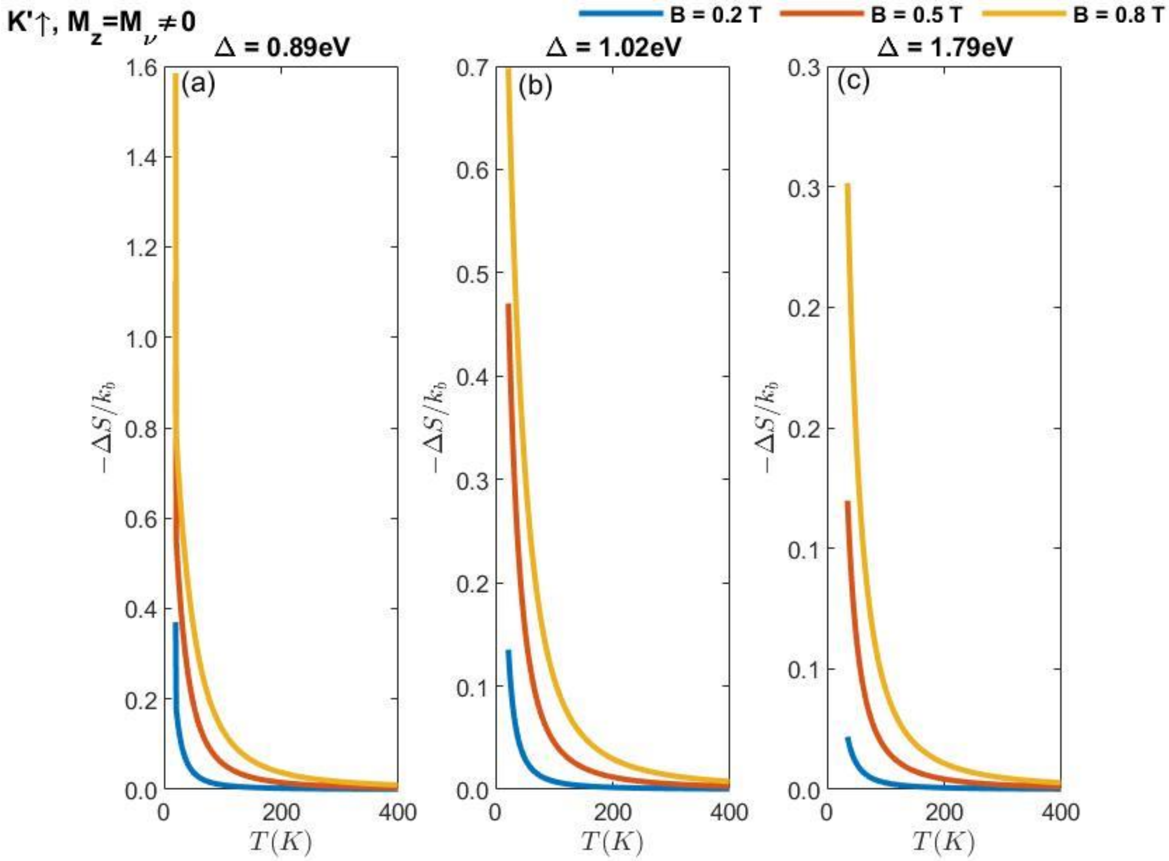

Fig.4.47: MCE for the K′ valley of WS_2 monolayer versus temperature at three strengths of magnetic field and for three values of band gaps when $M_z = M_\nu \neq 0$.

For the K′ valley of WS_2 monolayer the MCE was investigated in the absence and presence of Zeeman term and plotted in Fig.4.46 and 47.

4.4 Magnetic Properties

In this section, the magnetic properties of WS2 monolayer will be investigated in the cases of $M_z = M_\nu = 0$ and $M_z = M_\nu \neq 0$.

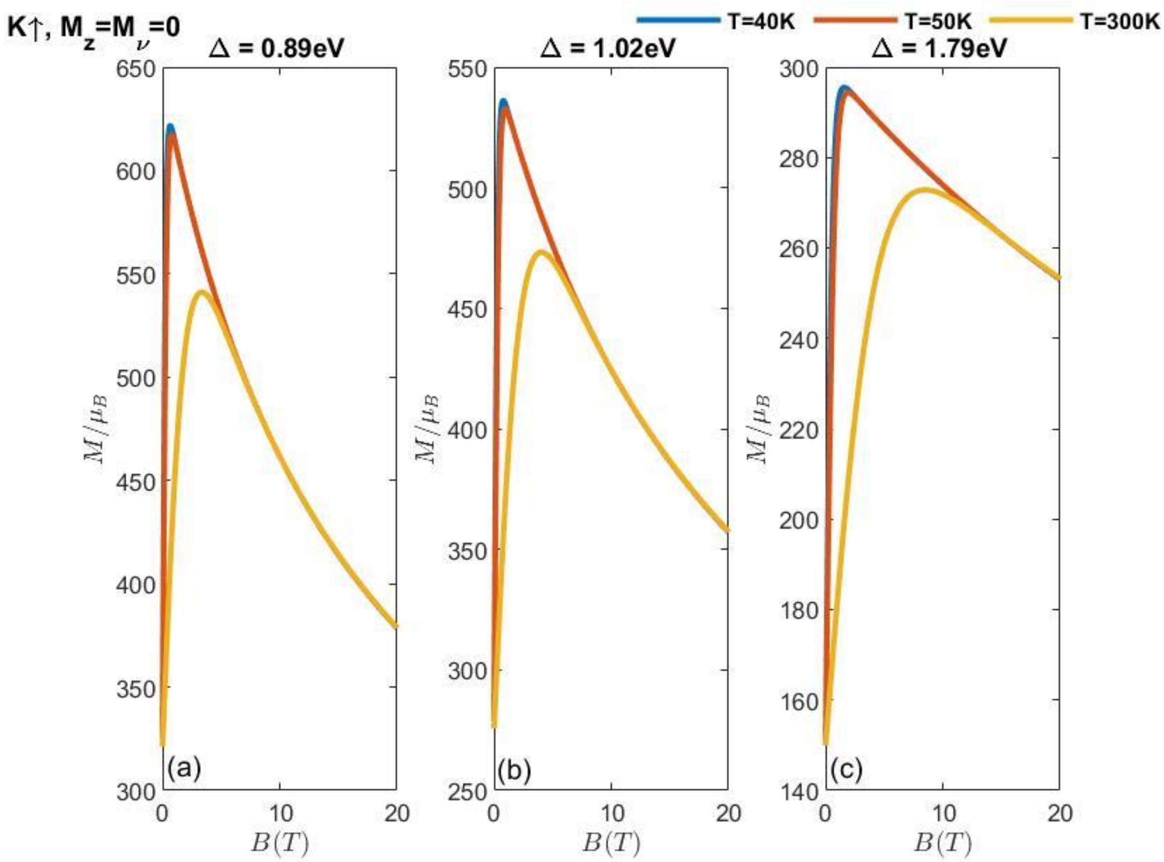

Fig.4.48: Magnetization for the K valley of WS_2 monolayer versus magnetic field strength at three different temperature and for three values of band gaps when $M_z = M_\nu = 0$.

A transition metal dichalcogenide (TMD) monolayer's magnetization versus magnetic field behavior displays interesting features that can be explained by its special structural and electrical properties (Zhang, Liu et al. 2016). The magnetization of WS_2 monolayer versus the magnetic field strength was investigated and plotted in Fig.4.48 at three different temperatures. As depicted by the figure, at temperatures of 40 and 50K, the magnetization increases rapidly with an increasing magnetic field, reaching its peak at about 1.0T for 40 and 50K; respectively, and subsequently starts decreasing at higher magnetic field strengths. Conversely, at a higher temperature of 300K, the magnetization exhibits a more gradual increase as the magnetic field rises, peaking around 6.57T before declining.

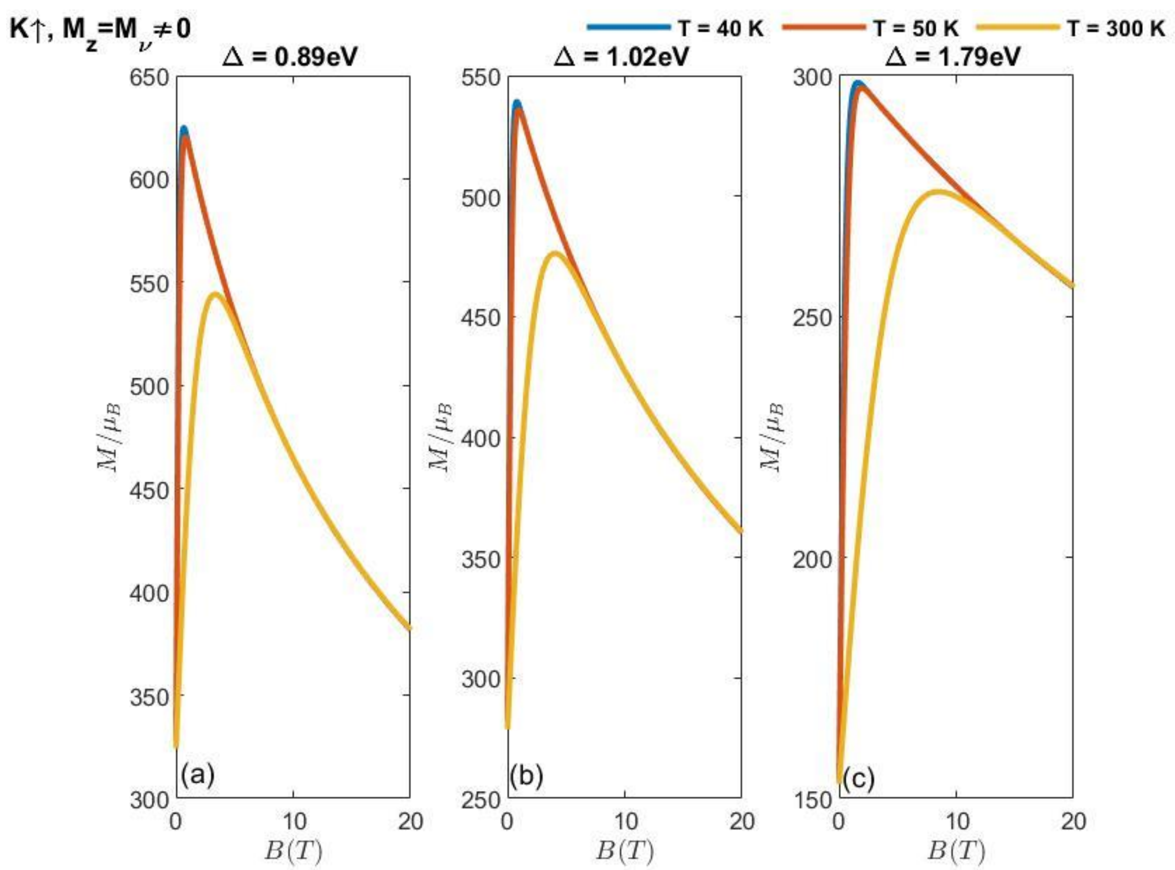

Fig.4.49: Magnetization for the K valley of WS_2 monolayer versus magnetic field strength at three different temperature and for three values of band gaps when $\mathrm{M_z} = \mathrm{M_\nu} \neq 0$.

The magnetization for the K valley of WS_2 monolayer versus magnetic field strength at three different temperature and for three values of band gaps when $\mathrm{M_z} = \mathrm{M_\nu} \neq 0$ is investigated and plotted in Fig.4.49. As it seen, at specific band gap, the magnetization decreases with increasing temperature. Also, the peak of magnetization is shifted toward higher magnetic field strengths when the temperature increases. In addition, at same temperature, the magnetization decreases with increasing the given band gap. Moreover, at specific temperature, the magnetization peak shifted toward higher magnetic field strengths with increasing the band gap.

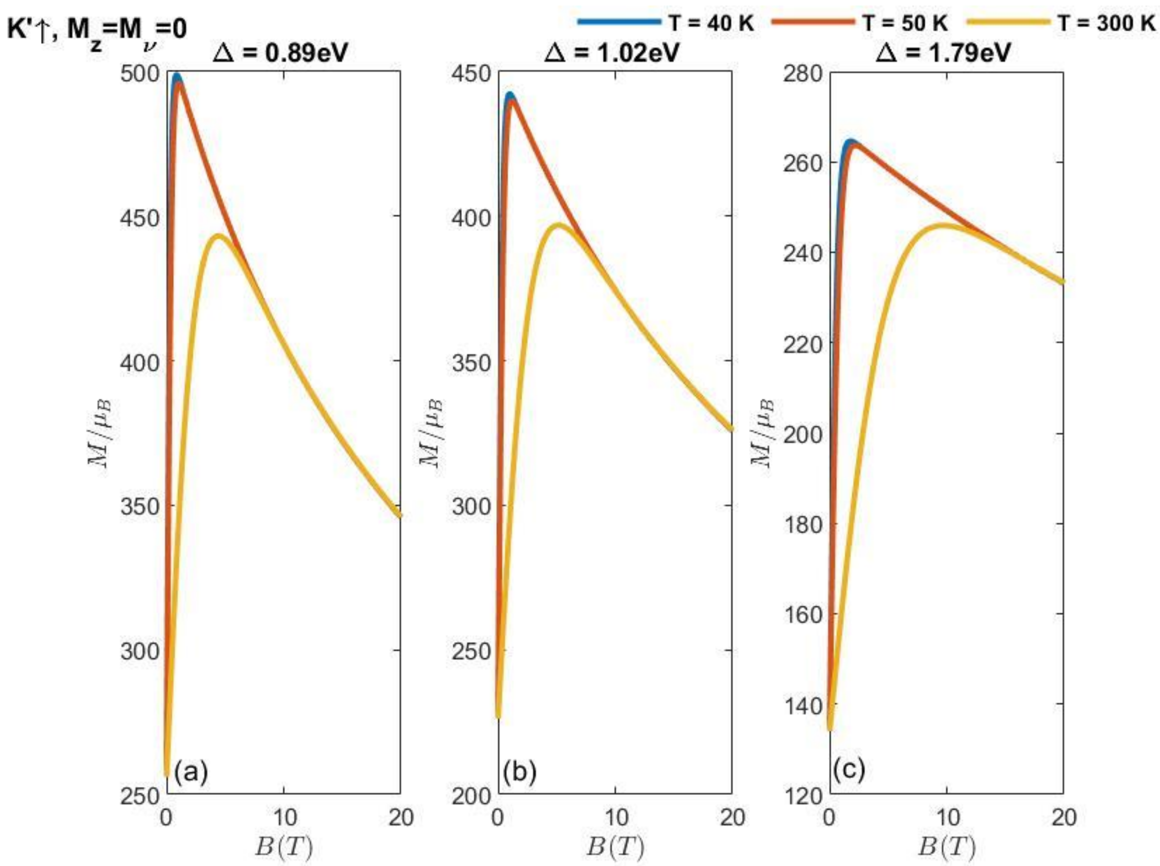

Fig.4.50: Magnetization for the K′ valley of WS_2 monolayer versus magnetic field strength at three different temperature and for three values of band gaps when $M_z = M_\nu = 0$.

The magnetization for the K′ valley of WS_2 monolayer versus magnetic field strength at three different temperature and for three values of band gaps when $M_z = M_\nu = 0$ is plotted in Fig.4.50. As it is shown, the magnetization of K′ valley is less than that for the K valley. The magnetization is rapidly increased with increasing the magnetic field strengths in the range of low magnetic field strength.

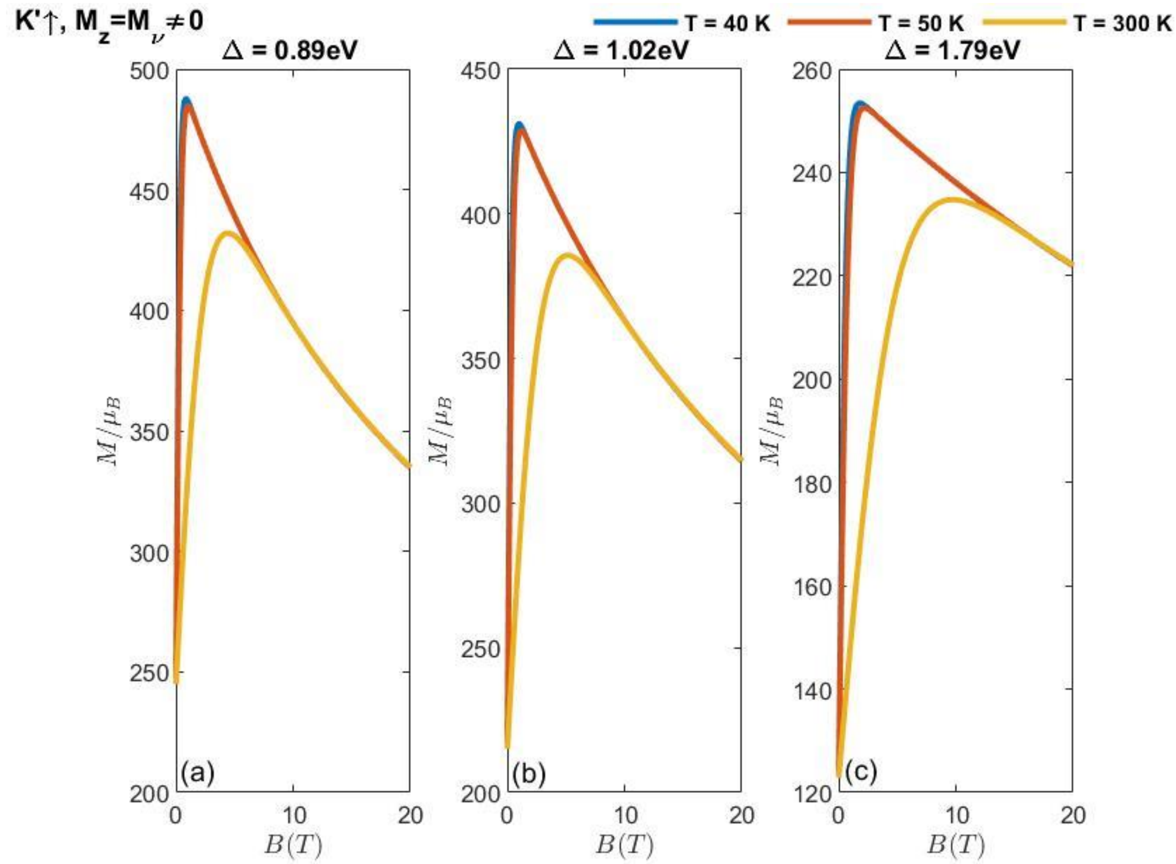

Fig.4.51: Magnetization for the K′ valley of WS_2 monolayer versus magnetic field strength at three different temperature and for three values of band gaps when $\mathrm{M_z} = \mathrm{M_\nu} \neq 0$.

The magnetization for the K′ valley of WS_2 monolayer versus magnetic field strength at three different temperature and for three values of band gaps when $\mathrm{M_z} = \mathrm{M_\nu} \neq 0$ is investigated and plotted in Fig.4.51. As can be shown, the magnetization decreases as temperature rises at a certain band gap. Additionally, when temperature rises, the magnetization peak shifts toward stronger magnetic fields. Additionally, as the band gap increases at the same temperature, the magnetization decreases. Additionally, as the band gap increased at a particular temperature, the magnetization peak moved in the direction of stronger magnetic fields.

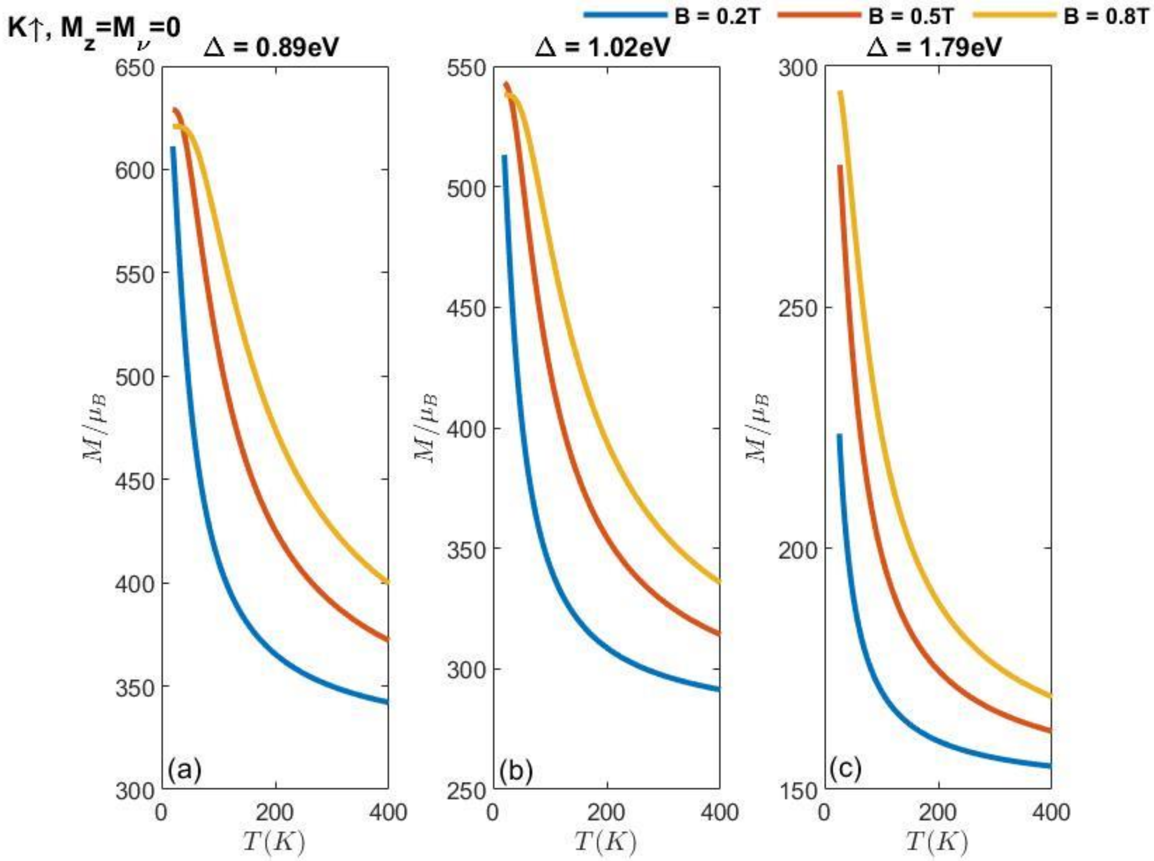

Fig.4.52: Magnetization for the K valley of WS_2 monolayer versus temperature at three values of magnetic field strengths and for three values of band gaps when $M_z = M_\nu = 0$.

The magnetization versus temperature behavior for the K valley of a transition metal dichalcogenide (TMD) monolayer demonstrates its magnetic characteristics under various thermal parameters. The magnetization of WS_2 monolayer versus temperature was investigated and plotted in Fig.4.52 at three values of magnetic field. As depicted in the figure, the magnetization decreases with increasing temperature. Additionally, it is observed that the magnetization increases with increasing magnetic field.

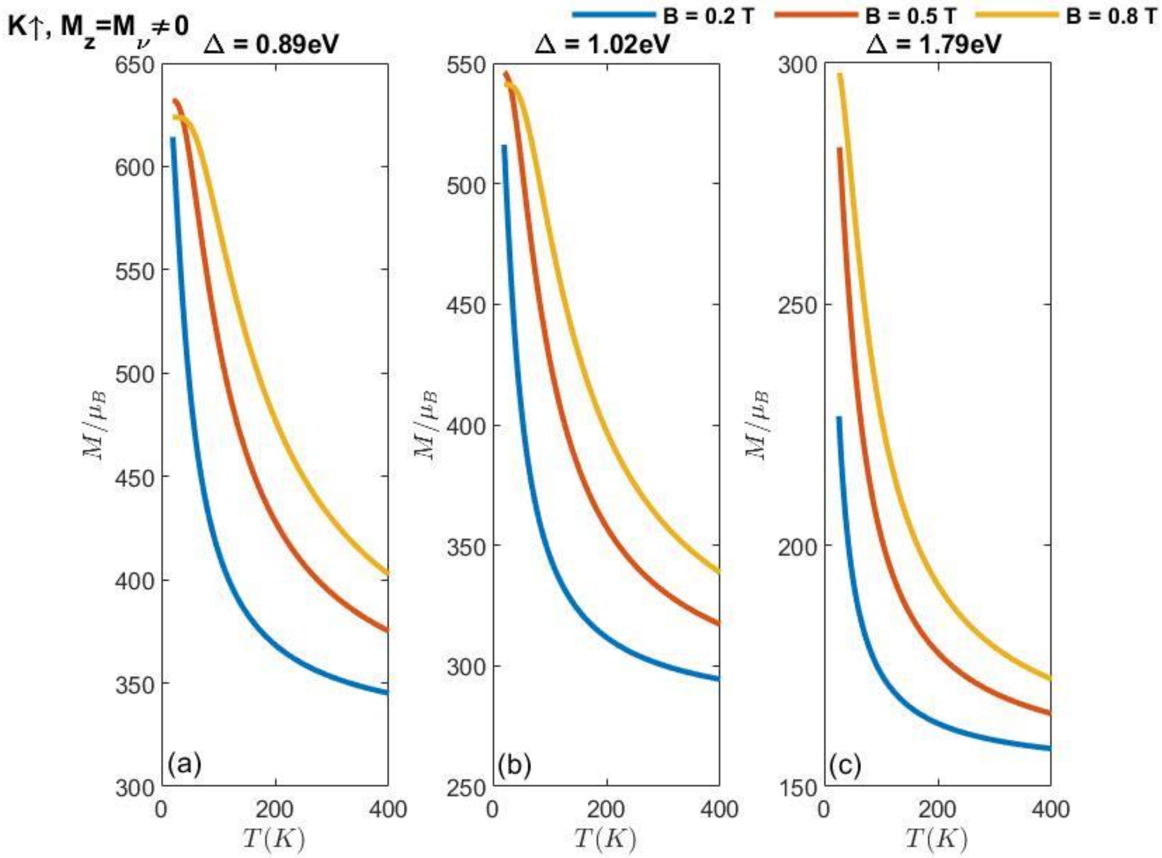

Fig.4.53: Magnetization for the K valley of WS_2 monolayer versus temperature at three values of magnetic field strengths and for three values of band gaps when $M_z = M_\nu \neq 0$.

The magnetization for the K valley of WS_2 monolayer versus temperature at three values of t magnetic field strengths and for three values of band gaps when $M_z = M_\nu \neq 0$ is plotted in Fig.4.53. As it is seen, at specific magnetic field strength, the magnetization decreases with increasing temperature. Also, the magnetization decreases with increasing the band gap for the same magnetic field strength.

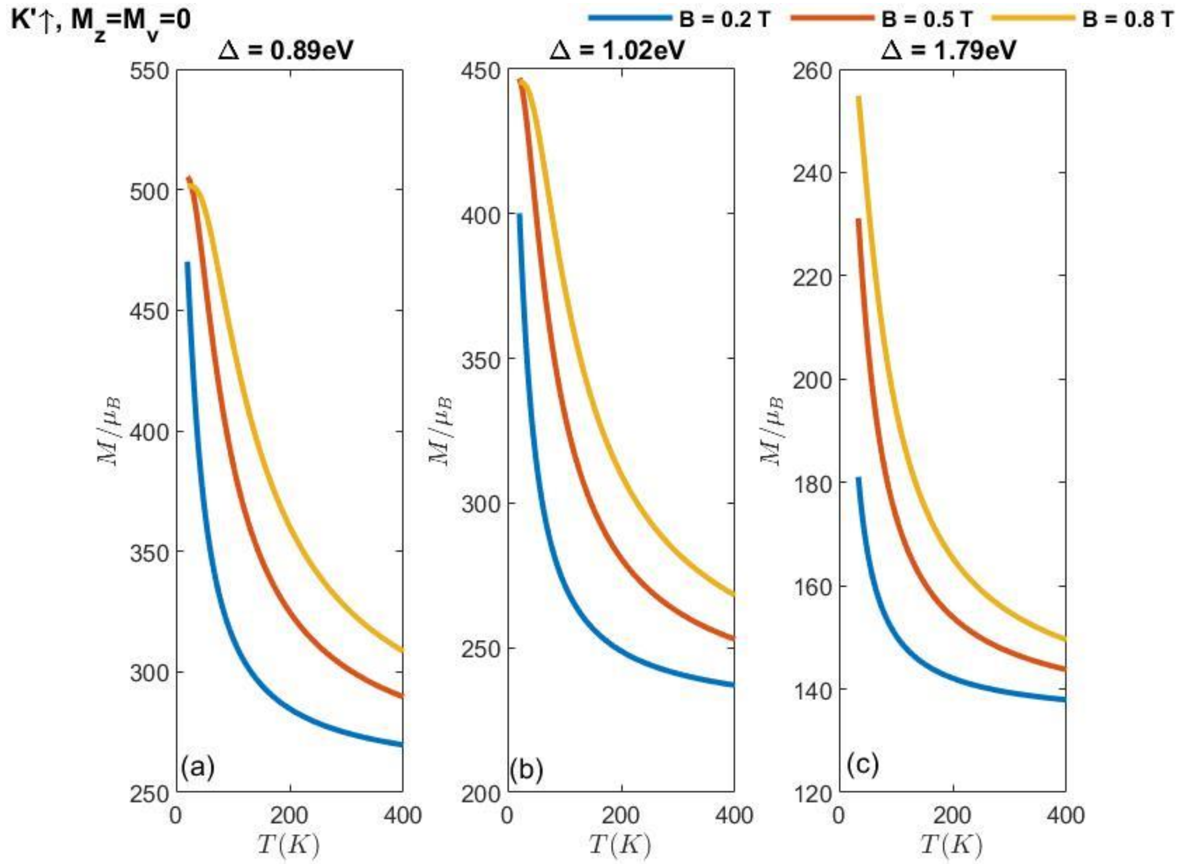

Fig.4.54: Magnetization for the K′ valley of WS_2 monolayer versus temperature at three strengths of magnetic fields and for three values of band gaps when $\mathrm{M_z} = \mathrm{M_\nu} = 0$.

The magnetization for the K′ valley of WS_2 monolayer versus temperature at three values of t magnetic field strengths and for three values of band gaps when $\mathrm{M_z} = \mathrm{M_\nu} = 0$ is plotted in Fig.4.54. As it is seen, the magnetization of K′ valley is lower the that for the K valley.

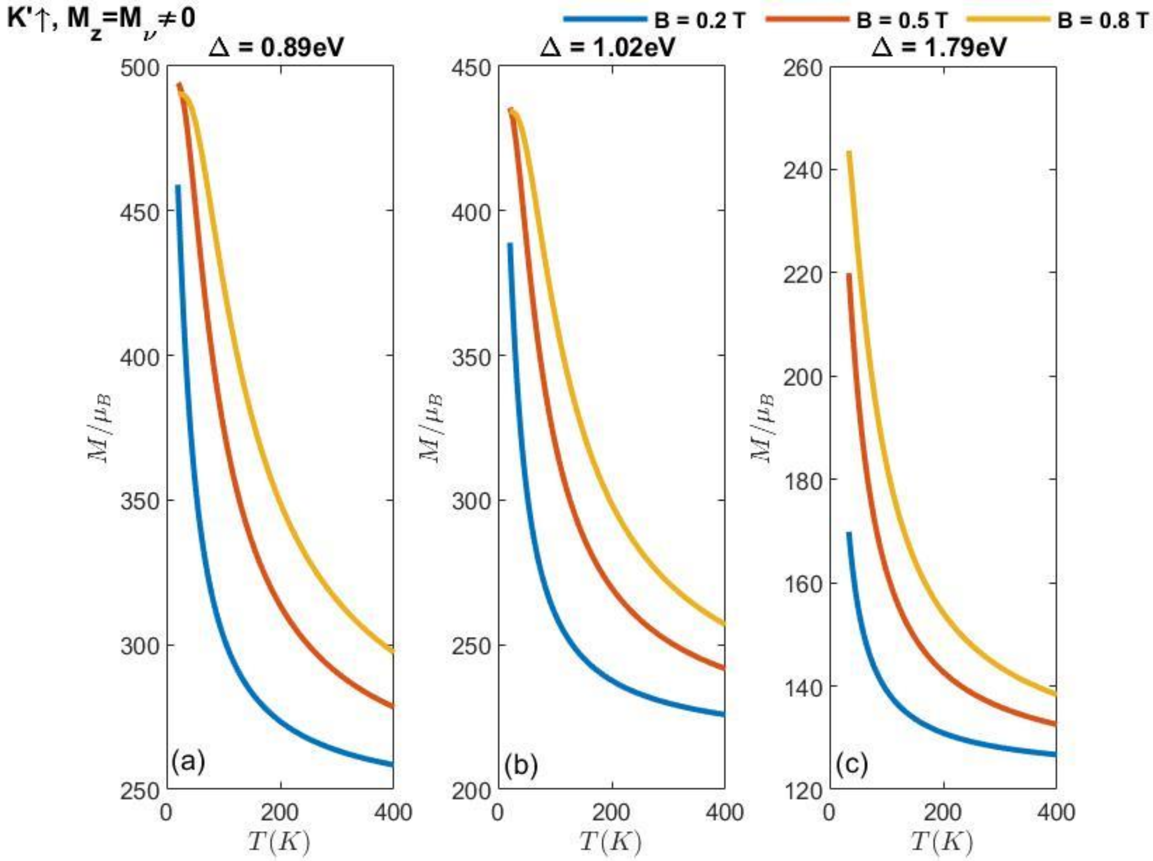

Fig.4.55: Magnetization for the K′ valley of WS_2 monolayer versus temperature at three values of magnetic field strengths and for three values of band gaps when $\mathrm{M_z} = \mathrm{M_\nu} \neq 0$.

The magnetization for the K′ valley of WS_2 monolayer versus temperature at three strengths of magnetic fields and for three values of band gaps when $\mathrm{M_z} = \mathrm{M_\nu} \neq 0$ is investigated in Fig.4.54. As it is seen, by adding the Zeeman term the magnetization acquires less magnitude of magnetization.

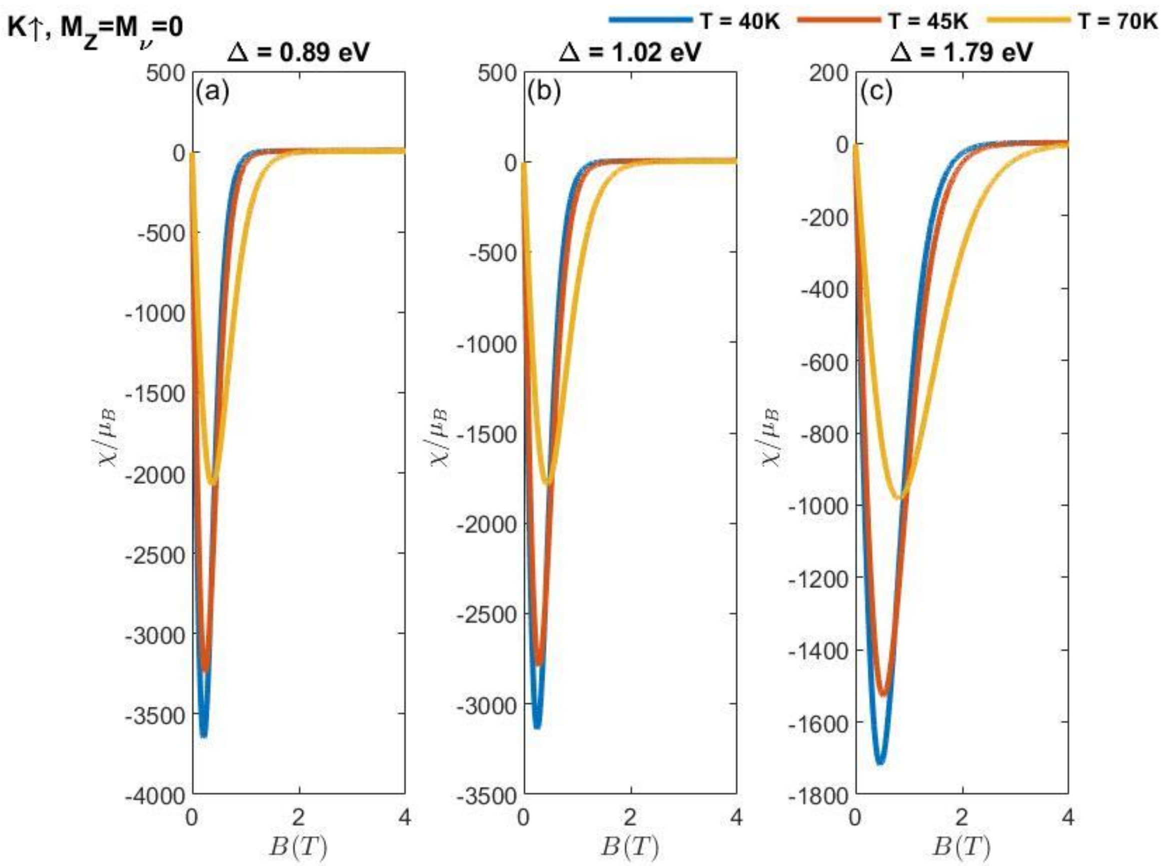

Fig.4.56: The magnetic susceptibility for the K valley of WS_2 monolayer versus magnetic field strength at three different temperature and for three values of band gaps when $M_z = M_\nu = 0$.

The amount that a material can get magnetized in response to an applied magnetic field is known as its magnetic susceptibility. It measures the amount of magnetization that a substance will acquire in the presence of a magnetic field. For many uses in physics, materials science, and engineering, including the creation of magnetic devices, sensors, and recording media, susceptibility offers insights into the way materials interact with magnetic fields (Elsaid, Shaer et al. 2020). The variation of magnetic susceptibility for the K valley of WS_2 monolayer with respect to the magnetic field strength is plotted in Fig.4.56 at three different temperature and for three values of band gaps in the case of absence of Zeeman term. As observed in the figure, the magnetic susceptibility decreases with increasing magnetic field at low magnetic field values, it begins to increase until reaching a plateau where it becomes independent of the magnetic field strength.

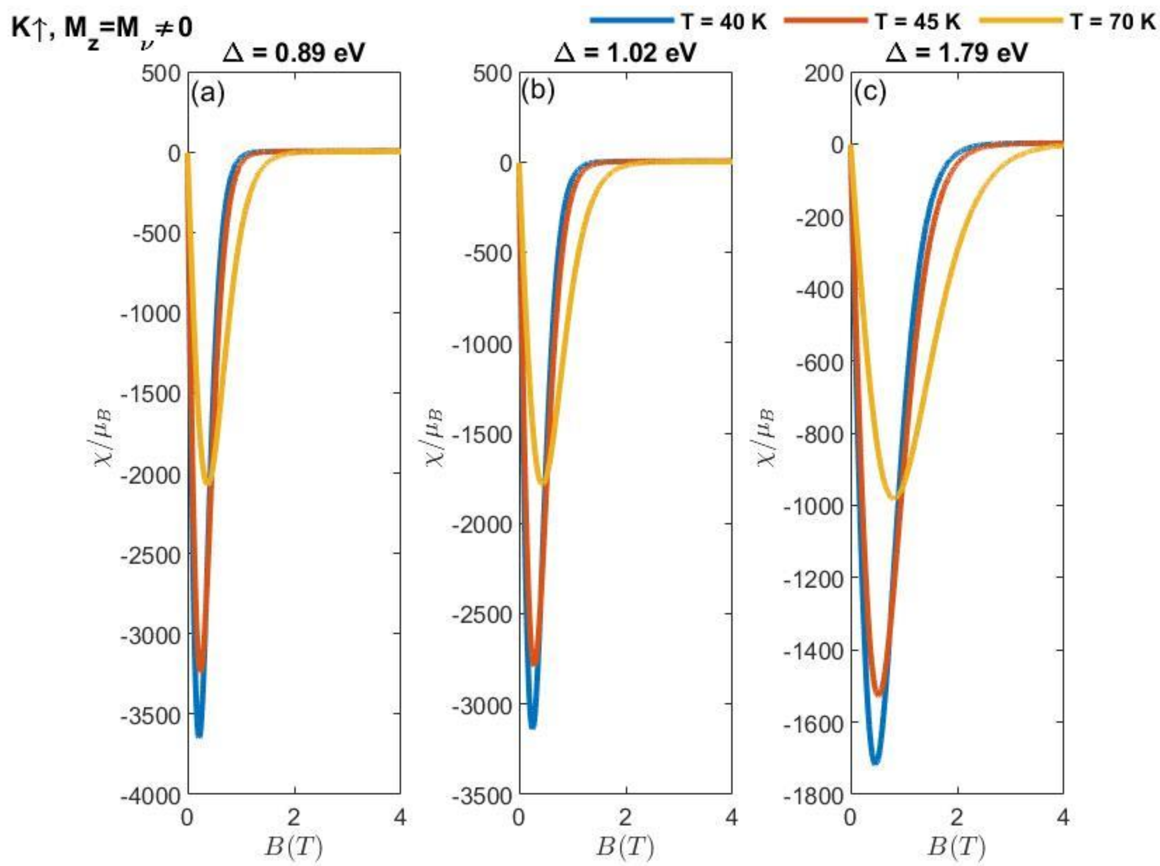

Fig.4.57: The magnetic susceptibility for the K valley of WS_2 monolayer versus magnetic field strength at three different temperature and for three values of band gaps when $M_z = M_\nu \neq 0$.

The variation of magnetic susceptibility for the K valley of WS_2 monolayer with respect to the magnetic field strength is plotted in Fig.4.57 at three different temperature and for three values of band gaps in the case of presence of Zeeman term. The rate of magnetic susceptibility decrease is notably faster at lower temperatures. However, as the temperature rises, the decrease in magnetic susceptibility slows down. Additionally, negative values of magnetic susceptibility are observed, suggesting that the material exhibits diamagnetic properties. Because of the induced currents that the applied magnetic field creates, diamagnetic materials typically repel magnetic fields weakly. A negative magnetic susceptibility and an extremely weak reaction to external magnetic fields are the outcomes of this behavior.

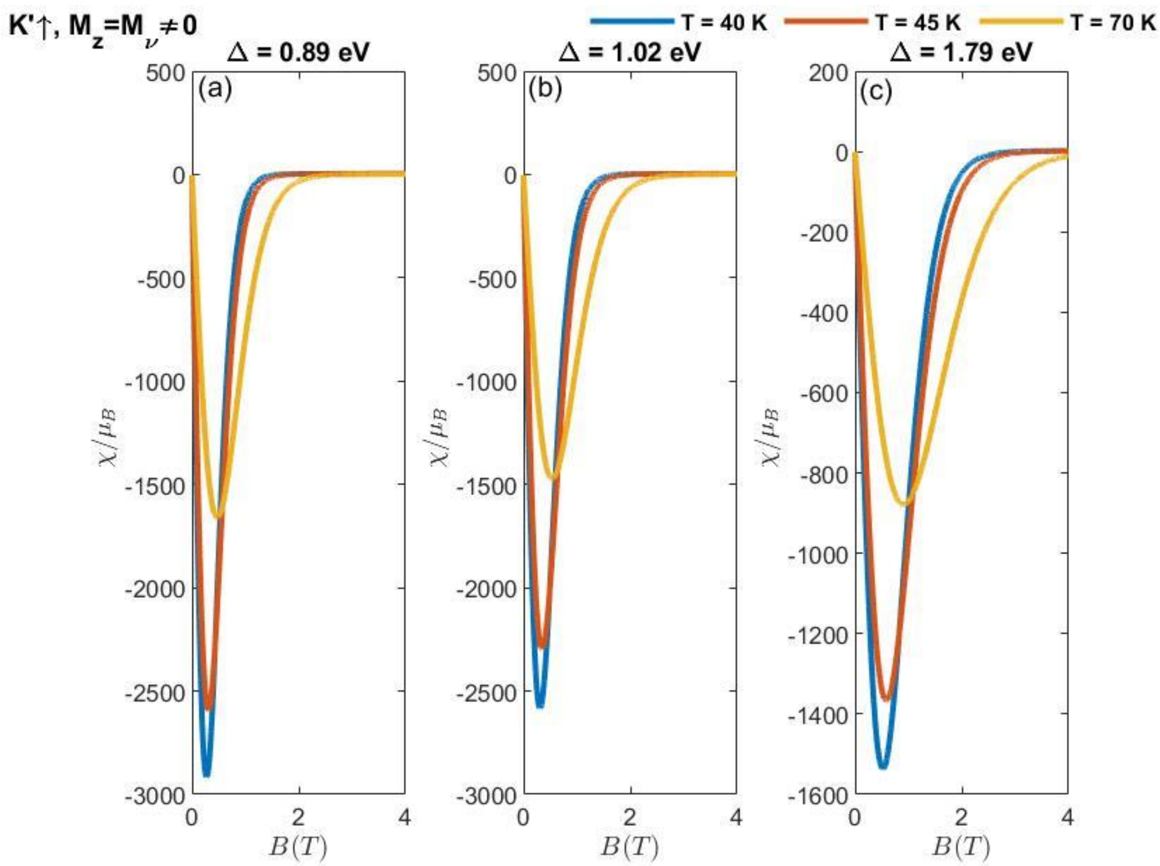

Fig.4.58: The magnetic susceptibility for the K′ valley of WS_2 monolayer versus magnetic field strength at three different temperature and for three values of band gaps when $M_z = M_\nu = 0$.

The variation of magnetic susceptibility for the K′ valley of WS_2 monolayer with respect to the magnetic field strength is plotted in Fig.4.58 at three different temperature and for three values of band gaps in the case of absence of Zeeman term.

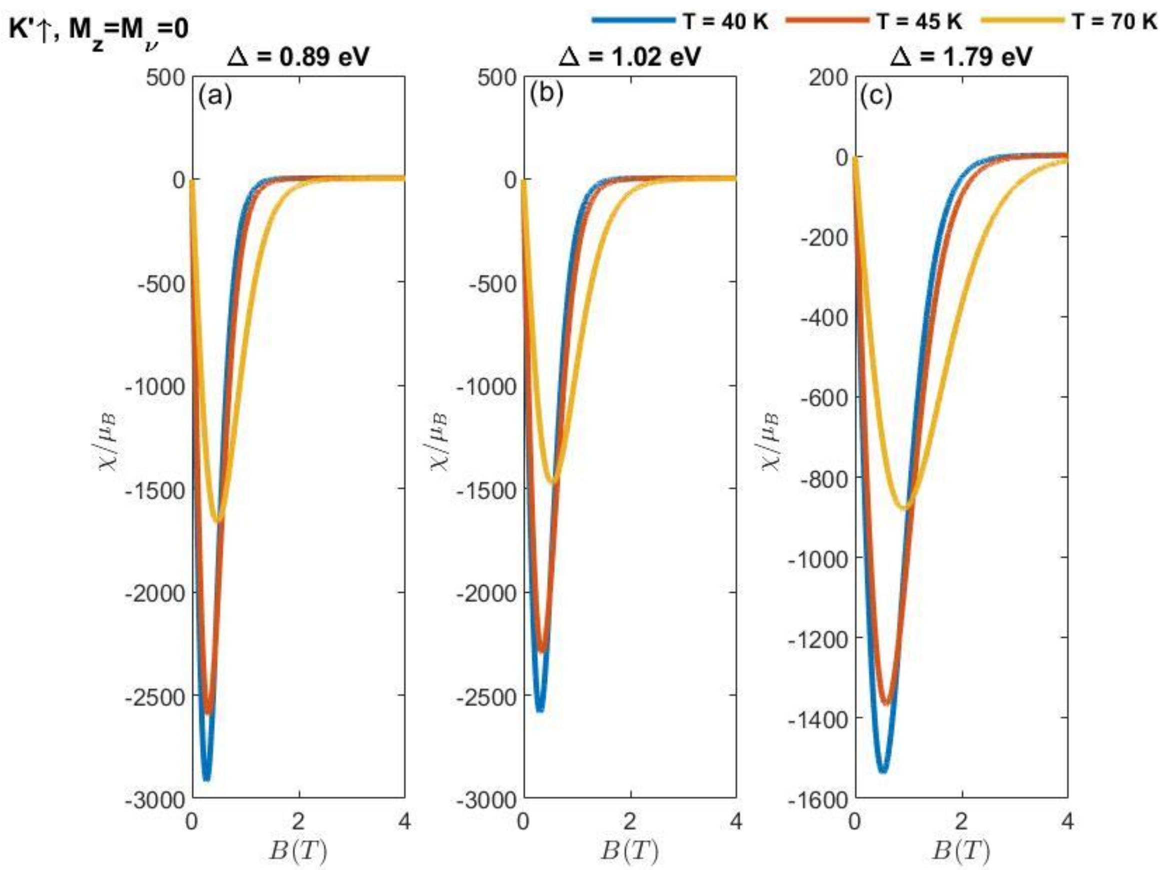

Fig.4.59: The magnetic susceptibility for the K′ valley of WS_2 monolayer versus magnetic field strength at three different temperature and for three values of band gaps when

$$M_z = M_\nu \neq 0.$$

Fig.4.59 shows a variation in magnetic susceptibility for the K′ valley of the WS_2 monolayer with relation to the strength of the magnetic field at three different temperatures and band gap values when $M_z = M_\nu \neq 0$.

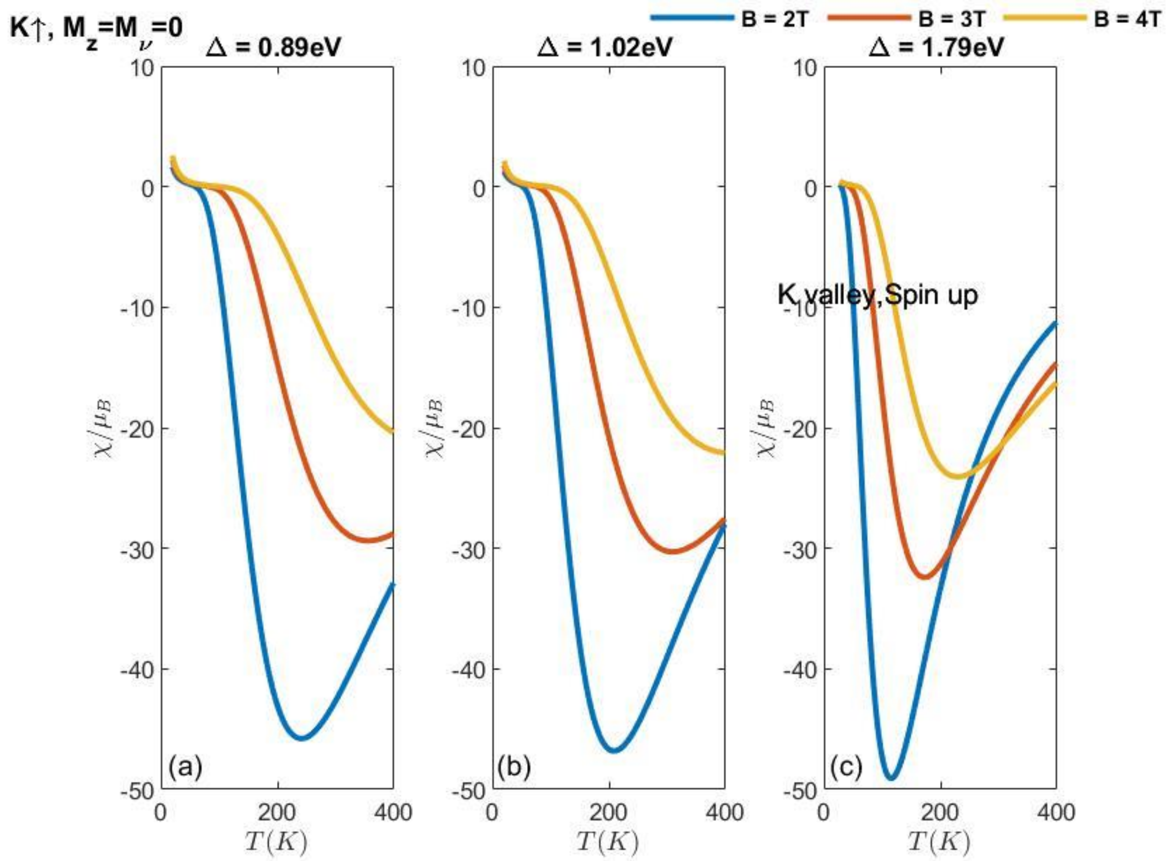

Fig.4.60: The magnetic susceptibility for the K valley of WS_2 monolayer versus temperature at three strengths of magnetic field and for three values of band gaps when $M_z = M_\nu = 0$.

Fig.4.60 reflects the magnetic susceptibility for the K valley of WS_2 monolayer versus temperature at three strengths of magnetic field and for three values of band gaps when $M_z = M_\nu = 0$. As it is seen from the figure, at the same magnetic field strength, the magnetic susceptibility decreases with increasing temperature until reaching the lowest point (shown in the table below). Subsequently, the magnetic susceptibility starts to increase with further temperature rise before stabilizing.

Table4.1: The lowest point of the magnetic susceptibility for the K valley of WS_2 monolayer when $M_z = M_\nu = 0$.

		Δ_1=0.89eV	Δ_2==1.02eV	Δ_3==1.79eV
	B= 2.0T	(238,-45.7)	(208,-46.8)	(121,-48.9)
(T,χ/μ_B)	B= 3.0T	(334,-29.2)	(293,-30.1)	(170,-32.4)
	B= 4.0T	(400,-20.4)	(393,-22.0)	(224,-24.1)

Table4.1 shows the lowest point of magnetic susceptibility for the K valley of WS_2 monolayer versus temperature at three strengths of magnetic field and for three values of band gaps when $M_z = M_\nu = 0$. As it seen from the table, at constant magnetic field, the magnetic susceptibility shifts towards lower temperature by increasing the band gap value. Also, by increasing the magnetic field strength, for the same band gap value, the magnetic susceptibility decreases and the lowest point occurs at higher temperatures.

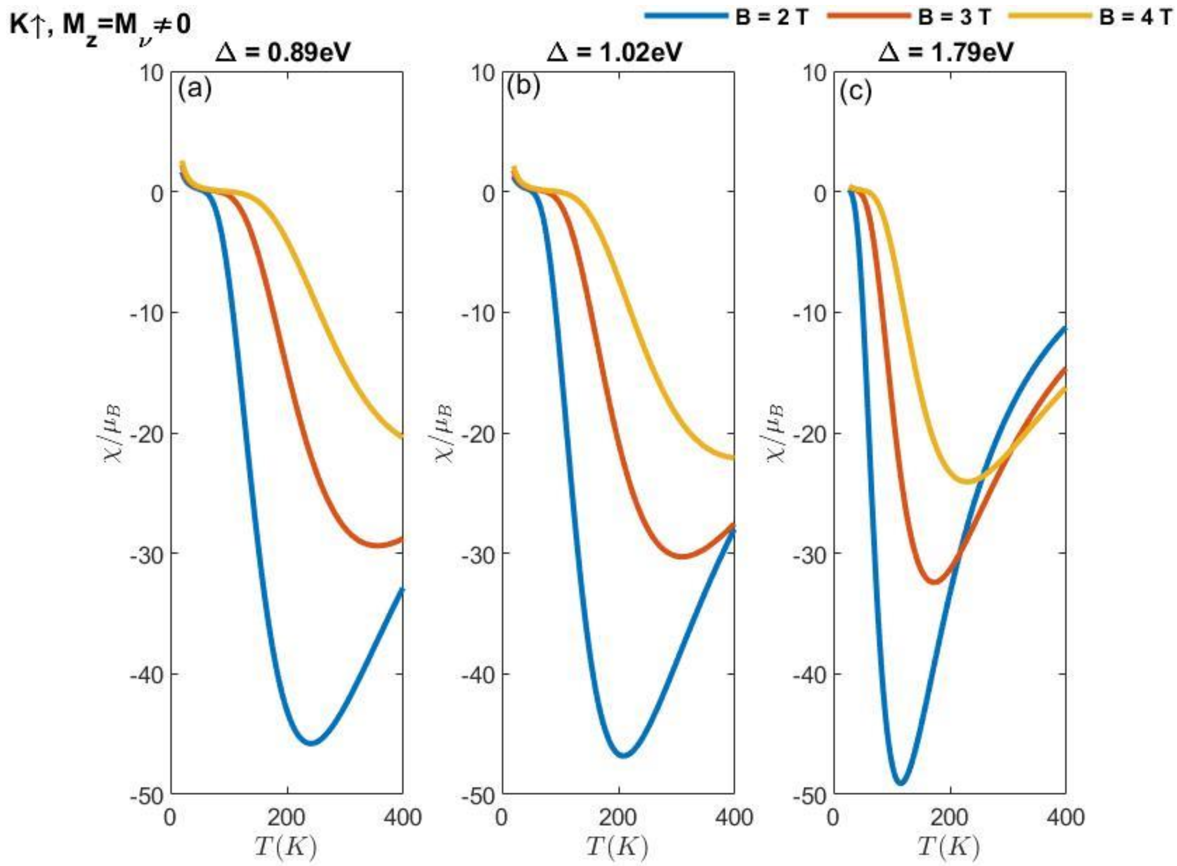

Fig.4.61: The magnetic susceptibility for the K valley of WS_2 monolayer versus temperature at three strengths of magnetic field and for three values of band gaps when $M_z = M_\nu \neq 0$.

Fig.4.61 reflects the magnetic susceptibility for the K valley of WS_2 monolayer versus temperature at three strengths of magnetic field and for three values of band gaps when $M_z = M_\nu \neq 0$. As demonstrated in the figure, for the same magnetic field strength, magnetic susceptibility declines with rising temperature until it reaches its lowest point (refer to the table below). As the temperature rises, the magnetic susceptibility gradually increases before stabilizing.

Table4.2: The lowest point of the magnetic susceptibility for the K valley of WS_2 monolayer when $\mathrm{M_z} = \mathrm{M_\nu} \neq 0$.

		Δ_1=0.89eV	Δ_2==1.02eV	Δ_3==1.79eV
	B= 2.0T	(246,-45.7)	(215,-46.7)	(123,-48.8)
(T,χ/μ_B)	B= 3.0T	(352,-29.4)	(309,-30.3)	(176,-32.4)
	B= 4.0T	$> 400K$	$> 400K$	(230,-24.1)

Table4.2 shows the lowest point of magnetic susceptibility for the K valley of WS_2 monolayer versus temperature at three strengths of magnetic field and for three values of band gaps when $\mathrm{M_z} = \mathrm{M_\nu} \neq 0$. As seen in the table, for a constant magnetic field, the magnetic susceptibility moves toward lower temperatures by increasing the band gap value. Furthermore, raising the magnetic field strength for the same band gap value reduces magnetic susceptibility, with the lowest point occurring at higher temperatures. Moreover, it is seen from table1 and table2, that adding the Zeeman term into energy function shifted the magnetic susceptibility toward higher temperatures around same value of magnetic susceptibility.

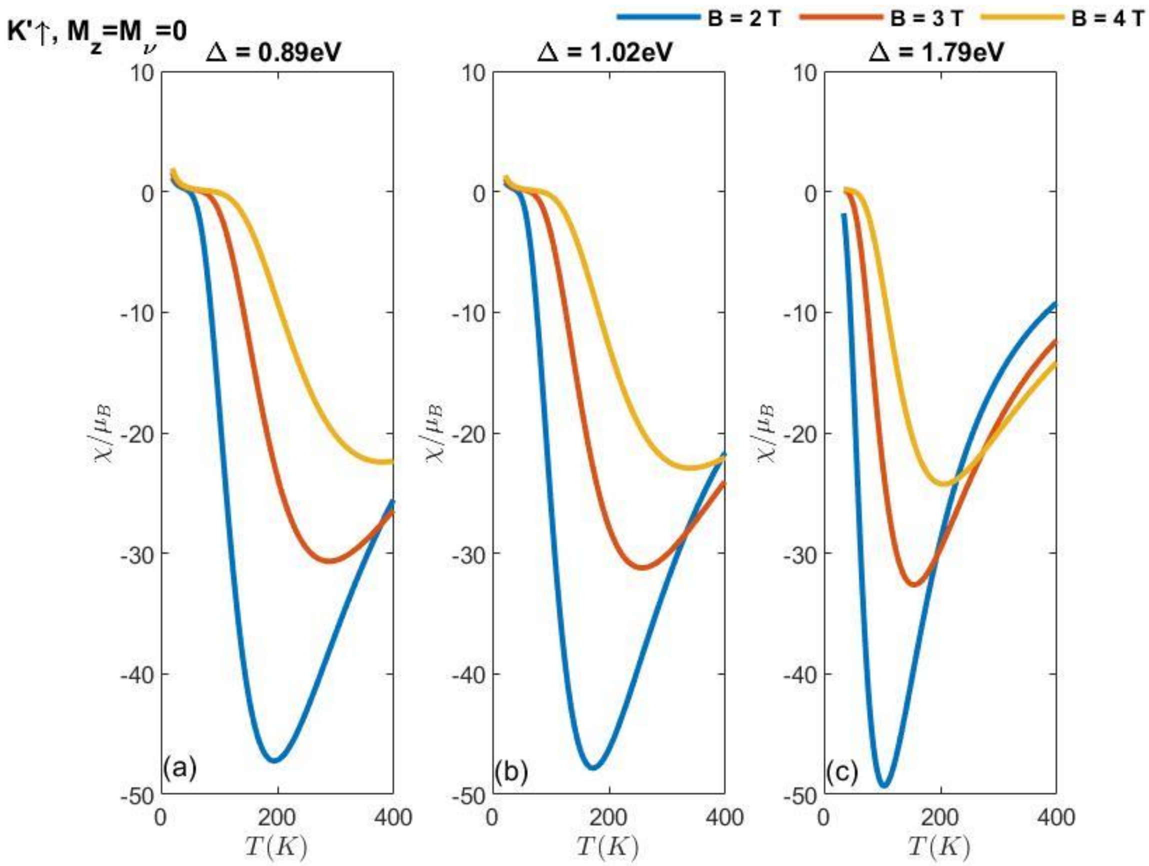

Fig.4.62: The magnetic susceptibility for the K′ valley of WS_2 monolayer versus temperature at three strengths of magnetic field and for three values of band gaps when $M_z = M_\nu = 0$.

Fig.4.62 shows the magnetic susceptibility for the K′ valley of WS_2 monolayer versus temperature at three strengths of magnetic field and for three values of band gaps when $M_z = M_\nu = 0$. As shown in the illustration, magnetic susceptibility decreases with increasing temperature until it reaches its lowest value (see table below). As the temperature rises, the magnetic susceptibility progressively increases before plateauing.

Table4.3: The lowest point of the magnetic susceptibility for the K′ valley of WS_2 monolayer when $M_z = M_\nu = 0$.

		Δ_1=0.89eV	Δ_2==1.02eV	Δ_3==1.79eV
	B= 2.0T	(198,-47.2)	(170,-47.8)	(99,-49.1)
(T,χ/μ_B)	B= 3.0T	(284,-30.6)	(253,-31.2)	(148,-32.5)
	B= 4.0T	(371,-22.4)	(343,-22.9)	(202,-24.3)

Table4.3 shows the lowest point of magnetic susceptibility for the K′ valley of WS_2 monolayer versus temperature at three strengths of magnetic field and for three values of band gaps when $M_z = M_\nu = 0$. As seen in the table, for a constant magnetic field, the magnetic susceptibility moves toward lower temperatures by increasing the band gap value. Furthermore, raising the magnetic field strength for the same band gap value reduces magnetic susceptibility, with the lowest point occurring at higher temperatures.

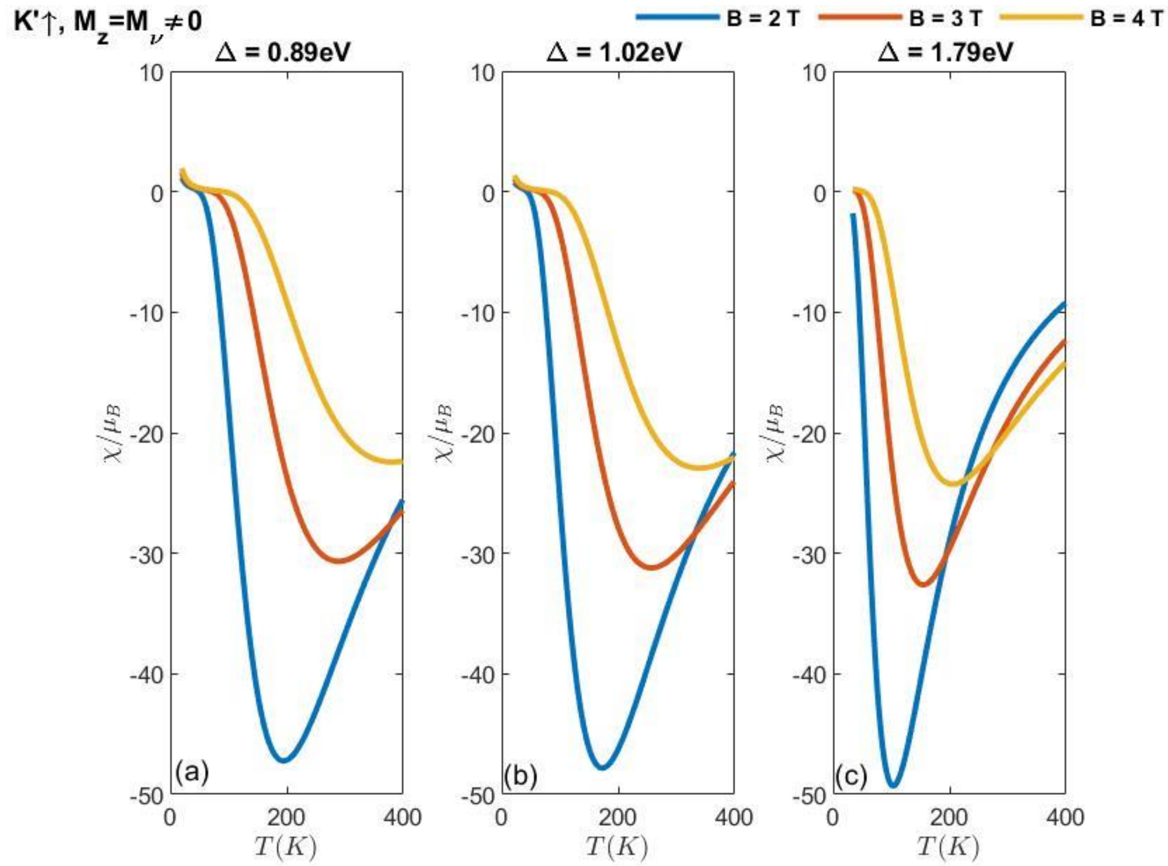

Fig.4.63: The magnetic susceptibility for the K′ valley of WS_2 monolayer versus temperature at three strengths of magnetic field and for three values of band gaps when $\mathrm{M_z} = \mathrm{M_\nu} \neq 0$.

Fig.4.63 shows the magnetic susceptibility for the K′ valley of WS_2 monolayer versus temperature at three strengths of magnetic field and for three values of band gaps when $\mathrm{M_z} = \mathrm{M_\nu} \neq 0$. The same behavior of magnetic susceptibility is shown in this case, the lowest point of magnetic susceptibility for this case is summarized in table below.

Table4.4: The lowest point of the magnetic susceptibility for the K′ valley of WS_2 monolayer when $M_z = M_v \neq 0$.

		Δ_1=0.89eV	Δ_2==1.02eV	Δ_3==1.79eV
	B= 2.0T	(200,-47,6)	(183,-47.5)	(103,-49.3)
(T,χ/μ_B)	B= 3.0T	(290,-30.7)	(259,-31.2)	(155,-32.6)
	B= 4.0T	(387,-22.4)	(350,-22.9)	(215,-24.2)

Table4.4 shows the lowest point of magnetic susceptibility for the K′ valley of WS_2 monolayer versus temperature at three strengths of magnetic field and for three values of band gaps when $M_z = M_v \neq 0$. As seen in the table, at a constant magnetic field, the magnetic susceptibility decreases with temperature as the band gap increases. Furthermore, increasing the magnetic field strength while maintaining the same band gap value reduces magnetic susceptibility, with the lowest point occurring at higher temperatures. Furthermore, Tables3.3 and 3.4 show that adding the Zeeman factor to the energy function changed the magnetic susceptibility toward higher temperatures.

In figures 3.60-63, a little drop in negative susceptibility results from thermal energy disrupting the induced currents that produce diamagnetic effects as temperature rises. Overall though, the susceptibility stays negative and doesn't change much with temperature. This stable and weakly repelling behavior of diamagnetic WS_2 TMD monolayers at various thermal regimes is shown by this consistent behavior. Comprehending these features is essential for uses requiring exact control over magnetic reactions, like magnetic levitation and highly sensitive magnetic field sensing devices (Stier, McCreary et al. 2016).

Chapter Five: Discussion

In this thesis, the effective Hamiltonian of a monolayer WS_2 in an electric field was analyzed. Information about enhancing the energy band gap of the monolayer WS_2 was obtained. Then, the effective Hamiltonian after an external and perpendicular magnetic field was applied along the z-axis of the WS_2 monolayer was studied in the case of absence and presence of Zeeman term.

The electronic properties such as the energy gap and the band structure of the monolayer in the presence of electric and magnetic fields were considered. Using the utilized information, other properties such as the density of states, and Fermi energy were discussed at different strengths of magnetic fields and temperatures.

The added magnetic field altered the electronic spectra and the Landau levels of the monolayer WS_2 was appeared. Using the partition function and the statistical physics approaches the average energy, specific heat capacity, the magnetization and magnetic susceptibility were studied in the presence and absence of Zeeman term.

In summary, the effect of increasing the band gap by increasing the applied electric field with varying temperatures and magnetic field strengths were investigated on the electronic, the thermal and the magnetic properties for the K valley and K′ valley of the WS_2 monolayer.

References

Aivazian, G., et al. (2015). "Magnetic control of valley pseudospin in monolayer WSe 2." .Nature Physics 11(2): 148-152

Alia, A. A., et al. (2019). "Magnetic properties of GaAs parabolic quantum dot in the of external tilted electric and magnetic presence of donor impurity under the influence .fields." Journal of Taibah University for Science 13(1): 687-695

Arora, S., et al. (2023). "Impact of Impurity on the Mean Energy, Heat Capacity, Free Quantum Wire." Journal Energy, Entropy and Magnetocaloric Effect of Ga 1-χ Al χ As .of Low Temperature Physics 212(1): 54-68

Boyacioglu, B. and A. Chatterjee (2012). "Heat capacity and entropy of a GaAs quantum .(8)dot with Gaussian confinement." Journal of applied physics 112

Brahim, M. (2023). A Computational Study of 2D Materials: Thermoelectric and Magnetic .Properties, 부경대학교

Bulatova, R. (2014). "Experimental tape casting of adjacently graded materials for ".magnetic refrigeration

liquid exfoliation Coleman, J. N., et al. (2011). "Two-dimensional nanosheets produced by .of layered materials." Science 331(6017): 568-571

Cortés, N., et al. (2022). "Proximity-induced spin-polarized magnetocaloric effect in .transition metal dichalcogenides." Physical Review B 105(1): 014443

Germanene: a novel two-dimensional germanium allotrope akin " .(2014) .Dávila, M., et al .to graphene and silicene." New Journal of Physics 16(9): 095002

Deatsch, A. E. and B. A. Evans (2014). "Heating efficiency in magnetic nanoparticle .hyperthermia." Journal of Magnetism and Magnetic Materials 354: 163-172

Diffo, T., et al. (2021). "Thermodynamic properties of a monolayer transition metal dichalcogenide (TMD) quantum dot in the presence of magnetic field." Physics Letters A .385: 126958

Elsaid, K., et al. (2021). "Thermophysical properties of graphene-based nanofluids." .International Journal of Thermofluids 10: 100073

Elsaid, M., et al. (2019). "The magnetization and magnetic susceptibility of GaAs Gaussian quantum dot with donor impurity in a magnetic field." Modern Physics Letters B 33(34): .1950422

Elsaid, M. K., et al. (2020). "Impurity effects on the magnetization and magnetic susceptibility of an electron confined in a quantum ring under the presence of an external .17-9 :magnetic field." Chinese Journal of Physics 64

".ELSAYED, M. "Numerical methods in the analysis of geometrically non-linear structures

Fang, H., et al. (2012). "High-performance single layered WSe2 p-FETs with chemically .doped contacts." Nano letters 12(7): 3788-3792

Gammag, R. and C. Villagonzalo (2012). "Persistent spin splitting of a two-dimensional .electron gas in tilted magnetic fields." The European Physical Journal B 85: 1-6

Geim, A. K. and I. V. Grigorieva (2013). "Van der Waals heterostructures." Nature .499(7459): 419-425

Gibertini, M., et al. (2019). "Magnetic 2D materials and heterostructures." Nature .nanotechnology 14(5): 408-419

.Gopal, E. (2012). Specific heats at low temperatures, Springer Science & Business Media

properties of cylindrical quantum dot Gumber, S., et al. (2015). "Thermal and magnetic .with asymmetric confinement." Canadian Journal of Physics 93(11): 1264-1268

Hoi, B. D. and M. Yarmohammadi (2018). "The Kubo-Greenwood spin-dependent and group-IV materials: A electrical conductivity of 2D transition-metal dichalcogenides .Green's function study." Journal of Magnetism and Magnetic Materials 451: 57-64

Kane, C. L. and E. J. Mele (2005). "Quantum spin Hall effect in graphene." Physical review .letters 95(22): 226801

Thermodynamic properties of a double ring-shaped " .(2018) Khordad, R. and H. R. Sedehi quantum dot at low and high temperatures." Journal of Low Temperature Physics 190: 200-.212

Kim, S.-Y. (2014). "Generalized Schottky Anomaly." Journal of the Korean Physical .2Society 65(7): 970-97

Kosogor, A. and V. A. L'vov (2023). "Calculation of magnetocaloric effect with regard for .dependence of heat capacity on magnetic field." Scientific Reports 13(1): 10004

in low Kosterlitz, J. and D. J. Thouless (1978). "Two-dimensional physics." Progress .temperature physics 7: 371-433

Leslie-Pelecky, D. L. and R. D. Rieke (1996). "Magnetic properties of nanostructured .materials." Chemistry of materials 8(8): 1770-1783

Li, X., et al. (2017). "Graphene and related two-dimensional materials: Structure-property .(2)relationships for electronics and optoelectronics." Applied Physics Reviews 4

Li, X., et al. (2013). "Unconventional quantum Hall effect and tunable spin Hall effect in Dirac materials: application to an isolated MoS 2 trilayer." Physical review letters 110(6): .066803

Li, Y. T., et al. (2020). "Graphene-based devices for thermal energy conversion and .utilization." Advanced Functional Materials 30(8): 1903888

aligned nanowire gate." -Liao, L., et al. (2010). "High-speed graphene transistors with a self .Nature 467(7313): 305-308

Liu, Y., et al. (2020). "Spintronics in two-dimensional materials." Nano-Micro Letters 12: .1-26

Lu, H.-Z., et al. (2013). "Intervalley scattering and localization behaviors of spin-valley .coupled dirac fermions." Physical review letters 110(1): 016806

Lu, Y. (2018). Theoretical analysis of lattice energy and morphology of transition metal .dichalcogenides

Lubchenko, V. and P. G. Wolynes (2003). "The origin of the boson peak and thermal conductivity plateau in low-temperature glasses." Proceedings of the National Academy of .Sciences 100(4): 1515-1518

Lv, R., et al. (2015). "Transition metal dichalcogenides and beyond: synthesis, properties, Accounts of chemical research 48(1): ".and applications of single-and few-layer nanosheets .56-64

Mak, K. F., et al. (2010). "Atomically thin MoS 2: a new direct-gap semiconductor." .Physical review letters 105(13): 136805

Marcos, J., et al. (2002). "Magnetic field induced entropy change and magnetoelasticity in .Ni-Mn-Ga alloys." Physical Review B 66(22): 224413

Mitioglu, A., et al. (2015). "Optical investigation of monolayer and bulk tungsten .diselenide (WSe2) in high magnetic fields." Nano letters 15(7): 4387-4392

High-mobility holes in dual-gated WSe2 field-effect " .(2015) .Movva, H. C., et al .transistors." ACS nano 9(10): 10402-10410

Muoi, D., et al. (2020). "Low-energy bands and optical properties of monolayer WS2." .Optik 209: 164581

Muoi, D., et al. (2019). "Electronic properties of WS2 and WSe2 monolayers with biaxial .strain: a first-principles study." Chemical Physics 519: 69-73

Murali, A., et al. (2021). "Emerging 2D nanomaterials for biomedical applications." .Materials Today 50: 276-302

Nasir, R., et al. (2009). "Thermodynamic properties of a weakly modulated graphene .monolayer in a magnetic field." Journal of Physics: Condensed Matter 22(2): 025503

Nersesyan, A., et al. (1995). "Disorder effects in two-dimensional Fermi systems with conical spectrum: exact results for the density of states." Nuclear Physics B 438(3): 561- .588

Peng, B., et al. (2016). "Thermal conductivity of monolayer MoS 2, MoSe 2, and WS 2: interplay of mass effect, interatomic bonding and anharmonicity." RSC advances 6(7): .5767-5773 et al. (2016). "Excitonic valley effects in monolayer WS2 under high ,.Plechinger, G .magnetic fields." Nano letters 16(12): 7899-7904

Radisavljevic, B., et al. (2011). "Single-layer MoS2 transistors." Nature nanotechnology .6(3): 147-150

Refrigeration in 2D: Electrostaticaloric effect in monolayer " .(Rehn, D. A., et al. (2018 .materials." Physical Review Materials 2(11): 114004

Sedehi, H. R. and R. Khordad (2021). "Magnetocaloric effect, magnetic susceptibility and specific heat of tuned quantum dot/ring systems." Physica E: Low-dimensional Systems .and Nanostructures 134: 114886

Sheikholeslami, M. and D. D. Ganji (2015). "Entropy generation of nanofluid in presence of magnetic field using Lattice Boltzmann Method." Physica A: Statistical Mechanics and .its Applications 417: 273-286

Sone, J., et al. (2014). "Epitaxial growth of silicene on ultra-thin Ag (111) films." New .Journal of Physics 16(9): 095004

Srivastava, A., et al. (2015). "Valley Zeeman effect in elementary optical excitations of .monolayer WSe 2." Nature Physics 11(2): 141-147

Stier, A. V., et al. (2016). "Exciton diamagnetic shifts and valley Zeeman effects in .monolayer WS2 and MoS2 to 65 Tesla." Nature communications 7(1): 10643

Tabert, C. J., et al. (2015). "Magnetic properties of Dirac fermions in a buckled honeycomb .lattice." Physical Review B 91(3): 035423

Tahir, M. and P. Vasilopoulos (2016). "Magneto-optical transport properties of monolayer .WSe 2." Physical Review B 94(4): 045415

of Thermomechanical Dynamics (TMD) to the Uechi, H., et al. (2023). "The Application Analysis of Nonequilibrium Irreversible Motion and a Low-Temperature Stirling Engine." .Journal of Applied Mathematics and Physics 11(1): 332-359

Wei, S., et al. (2020). "Emerging intrinsic magnetism in two-dimensional materials: theory .and applications." 2D Materials 8(1): 012005

Xiao, D., et al. (2012). "Coupled spin and valley physics in monolayers of MoS 2 and other .group-VI dichalcogenides." Physical review letters 108(19): 196802

Yahyah, N. S., et al. (2019). "Heat capacity and entropy of Gaussian spherical quantum dot in the presence of donor impurity." Journal of Theoretical and Applied Physics 13: 277-.288

Yarmohammadi, M. (2016). "Role of Spin–Orbit Interaction and Impurity Doping in Thermodynamic Properties of Monolayer MoS 2." Journal of Electronic Materials 45: .4958-4965

Zhang, Z., et al. (2016). "Tunable electronic and magnetic properties of two-dimensional materials and their one-dimensional derivatives." Wiley Interdisciplinary Reviews: .Computational Molecular Science 6(4): 324-350

Zong, X., et al. (2008). "Enhancement of photocatalytic H2 evolution on CdS by loading MoS2 as cocatalyst under visible light irradiation." Journal of the American Chemical .Society 130(23): 7176-7177

الخواص المغناطيسية والحرارية لطبقة أحادية من ثنائي كالكوجينيدات المعادن الانتقالية لمادة التنغستون سلفايد في مجال مغناطيسي

إيمان عمر حسن نزال

د.مؤيد أبو صاع

د.عدلي صالح

أ.د. محمد السعيد

أ.د. حازم خنفر

أ.د. سامي جبر

أ.د. جهاد أسعد

ملخص

في هذه الأطروحة، سيتم تحليل اقتران الطاقة الفعال لطبقة أحادية من كبريتيد التنغستون في مجال كهربائي من أجل الحصول على معلومات حول تعزيز فجوة الطاقة في كبريتيد التنغستون أحادي الطبقة. بعد ذلك، سيتم دراسة اقتران الطاقة الفعال بعد تطبيق مجال مغناطيسي خارجي وعمودي على طول المحور ع للطبقة الأحادية من كبريتيد التنغستون في حالة غياب ووجود جزء زيمان. سيتم النظر في الخصائص الإلكترونية مثل فجوة الطاقة وبنية النطاق للطبقة الأحادية في وجود المجالات الكهربائية والمغناطيسية. باستخدام المعلومات المستخدمة سيتم مناقشة خصائص أخرى مثل كثافة الحالات وطاقة فيرمي عند قيم مختلفة لشدة المجال المغناطيسي ودرجات الحرارة. سيغير المجال المغناطيسي المضاف الأطياف الإلكترونية وستظهر مستويات لانداو للطبقة الأحادية من كبريتيد التنغستون. باستخدام الفيزياء الإحصائية سوف ندرس متوسط الطاقة والسعة الحرارية النوعية والمغنطة والقابلية المغناطيسية في وجود وغياب الجزء الخاص بزيمان في اقتران الطاقة. سيتم أخذ تأثير زيادة

فجوة الطاقة عن طريق زيادة المجال الكهربائي المطبق على الخواص الإلكترونية والحرارية والمغناطيسية ل K و K′ من الطبقة الأحادية من كبريتيد التنغستون.

كلمات افتتاحية: كبريتيد التنغستون، حراري، مغناطيسي، فيرمي، مجال مغناطيسي.